



MIT
International Center for
Air Transportation

**DATA-DRIVEN PREDICTIVE ANALYTICS OF RUNWAY
OCCUPANCY TIME FOR IMPROVED CAPACITY AT AIRPORTS**

Nicolas P. Meijers and R. John Hansman

This report is based on the Master's Thesis of Nicolas P. Meijers submitted to the Department of Aeronautics and Astronautics in partial fulfillment of the requirements for the degree of Master of Science at the Massachusetts Institute of Technology.

Report No. ICAT-2019-14
December 2019

MIT International Center for Air Transportation (ICAT)
Department of Aeronautics & Astronautics
Massachusetts Institute of Technology
Cambridge, MA 02139 USA

Data-Driven Predictive Analytics of Runway Occupancy Time for Improved Capacity at Airports

by
Nicolas Pierre Meijers

Submitted to the Department of Aeronautics and Astronautics
on December 11, 2019, in partial fulfillment of the
requirements for the degree of
Master of Science in Aeronautics and Astronautics

Abstract

Runway Occupancy Time (ROT) is a major constraint for runway throughput. An incentive exists to reduce ROT at capacity-constrained airports and accommodate additional air transportation demand. The availability of a large quantity of surveillance data on landing operations at major US airports provides an opportunity to understand the factors driving ROT and develop reliable methods to reduce ROT by optimizing runway exit systems.

This thesis presents a data-driven approach to understanding the factors influencing Runway Occupancy Time (ROT). Airport Surface Detection Equipment - model X (ASDE-X) data, from the 36 largest airports in the US, provided detailed flight track data that were combined with airport and weather data to analyze ROT. The relative importance of different factors driving ROT was first assessed using a random-forest algorithm. The dominant factors identified were then studied individually to obtain a better understanding of ROT behavior.

Based on this improved understanding of ROT, predictive models of ROT were designed and presented in this thesis. Using a two-step process, these models are able to stochastically predict ROT for aircraft landing in specific conditions on a runway characterized by its exit system. First, a Recurrent Neural-Network model predicts the probability of use of each available runway exit. Second, a set of Feed-Forward Neural-Networks predicts the average and variance of ROT that would be observed if the aircraft was vacating the runway using each exit. These two predictions were combined to obtain a predicted gaussian-mixture distribution of ROT for the landing aircraft. These models were used to predict the distribution of ROT of a given runway by making stochastic predictions of ROT for thousands of flights.

The impact on ROT of different changes to the exit system of the runways at Keflavík airport in Iceland was assessed using these models. Keflavík airport currently has a poor Runway Occupancy Time performance with an 80s average ROT. The predictive models were used to identify the location of new exits providing the best ROT reduction. According to the models, modifications to the exit system would potentially provide up to 23s of reduction in average ROT observed during peak-hour operations.

Thesis Supervisor: R. John Hansman
Title: T. Wilson Professor of Aeronautics and Astronautics

Acknowledgments

This thesis is partly based upon work sponsored by the Federal Aviation Administration (FAA) under a NEXOR II research contract. I would like to acknowledge the support of Pr. Antonio Trani from Virginia Tech, Pr. John Shortle from George Mason University, and of Paul Strande, Thomas Proeschel and Edward Johnson at the FAA.

The work presented in this thesis was also sponsored by ISAVIA. I would like to thank Hjalti Pálsson and Atli Norðmann Sigurðarson for their precious support.

THIS PAGE INTENTIONALLY LEFT BLANK

Contents

List of Figures	9
List of Tables	13
1 Introduction	15
2 Literature Review	19
2.1 Understanding Factors Driving Runway Occupancy Time	19
2.2 Modelling Runway Occupancy Time	21
3 Runway Occupancy Time Data Collection using Landing Data	23
3.1 Runway Occupancy Time Measurements	23
3.2 Determining Deceleration Information and Landing Parameters	28
4 Identifying Factors Driving Runway Occupancy Time	31
4.1 Analyzing the Variability of Runway Occupancy Time	31
4.2 Identifying Factors Driving ROT using a Random Forest Algorithm	32
4.2.1 Random Forest Models	33
4.2.2 Training a Random Forest Algorithm to Predict ROT	34
4.3 Ranking the Factors Driving ROT	36
5 Understanding the Impact of Dominant ROT Factors	37
5.1 Analysis of the Impact of Aircraft Type	37
5.2 Analysis of the Impact of the Runway Exit Used	38
5.2.1 Impact of the Runway Exit Location	39
5.2.2 Impact of the Runway Exit Angle	40
5.3 Analysis of the Impact of the Airline	42
5.4 Analysis of the Impact of the Final Approach Speed	43
5.5 Analysis of the Impact of a Following Aircraft on Approach	46
6 Developing Predictive Models of Runway Occupancy Time	49
6.1 Overview of Predictive Models of Runway Occupancy Time	49
6.2 Predictive Modelling of Exit Use	51

6.2.1	Recurrent Neural Network Models	51
6.2.2	Training Recurrent Neural Networks to Predict Exit Use	53
6.3	Predictive Modelling of Mean/Variance of ROT	56
6.3.1	Neural Network Models	56
6.3.2	Prediction Process of Mean/Variance Estimates of ROT	57
6.3.3	Training Neural Networks to Predict Mean/Variance Estimates of ROT	58
6.4	Predicting the ROT Distribution for a Landing Aircraft	61
6.5	Predicting ROT Distributions by Runway	63
6.6	Performance of Models in Predicting ROT Distributions by Runway	64
7	Case Study - Reducing ROT at Keflavík Airport	67
7.1	Understanding Current Landing Operations at Keflavík Airport	67
7.1.1	Collecting ROT Measurements and Landing Data	69
7.1.2	Understanding the Characteristics of Landing Operations	71
7.1.3	Assessing the Current Runway Occupancy Time performance	74
7.2	Reducing Runway Occupancy Time at Keflavík Airport	76
7.3	Reducing Runway Occupancy Time for Runway 28	77
7.3.1	Assessing the Performance of the Current Runway 28 Exit System	77
7.3.2	Assessing the Performance of Predictive Models for Runway 28	78
7.3.3	Evaluating Modifications to the Current Runway 28 Exit System	78
7.4	Reducing Runway Occupancy Time for Runway 19	82
7.4.1	Assessing the Performance of the Current Runway 19 Exit System	82
7.4.2	Assessing the Performance of Predictive Models for Runway 19	83
7.4.3	Evaluating Modifications to the Current Runway 19 Exit System	84
7.5	Reducing Runway Occupancy Time for Runway 01	85
7.5.1	Assessing the Performance of the Current Runway 01 Exit System	85
7.5.2	Assessing the Performance of Predictive Models for Runway 01	87
7.5.3	Evaluating Modifications to the Current Runway 01 Exit System	87
7.6	Reducing Runway Occupancy Time for Runway 10	93
7.6.1	Assessing the Performance of the Current Runway 10 Exit System	93
7.6.2	Assessing the Performance of Predictive Models for Runway 10	94
7.6.3	Evaluating Modifications to the Current Runway 10 Exit System	94
7.7	Summary of Potential Modifications to the Exit System	98
8	Conclusion	101
A	List of Aircraft Used to Develop Predictive Models	109
B	Performance of Predictive Model of Exit Use	111
C	Performance of Predictive Models of ROT	117
D	ROT Distribution Prediction Performance	123

List of Figures

1-1	Interaction between Runway Occupancy Time and final approach separation	15
1-2	Example of the two most popular runway exit angles	17
3-1	Example of runway exit measurements (KATL, exit SG14)	24
3-2	Example of the identification of landing flights at San Francisco airport (KSFO on 04-01-2015)	25
3-3	Example of projected tail length of aircraft using exit SG14 (KATL)	26
3-4	Example of the runway threshold and runway exit identified for a landing flight at Boston Logan International airport (KBOS)	26
3-5	Runway Occupancy Time extraction process	27
3-6	Example of leading and following aircraft at Atlanta Hartsfield airport (KATL)	28
3-7	Example of speed and deceleration profiles of an A320 landing at Charlotte Douglas International airport (KCLT)	29
3-8	Example of recorded gate locations at Honolulu International airport (PHNL)	30
4-1	Cumulative distribution of ROT at the system level (36 US airports)	32
4-2	Cumulative distributions of ROT for the 36 US Airports	32
4-3	Training process of a random-forest algorithm	33
4-4	Example of a single random forest tree of depth 5	35
4-5	Ranking of the importance of ROT factors	36
5-1	Cumulative distributions of ROT per wake category	38
5-2	Cumulative distributions of ROT for 6 common "Large" aircraft types	38
5-3	Example of the two most popular runway exit angles	39
5-4	Evolution of A320 ROT depending on exit location and exit type	39
5-5	Cumulative distributions of A320 ROT depending on the type of exit	40
5-6	Cumulative distributions of A320 exit speed depending on the type of exit	40
5-7	Example of similarly located high-speed (30°) and right-angle (90°) exits	41
5-8	Example of comparison of average A320 speed profiles for two similarly located high-speed (30°) and right-angle (90°) exits	41
5-9	Example of comparison of average A320 deceleration profiles for two similarly located high-speed (30°) and right-angle (90°) exits	42

5-10	Cumulative distribution of A320 ROT depending on airline	42
5-11	Observed A320 ROT depending on approach speed	43
5-12	Example of comparison of average A320 speed profiles for different final approach speeds (exit K4, KPHL)	44
5-13	Example of comparison of average A320 deceleration profiles for different final approach speeds (exit K4, KPHL)	44
5-14	Contour plot of ROT depending on final approach speed and exit location for A320 using high-speed exits (30°)	45
5-15	Contour plot of ROT depending on final approach speed and exit location for A320 using right-angle exits (90°)	45
5-16	Example of arrival pressure categories at LaGuardia airport (KLGA)	47
6-1	Overall prediction process of ROT	50
6-2	Simplified functioning of a recurrent neural network	52
6-3	Final architecture of the predictive model of exit use	54
6-4	RNN training and validation loss depending on number of units	55
6-5	General predictive process of mean/variance of ROT	58
6-6	Validation loss of average ROT predictive model depending on number of units	59
6-7	Distribution of mean squared error in the prediction of average ROT on testing dataset	60
6-8	Example of predicted ROT distribution and weighted components per exit for an aircraft landing on runway 34L (KSLC)	62
6-9	Predicted ROT distribution for runway 25L at Phoenix Sky Harbor International airport (KPHX)	63
6-10	Predicted ROT distribution with larger left tail for runway 17 at Philadelphia International airport (KPHL)	65
7-1	Runway configuration of Keflavík airport (BIKF)	68
7-2	Aerodrome chart of Keflavík airport (BIKF)	69
7-3	Example of flight tracks at Keflavík airport (BIKF on 01-01-2018)	70
7-4	Example of the runway threshold and runway exit identified for a landing flight at Keflavík airport (BIKF)	70
7-5	Distribution of wind at Keflavík airport (BIKF)	72
7-6	Distribution of temperature at Keflavík airport (BIKF)	72
7-7	Observed fleet-mix of landing aircraft at Keflavík airport (BIKF)	72
7-8	Average daily distribution of landings at Keflavík airport (BIKF)	73
7-9	Terminal locations for aircraft landing at Keflavík airport (BIKF)	73
7-10	Runway Occupancy Time distribution at US airports and during peak-hours at Keflavík airport (BIKF)	74
7-11	Exit system of runway 28	77
7-12	Potential new exit system for runway 28	79
7-13	Average Runway Occupancy Time of runway 28 depending on new high-speed exit location	79

7-14 Potential new exit system for runway 28	80
7-15 Average ROT of runway 28 depending on 2 nd new high-speed exit location	81
7-16 Exit system of runway 19	82
7-17 Potential new exit system for runway 19	84
7-18 Average Runway Occupancy Time of runway 19 depending on new high-speed exit location	85
7-19 Exit system of runway 01	86
7-20 Exit system of runway 01 with planned taxiway	88
7-21 Potential new exit system for runway 01	89
7-22 Average Runway Occupancy Time of runway 01 depending on new high-speed exit location	90
7-23 Exit system of runway 01 with pilot incentive to exit early	91
7-24 Average Runway Occupancy Time of runway 01 depending on new high-speed exit location with pilot incentive to vacate the runway early	92
7-25 Exit system of runway 10	93
7-26 Potential new exit system for runway 10	95
7-27 Potential new exit system for runway 10	96
7-28 Average Runway Occupancy Time of runway 10 depending on new high-speed exit location	96
7-29 Potential new exit system for runway 10	97
7-30 Summary of potential modifications to the exit system	100

THIS PAGE INTENTIONALLY LEFT BLANK

List of Tables

1.1	Legacy aircraft wake categories - FAA order JO 7110.65Y	16
1.2	Final approach wake turbulence separation minima (IFR) - FAA order JO 7110.65Y	16
3.1	List of the 36 airports with available ASDE-X data	24
3.2	Collected landing data, airport data and weather data	30
5.1	Average A320 ROT for 7 airlines and 8 airports	43
5.2	Average A320 ROT and exit location depending on arrival pressure for 26 airports	48
6.1	Parameters used by predictive models	51
6.2	Example of sequence of input for an aircraft landing on runway 34L (KSLC) . .	53
6.3	Example of parameters of aircraft landing on runway 34L (KSLC)	62
6.4	Example of runway exit system of runway 34L (KSLC)	62
6.5	Example of exit use and ROT predictions for aircraft landing on runway 34L (KSLC)	62
7.1	Average Runway Occupancy Time for each runway at Keflavík airport (BIKF) . .	68
7.2	Collected landing data, airport data and weather data at Keflavík airport (BIKF)	71
7.3	Average Runway Occupancy Time during peak-hours for each runway at Keflavík airport (BIKF)	74
7.4	Legacy ICAO aircraft wake categories - ICAO DOC 4444	75
7.5	Final approach wake turbulence separation minima (IFR) - ICAO DOC 4444 . .	75
7.6	Average exit use and Runway Occupancy Time observed for each exit of runway 28	77
7.7	Average exit use and Runway Occupancy Time predicted for each exit of runway 28	78
7.8	Average exit use and Runway Occupancy Time predicted for each exit of runway 28 with additional high-speed exit	80
7.9	Average exit use and Runway Occupancy Time predicted for each exit of runway 28 with a 2 nd additional high-speed exit	81
7.10	Average exit use and Runway Occupancy Time predicted for each exit of runway 28 with two simultaneously optimized additional high-speed exits	82
7.11	Average exit use and Runway Occupancy Time observed for each exit of runway 19	83

7.12	Average exit use and Runway Occupancy Time predicted for each exit of runway 19	83
7.13	Average exit use and Runway Occupancy Time predicted for each exit of runway 19 with an additional high-speed exit	85
7.14	Average exit use and Runway Occupancy Time observed for each exit of runway 01	86
7.15	Average exit use and Runway Occupancy Time predicted for each exit of runway 01	87
7.16	Average exit use and Runway Occupancy Time predicted for each exit of runway 01 with a bypassing taxiway	89
7.17	Average exit use and Runway Occupancy Time predicted for each exit of runway 01 with new high-speed exit	90
7.18	Average exit use and Runway Occupancy Time predicted for each exit of runway 19 with pilot incentive to vacate the runway early	91
7.19	Average exit use and Runway Occupancy Time predicted for each exit of runway 01 with new high-speed exit and pilot incentive	92
7.20	Average exit use and Runway Occupancy Time observed for each exit of runway 10	93
7.21	Average exit use and Runway Occupancy Time predicted for each exit of runway 10	94
7.22	Average exit use and Runway Occupancy Time predicted for each exit of runway 10 with new right-angle exit	95
7.23	Average exit use and Runway Occupancy Time predicted for each exit of runway 10 with new taxiway and additional high-speed exit	97
7.24	Average exit use and Runway Occupancy Time predicted for each exit of runway 10 with new taxiway and coupled high-speed exit	98
7.25	Predicted reductions in average ROT with potential modifications	98
A.1	List of aircraft used to develop predictive models	109
B.1	Detailed performance of the predictive model of exit use	111
C.1	Detailed performance of the predictive models of average ROT	117
D.1	Performance of models in the prediction of Runway Occupancy Time distributions	123

Chapter 1

Introduction

Motivation

Runway Occupancy Time (ROT) is one of the main elements limiting the throughput of runways at airports. Runway Occupancy Time can be formally defined as the "time interval between the aircraft crossing the threshold and its tail vacating the runway" according to Eurocontrol [1]. Under current regulations [2], the simultaneous occupancy of a runway by multiple landing airplanes is prohibited and an aircraft cannot be cleared to land if the previous aircraft has not vacated the runway. This rule limits the number of aircraft that can land on a runway on a given time period. A high average Runway Occupancy Time on a runway will considerably limit runway throughput. To prevent simultaneous runway occupancy, pilots are incentivized to vacate the runway as soon as possible [3] and air traffic controllers insure proper separations between aircraft on final approach as per Figure 1-1. These separations aim at leaving enough time for the leading aircraft to vacate the runway before the trailing aircraft reaches the runway threshold.

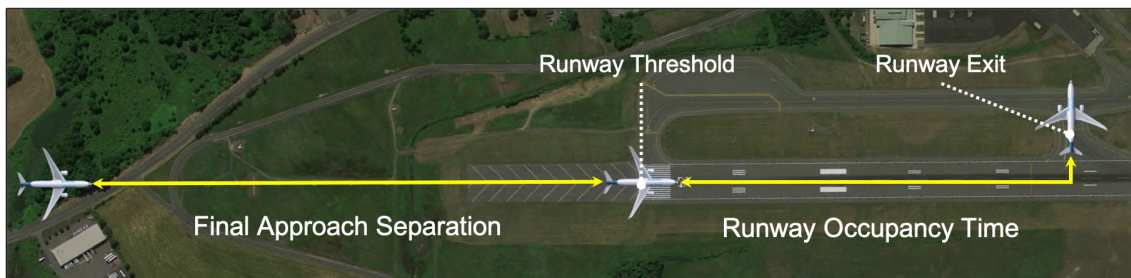


Figure 1-1: Interaction between Runway Occupancy Time and final approach separation

Current separations between aircraft on final approach are however mainly driven by wake-vortex turbulence. To reduce the risk of wake turbulence encounter on approach, strict separation minima are enforced and are usually more conservative than what Runway Occupancy

Time requires. These minima are based on categories of aircraft defined using the aircraft Maximum Take-Off Weight (MTOW). Tables 1.1 and 1.2 present the aircraft legacy wake categories and final approach separation minima for IFR operations in application in the US.

Table 1.1: Legacy aircraft wake categories - FAA order JO 7110.65Y

	Small	Large	B757	Heavy	Super
MTOW (lb)	MTOW ≤ 41,000	41,000 < MTOW < 300,000	B757	MTOW ≥ 300,000	A380, AN225

Table 1.2: Final approach wake turbulence separation minima (IFR) - FAA order JO 7110.65Y

Separation Minimum (NM)		Following Aircraft				
		Super	Heavy	B757	Large	Small
Leading Aircraft	Super	MRS*	6	7	7	8
	Heavy	MRS*	4	5	5	6
	B757	MRS*	MRS*	MRS*	MRS*	4
	Large	MRS*	MRS*	MRS*	MRS*	4
	Small	MRS*	MRS*	MRS*	MRS*	MRS*

*Minimum Radar Separation (2.5, 3 or 5NM)

In recent years, the US Federal Aviation Administration (FAA) and its European counterpart, Eurocontrol, have focused research efforts on reducing separation minima thanks to aircraft re-categorization programs (RECAT). These re-categorization programs have introduced more complex wake-turbulence classifications of aircraft based on both wingspan and MTOW leading to more aircraft categories and reduced separation minima on average. However, as wake vortex separation minima are reduced for aircraft on final approach, inter-arrival times are progressively getting closer to the observed Runway Occupancy Time. This increases the constraining impact of Runway Occupancy Time on runway throughput.

The average Runway Occupancy Time observed on a runway also drives the Minimum Radar Separation (MRS) used on final approach. This Minimum Radar Separation can be equal to 5.0, 3.0 or 2.5NM. According to ICAO PANS-ATM (Procedures for Air Navigation Services related to Air Traffic Management) [4], the Minimum Radar Separation may be reduced from 5.0 to 3.0NM if the radar capabilities enable it. An additional reduction to 2.5NM may be provided if 8 different conditions are fulfilled. These include observing an average ROT below 50s for a considered runway. By complying with the multiple requirements established by ICAO and reducing ROT below 50s, airport operators may reduce MRS and increase runway throughput.

The Runway Occupancy Time of a landing aircraft is the result of the aircraft braking performance in its landing environment. This braking performance enables the aircraft to potentially

vacate the runway after a specific braking distance where the aircraft reached an acceptable ground-speed. The main leverage airport operators have to reduce ROT consists in optimizing the exit system of runways. The exit system needs to be adapted to the expected landing operations. By designing runway exits with optimal parameters, airport operators can reduce the Runway Occupancy Time of aircraft and recover additional movement for their runways. The key exit parameters include the distance of the exits from the runway threshold and the angle of the exits with the runway axis, ranging from 0° to 180° . The most popular exit angles are 90° (i.e. right-angle exits) and 30° (i.e. high-speed exits), depicted in Figure 1-2. Compared to right-angle exits, high-speed exits are designed to enable aircraft to vacate the runway at a higher speed which reduces the braking distance on the runway. Finding optimal exit parameters is however difficult for airport operators as different aircraft types landing in different conditions can have very different braking behaviors.

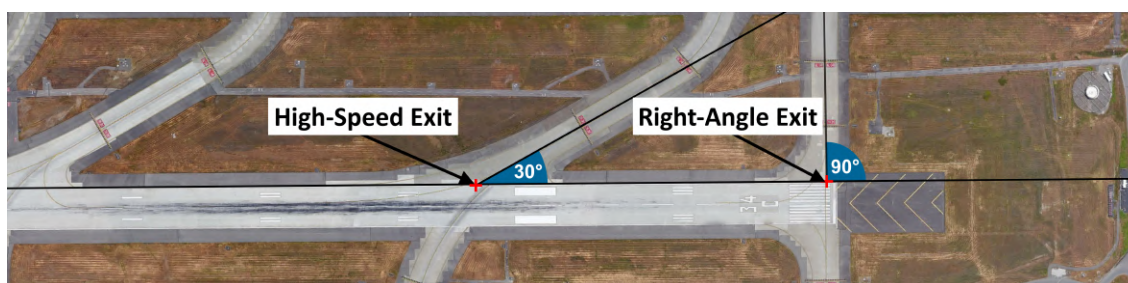


Figure 1-2: Example of the two most popular runway exit angles

With the large amount of data on landing operations available today from surveillance systems, an opportunity exists to better understand the factors driving runway occupancy time and to design data-driven solutions to optimally locate runway exits and reduce ROT. Available data on landing operations includes large amounts of flight track data around airports (e.g. Airport Surface Detection data, ADS-B data), weather surface data and information on airport geometry and runway characteristics. By fusing multiple sources of data, a comprehensive picture of braking performance under various conditions can be obtained.

This thesis aims at leveraging operational data to analyze the roots of ROT and develop predictive models of Runway Occupancy Time to optimize runway exit systems. A large volume of ROT measurements and associated landing parameters was first extracted from several data sources such as the Airport Surface Detection Equipment, Model X (ASDE-X) and the Automated Dependent Surveillance-Broadcast (ADS-B). These measurements were linked to weather and airport data derived from the Automated Surface Observing System (ASOS) and Google-Earth. Data-mining techniques were then applied to the collected data to identify precursors of Runway Occupancy Time. A Random-Forest algorithm provided a ranking of landing parameters explaining the variance of ROT. The dominant factors influencing ROT were analyzed using observed speed and deceleration profiles on the runway. Based on this understanding, data-driven models were developed to predict Runway Occupancy Time. These models, based on Recur-

rent and Feed-Forward Neural Networks and trained on the collected data, give high-fidelity stochastic predictions of ROT for landing aircraft using a given set of available runway exits. At the runway level, by predicting ROT for thousands of landing flights with different landing parameters, runway-specific ROT probability distributions can be predicted. These models enable the assessment of modifications to a runway exit system by evaluating their impact on the predicted ROT distribution. They were used to propose modifications to the exit system of an airport in Iceland showcasing a poor Runway Occupancy Time performance.

Research Objectives

The research objectives of this thesis can be summarized as follow:

- Develop data driven solutions to reduce Runway Occupancy Time by:
 - Identifying and understanding factors driving Runway Occupancy Time using flight-track data
 - Developing predictive models of Runway Occupancy Time based on the identified precursors
 - Using the predictive models to optimize runway exit systems at capacity constrained airports

Thesis Outline

This thesis is organized in the following manner. First, a literature review is presented in Chapter 2. Second, a methodology to extract Runway Occupancy Time measurements and exogenous landing data is introduced in Chapter 3. Chapter 4 presents a method used to identify the factors driving ROT. Fourth, a detailed analysis of the impact of each driving factor on Runway Occupancy Time is described in Chapter 5. Chapter 6 presents the methodology used to develop predictive models of Runway Occupancy Time and assess their performance. Finally, a case study on reducing Runway Occupancy Time at Keflavík airport (Iceland) by optimizing the runway exit system is presented in Chapter 7. Chapter 8 presents the conclusions drawn from this study.

Chapter 2

Literature Review

This thesis presents a data-driven approach to understanding and reducing Runway Occupancy Time at capacity-constrained airports. Runway Occupancy Time has been identified as a potential limitation to runway throughput more than 60 years ago and several studies have focused on identifying factors driving Runway Occupancy Time. Several approaches were developed as well to model Runway Occupancy Time and be able to propose runway exit systems minimizing the Runway Occupancy Time of landing aircraft. This section presents a comprehensive review of the different research efforts aiming at understanding and modelling Runway Occupancy Time.

2.1 Understanding Factors Driving Runway Occupancy Time

Several studies have been conducted in the past to identify the factors influencing Runway Occupancy Time. They used various collection methods to obtain ROT measurements and conduct statistical analysis.

Some of the first studies of Runway Occupancy Time date back to the 1980s to identify potential limitations at reducing separations between aircraft on final approach. The MITRE corporation was tasked by the FAA to study the interaction between inter-arrival times and ROT and needed to understand the variability of ROT depending on multiple factors. Using data collected by visual means between 1972 and 1973 at 6 US airports, Koenig [5] identified that Runway Occupancy Time was not solely driven by braking performance but also influenced by pilot motivational factors. These motivational factors were driving the choice of the exit used to vacate the runway and encompassed the time to gate, airline-specific procedures and traffic density for instance.

In 1983, additional studies of ROT were funded by the FAA. As a contractor, the MITRE corporation collected 1755 Runway Occupancy Time measurements at LaGuardia airport (KLGA), Newark airport (KEWR) and Boston Logan International airport (KBOS). These measurements

were obtained by visually observing multiple landings from the control tower. Using this data, the Runway Occupancy Time dependence on the wake category of the landing aircraft and the observed runway condition (dry/wet) was analyzed by Weiss and Barrer [6]. It was found that the runway condition had a relatively small impact on Runway Occupancy Time. The data used for this study was however limited to a few airports and not highly reliable due to the difficulty of measuring ROT from the control tower. The main difficulty encountered was to reliably measure the time when the aircraft was crossing the runway threshold and vacating the runway from the control tower.

This difficulty was overcome by NASA in 1999 with the development of the Dynamic Runway Occupancy Measurement System (DROMS). Using mode-S transponders and multilateration, precise aircraft position could be collected at Atlanta Hartford International airport (KATL) and Runway Occupancy Time measurements could be calculated. Lee et al. [7] used this system to collect more than 3000 ROT measurements at Atlanta during 15 days and analyze factors influencing ROT. They found that ROT was equally influenced by the approach speed and weight of the aircraft, barely influenced by winds observed on approach and increased by less than 5% with wet runway conditions versus dry conditions. It was also observed that ROT was not dependent on the airline, contradicting MITRE previous findings.

More recently, the collection of Runway Occupancy Time measurements was eased by the availability of modern detection systems around airports. The Airport Surface Detection Equipment - Model X (ASDE-X) was installed by the FAA at 36 US airports starting in 2004 and provided a large amount of data regarding flight tracks around airports. In 2009, Kumar, Sherry, and Kicinger [8] were the first to leverage this data to analyze Runway Occupancy Time. They developed a simple method to extract ROT measurements from ASDE-X data and collected 2035 Runway Occupancy Time measurements at Dallas Fort Worth airport (KDFW). Kumar, Sherry, and Kicinger [8] used this data to analyze the correlation of ROT with the momentum of landing aircraft.

ASDE-X flight track data was also used by Kolos-Lakatos [9] in 2013 to understand the interaction between Runway Occupancy Time and Wake Vortex separation. ROT data was collected at Boston Logan airport (KBOS), LaGuardia airport (KLGA), Newark airport (KEWR) and Philadelphia airport (KPHL) by modelling runways as polygons and computing the time each landing aircraft spent in the runway polygon. Using numerous ROT measurements, Kolos-Lakatos [9] studied the dependency of ROT with the aircraft size, the type of runway exit used and IMC/VMC weather conditions. It was found that ROT generally increases with the size of the aircraft although small aircraft sometime had a similar ROT to large aircraft due to the optimization of exits for larger aircraft. Runways equipped with high-speed exits (30°) were also observed to have a lower Runway Occupancy Time. Finally, no significant difference was observed regarding the ROT of aircraft landing in IMC conditions and VMC conditions.

The studies conducted so far to analyze Runway Occupancy Time highlighted the influence of specific factors on Runway Occupancy Time. They were however limited to a few airports in the US and based on a limited set of Runway Occupancy Time measurements. They also

focused on specific factors that could influence Runway Occupancy Time and were sometimes contradictory. An opportunity exists today to use the large amount of flight track data available around airports in the US to conduct a system level analysis of the factors driving Runway Occupancy Time. Collected data regarding landing aircraft would need to encompass all potential factors that could influence Runway Occupancy Time to get a full picture of ROT precursors and assess their relative importance.

2.2 Modelling Runway Occupancy Time

Based on the understanding of factors driving ROT, built over time, multiple models have been developed in the past to optimize the exit system of runways to reduce ROT.

Horonjeff et al. [10] were the first to develop a probabilistic method to optimally locate runway exits in 1959. The braking distance and time needed by an aircraft type to reach a specific ground speed were modelled by a joint probability distribution. Using this joint probability distribution, the model solved an optimization problem to find the exit locations providing the lowest go-around probability given the observed fleet-mix and separations on final approach at the airport. Daellenbach [11] improved this model in 1974 using dynamic programming to solve the optimization problem.

In 1990, Ruhl [12] proposed a new method to design optimally located runway exits by modelling the deceleration of aircraft on the runway. These models broke-down the landing phase in multiple sub-phases of deceleration described by a finite number of parameters. The distributions of these parameters were obtained using 180 video records of aircraft landing at 4 airports in the US. The impact of multiple landing factors on these parameters was assessed using statistical analysis. For each landing aircraft, the model computed the speed of the aircraft at each runway exit and compared it to the exit acceptance velocity. The first exit with an exit acceptance velocity higher than the speed of the aircraft was assumed to be used by the aircraft to vacate the runway. The model then assumed that the aircraft would have adjusted its deceleration to reach the exit at the acceptance velocity and predicted a Runway Occupancy Time value. In the end, the model would predict the Runway Occupancy Time and exit use of a landing aircraft given its aircraft type, airline, final approach speed and multiple environmental conditions. By using a Monte-Carlo simulation, optimal exit locations could then be investigated for a specific airport.

In 1993, Hobeika et al. [13] used a similar approach to create the Runway Exit Design Interactive Model (REDIM). This tool modeled the deceleration of a landing aircraft on the runway for 4 different categories of aircraft. The landing phase was broken-down in five different deceleration sub-phases described by a set of kinematic equations and parameters. These different parameters were calibrated using both simulation and collected ROT data at US airports. The braking phase and flare phase were represented as random events to stochastically model deceleration. Using this decomposition of deceleration, the model could predict the mean and variance of the landing distance and ROT required by an aircraft to reach a specific

exit speed. Using these predicted values, constraints regarding exit location could be derived for each aircraft type. These constraints were used to design an optimization problem solved using dynamic programming to find a set of exits minimizing the average ROT for an observed fleet-mix.

This model was improved successively over the years and used by the FAA to modify the runway exit system of major US airports. Changes included the addition of new parameters in the modelling of Runway occupancy Time such as the weight of the landing aircraft and more flexibility in the recommendation of optimal exit locations. Both of these changes were implemented in the second version of the model by Trani et al. [14]. In 1995, Gu, Trani, and Zhong [15] modified the model to account for the impact of gate location on the choice of the exit used to vacate the runway. This was done by either adapting the assumed deceleration rates or assigning exits minimizing Runway Occupancy Time plus the weighted taxi-time to gate to the landing aircraft. A third version of the model is planned and will use ASDE-X data to better estimate kinematic parameters and will propose aircraft-specific modelling.

In 2007, Barbas, Vázquez, and López [16] proposed an alternative approach to model Runway Occupancy Time and assess changes to runway exit systems. Their approach consisted in using a two-step predictive model combined with a Monte-Carlo simulation to get an estimate of the average ROT of a runway. Predictions of exit use and Runway Occupancy Time were made for thousands of landing aircraft to obtain this average estimate. For each landing aircraft, the probabilities of use of the different available exits were first predicted using a logistic regression. Then, an exit was assigned to the aircraft, sampled at random from the predicted distribution of exit use. Given this exit, the ROT of the aircraft was predicted by modelling the speed profile of the aircraft on the runway using a non-linear speed function. The exit system of a runway could then be optimized by assessing the impact of potential modifications on the predicted average ROT. The different models were calibrated using 1550 ROT measurement collected at Madrid Barajas airport (LEMD) using visual observations.

Since 1959, multiple predictive methods have been designed to optimize runway exit systems and reduce Runway Occupancy Time. They mostly consisted in modelling Runway Occupancy Time and exit usage. Their performance and complexity have increased over time, accounting for more and more factors impacting Runway Occupancy Time. These methods were based on the modelling of the deceleration of aircraft on the runway and were calibrated using small sets of landing observations. The advent in recent years of advanced supervised machine-learning algorithms, able to model non-linear phenomenon, gives the opportunity to develop new predictive methods of Runway Occupancy Time. These methods would not require making assumptions on the braking physics of landing aircraft while still providing a high predictive performance. The large amount of operational data available today could be used to develop such models. These models could be leveraged to optimize runway exit systems at capacity-constrained airports.

Chapter 3

Runway Occupancy Time Data Collection using Landing Data

To analyze the roots of Runway Occupancy Time and propose data-driven solutions to reduce ROT at airports, a significant amount of Runway Occupancy Time measurements around major US airports were first collected. These measurements were extracted based on landing flight tracks at 36 US airports. Landing parameters and deceleration information associated to each ROT measurement were gathered as well to understand the influence of several factors on ROT. This section presents the methodology used to collect a significant amount of Runway Occupancy Time measurements around major US airports and the associated landing parameters and deceleration information.

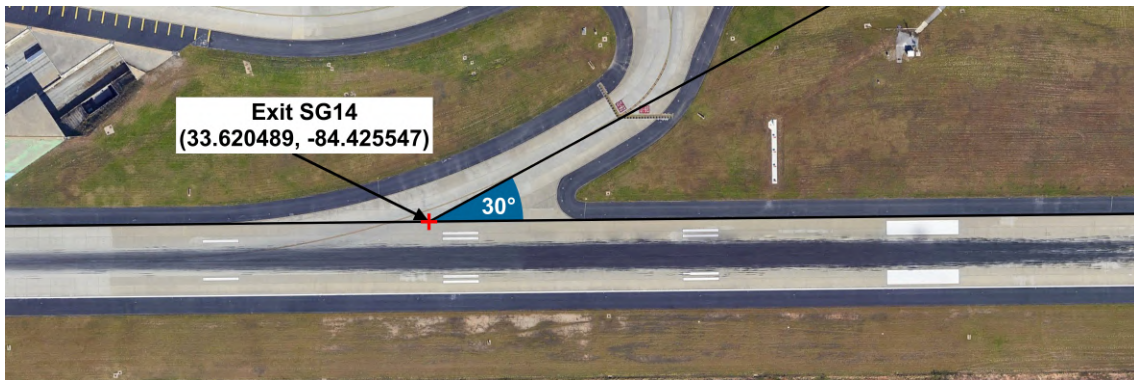
3.1 Runway Occupancy Time Measurements

To gather Runway Occupancy Time measurements, Airport Surface Detection Equipment - model X (ASDE-X) data was collected from 36 major US airports listed in Table 3.1 between March 2015 and April 2016. Additional ASDE-X data regarding A320/A321 NEO and B737 MAX 8/9 aircraft observed in 2018 at the same airports was gathered as well and used solely to develop the predictive models of ROT, described in Section 6. The Airport Surface Detection Equipment - model X is a detection system, implemented progressively since 2003 around major US airports, and fusing data from multiple sources such as ADS-B receivers, surface surveillance radar, airport surveillance radars, terminal automation system and multilateration sensors [17]. The system is used by tower controllers to visualize airport operations and aircraft movements in real-time. The collected data includes raw flight tracks of departing and arriving aircraft detected within a 10NM radius around each airport. Each flight track is composed of position parameters (latitude, longitude and sea-level altitude) and kinematic parameters (ground speed) sampled at a rate of one second and also includes general aircraft identification parameters such as the aircraft type, the airline and the callsign of the aircraft.

Table 3.1: List of the 36 airports with available ASDE-X data

KATL	KBDL	KBOS	KBWI	KCLT	KDCA	KDEN	KDFW	KDTW
KEWR	KFLL	KHOU	KIAD	KIAH	KJFK	KLAS	KLAX	KLGA
KMCO	KMDW	KMEM	KMIA	KMKE	KMSP	KORD	KPHL	KPHX
KPVD	KSAN	KSDF	KSEA	KSFO	KSLC	KSNA	KSTL	PHNL

Additional data was collected regarding runway characteristics at the 36 airports using the 28-Day NASR Subscription Aeronautical Data from the FAA, effective October 12, 2017 [18]. This source of data gives up-to-date runway information such as displaced runway threshold coordinates, runway width, length or pavement description. Information regarding runway exits, existing in 2015, was also gathered manually based on airport diagrams and geospatial data extracted from Google Earth. For each runway of the 36 airports, the coordinates and angle of each runway exit were measured as per Figure 3-1. Information regarding a total of 4442 exits corresponding to 284 runways was obtained. Finally, the length from nose to tail of 504 common aircraft types observed in the National Airspace System (NAS) was collected using data from the FAA aircraft characteristics database [19], aircraft manufacturer websites [20].

**Figure 3-1:** Example of runway exit measurements (KATL, exit SG14)

To extract ROT measurements from the different ASDE-X flight tracks, some data-processing was required. This data processing, presented in the following part is generic and was applied to flight tracks obtained using various data sources such as ASDE-X or ADS-B.

First, the different flight tracks needed to be distinguished from each other. Based on the track identification numbers, a first set of separate flight tracks was identified. These flight tracks were then sub-divided to create a new set of refined flight tracks by identifying successive data-points separated by more than ten minutes. This enables the separation of successive flights for aircraft with the same track identification number.

Second, flight tracks corresponding to landing flights were separated from the rest of the tracks

using a set of logical rules. A flight track corresponded to a landing flight when the initial broadcasted ground speed was higher than 80kt and when the aircraft was flying below a 100ft AGL (Above Ground Level) at some point during its flight. These two thresholds were chosen based on repeated trials to identify most of the landing aircraft using flight tracks visualisation. An example of the landing flight tracks identified at San Francisco airport (KSFO) on 04-01-2015 using this separation process is depicted in Figure 3-2.

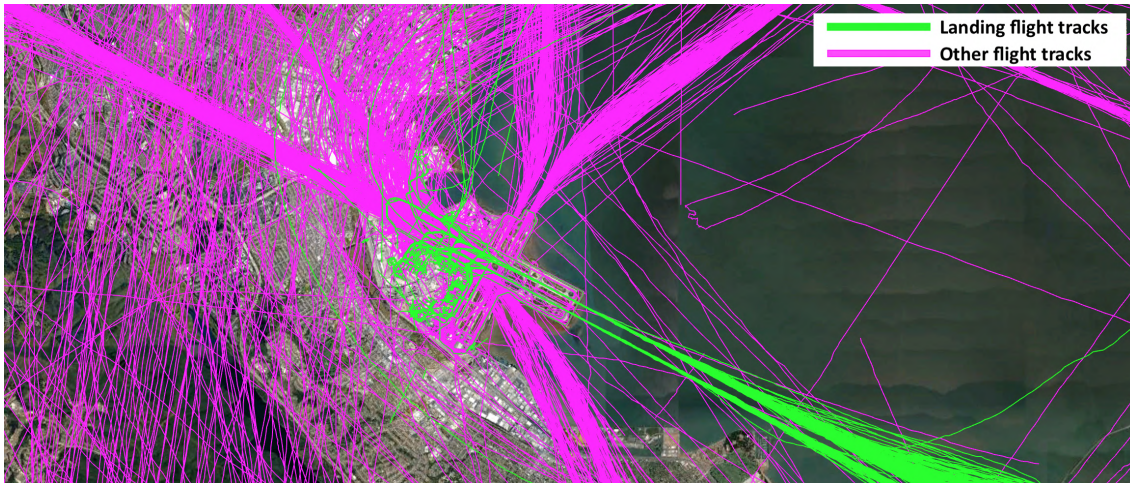


Figure 3-2: Example of the identification of landing flights at San Francisco airport (KSFO on 04-01-2015)

Third, the runway used for landing was identified for each flight track corresponding to a landing flight. During the first 10 seconds when the aircraft flew below 50ft AGL, its distance to each of the displaced runway thresholds of the airport was computed. The runway used for landing corresponded to the threshold associated to the minimum computed distance, as each aircraft is flying straight above it during landing.

Fourth, based on the Eurocontrol definition of ROT [1], two timestamps needed to be computed to measure ROT. These timestamps correspond to the time when the aircraft flew above the runway threshold t_0 and the time when its tail vacated the runway t_{end} . While the first timestamp t_0 was simply identified based on the closest point of the flight track to the displaced runway threshold, the process used to identify the second timestamp t_{end} is more complex. It was assumed that the aircraft position coordinates, recorded by the detection system (ASDE-X or ADS-B), corresponded to the GPS antennas of the aircraft, usually located around the center of modern jet aircraft. Based on this hypothesis, the tail of the aircraft is assumed to be clear of the runway when the distance between the center of the aircraft and the runway boundary is more than half the length of the aircraft projected on a perpendicular axis to the runway. This projected tail length can be computed using Equation 3.1 and is depicted in Figure 3-3.

$$D = \sin(\alpha) * \frac{L}{2} \quad (3.1)$$

with α the angle of the runway exit and L the total length of the aircraft

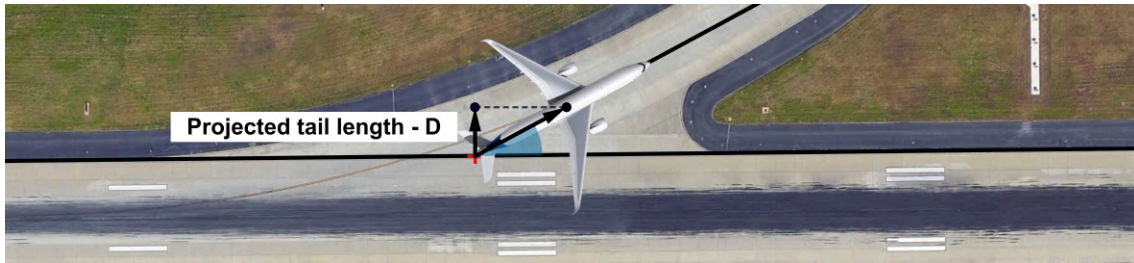


Figure 3-3: Example of projected tail length of aircraft using exit SG14 (KATL)

This criteria was used to identify t_{end} . The exit used to vacate the runway was first identified to get access to the angle of the exit. The distance between the center of the aircraft and the runway centerline was computed successively for all the points following t_0 . When this distance was more than half the runway width, the distance between the aircraft and each of the exits of the runway was computed and the closest runway exit was assumed to be used by the aircraft to vacate the runway. Figure 3-4 shows the runway threshold and runway exit identified for a given landing flight at Boston Logan International airport (KBOS).



Figure 3-4: Example of the runway threshold and runway exit identified for a landing flight at Boston Logan International airport (KBOS)

Second, the projected tail length of the aircraft was computed by projecting half of the length of the aircraft to an axis perpendicular to the runway using the exit angle. The distance between the center of the aircraft and the runway centerline was compared to the projected tail-length for all the points following t_0 . When this distance was higher than the projected tail-length plus half the runway width, the tail of the aircraft was assumed to be cleared of the runway boundary and t_{end} was identified. The Runway Occupancy Time was then measured by computing the difference between t_{end} and t_0 .

Finally, values of ROT less than 20 seconds were dismissed. These values usually corresponded to poor quality flight track data with unreliable values of position, speed or altitude. In total, 3,446,460 Runway Occupancy Time measurements with a 1 second precision were extracted from ASDE-X flight tracks at the 36 airports. The overall process used to extract ROT measurements from flight tracks is summed-up in Figure 3-5.

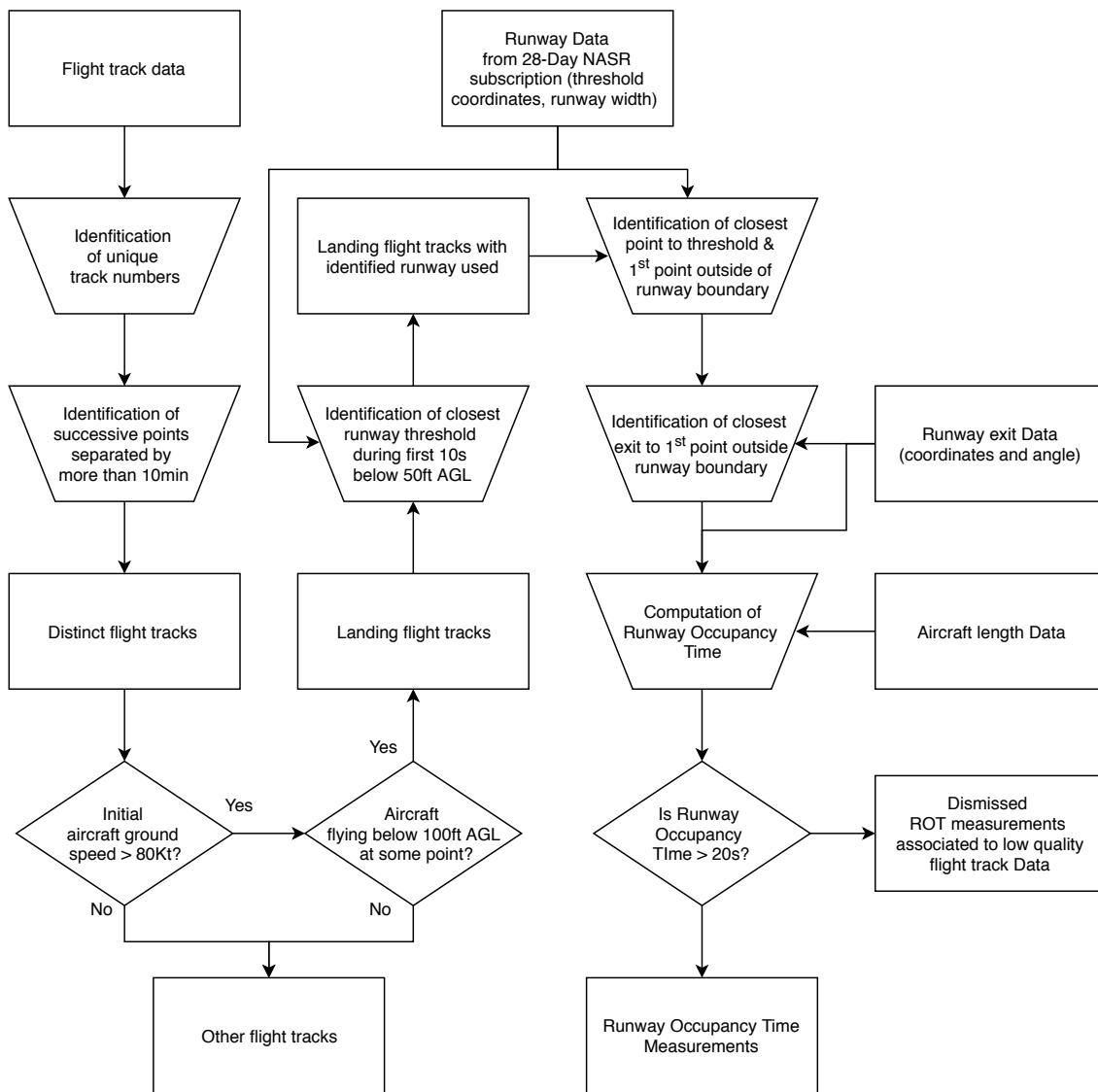


Figure 3-5: Runway Occupancy Time extraction process

3.2 Determining Deceleration Information and Landing Parameters

For each landing flight, additional data characterizing the landing was collected. First, the aircraft type (i.e. ICAO aircraft code), airline and final approach ground speed of the aircraft were gathered. The final approach ground speed of the aircraft corresponds to the aircraft ground speed above the runway threshold (t_0). Data was also gathered regarding the runway exit used to vacate the runway and more specifically its distance from the runway threshold and its angle. It was suspected that the presence of another aircraft following on final approach might have an influence over ROT. For each landing flight, information about the number of following aircraft detected on approach was collected. The type of the first following aircraft and its distance from the landing aircraft when crossing the runway threshold were also extracted. An example of a leading and trailing aircraft on final approach at Atlanta Hartsfield airport (KATL) and the computed distance between them is depicted in Figure 3-6.



Figure 3-6: Example of leading and following aircraft at Atlanta Hartsfield airport (KATL)

The observed weather during landing could have an impact on Runway Occupancy Time. Weather parameters (temperature, wind, visibility, day/night indicator, pressure altitude, type and amount of precipitation) were collected at 5-minute time intervals at each airport using ASOS (Automated Surface Observing System) data archives and temporarily linked with the identified landing observations at t_0 . More than 900 ASOS weather stations have been installed in the US since 1991 and are managed by the National Weather Service (NWS), the Federal Aviation Administration (FAA) and the Department of Defense [21]. They are mostly used to assess surface weather for aviation purposes around airports. Data is recorded every 1 or 5 minutes depending on the gathered weather information and is available online [22]. General flight conditions (VMC/IMC) were derived from the visibility and ceiling data provided by ASOS data archives and also obtained from the FAA Aviation System Performance Metrics (ASPM) data service.

Information was also gathered regarding the braking performance of each aircraft. The ground speed of each landing aircraft was collected from the runway threshold crossing (t_0) to the moment the aircraft vacated the runway (t_{end}). The ground speed profiles, corresponding to the aircraft braking on the runway, were post-processed to guarantee data-quality. First, the

speed data points of each profile were re-sampled to be regularly spaced in time (i.e. every second). Duplicates were removed and the speed profiles were smoothed using a moving average filter with a 5s span. Deceleration profiles were then derived by differentiating the smoothed speed profiles. An example of the speed and deceleration profiles obtained using this process is depicted in Figure 3-7. The collected speed and deceleration profiles were used later to understand the impact of certain parameters on the braking performance of aircraft and therefore on Runway Occupancy Time.

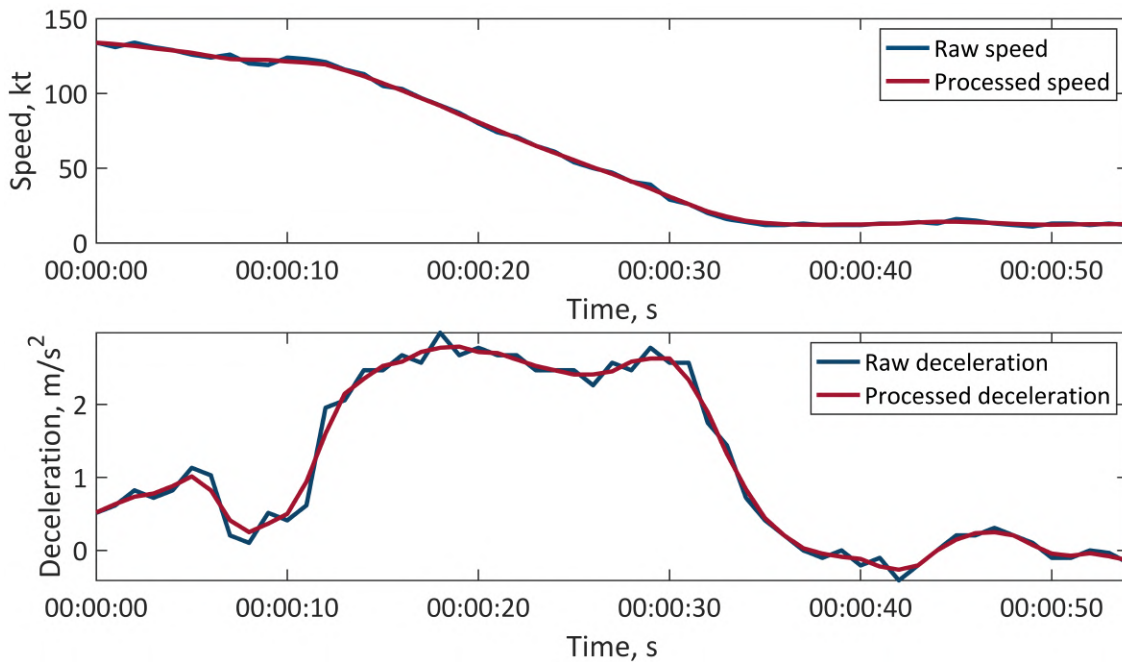


Figure 3-7: Example of speed and deceleration profiles of an A320 landing at Charlotte Douglas International airport (KCLT)

Finally, data was collected regarding the location of the gates reached by aircraft after landing. The last recorded ASDE-X coordinates for each landing aircraft were used as a surrogate for gate location. For approximately 99% of the landing flights, these coordinates corresponded to the gate location. In nearly 1% of the cases, however, they did not seem to correspond to a gate location and the ASDE-X system stopped too early recording data. This might be due to the pilot switching-off the transponder of the aircraft after landing. An example of the last coordinates of each landing flight track recorded at Honolulu airport (PHNL) is depicted in Figure 3-8. These coordinates were used to compute the distance between the runway exit used by each aircraft to vacate the runway and its terminal gate. They were also used to assess whether the runway exit was on the same side as the final gate location relative to the runway axis. This data, regarding the gate location, was used solely for the the development of the predictive models of ROT detailed in Chapter 6.



Figure 3-8: Example of recorded gate locations at Honolulu International airport (PHNL)

In the end, the database was composed of 3,446,460 aircraft landing observations at 36 airports, described by 23 discrete parameters and by their associated speed and deceleration profiles on the runway. These parameters, listed in Table 3.2, are meant to encompass the main factors that could drive Runway Occupancy Time under normal braking conditions.

Table 3.2: Collected landing data, airport data and weather data

Landing Data	Airport Data	Weather Data
<ul style="list-style-type: none"> • Runway Occupancy Time • Aircraft type • Airline • Approach speed • Number of following aircraft • Following aircraft type • Distance of the following aircraft • Speed profile on the runway • Deceleration profile on the runway 	<ul style="list-style-type: none"> • Airport • Runway used • Location of the runway exit used • Angle of the runway exit used • Distance between the runway exit used and the gate location • Relative position of the runway exit used with the runway axis and the gate location 	<ul style="list-style-type: none"> • Day/night indicator • Temperature • Headwind • Crosswind • VMC/IMC conditions (based on airport operating mode) • VMC/IMC conditions 2 (based on measured visibility and ceiling) • Type of precipitation • Amount of precipitation • Pressure altitude • Visibility

Chapter 4

Identifying Factors Driving Runway Occupancy Time

The landing data, described in Chapter 3 was used to identify factors driving Runway Occupancy Time¹. The following section first analyzes the variability of ROT observed in the landing data before presenting the method used to identify the factors driving ROT and its results.

4.1 Analyzing the Variability of Runway Occupancy Time

According to Figure 4-1, depicting the cumulative distribution of ROT measured at the 36 US airports, a large variability in Runway Occupancy Time measurements was observed in the landing data. While aircraft spend on average 49s on the runway, 95% of ROT values are encompassed between 34s and 74s. The observed ROT variability at the system level is due to various ROT performances among airports and a significant ROT variability within each airport.

Figure 4-2, depicting the cumulative distribution of ROT for each of the 36 airports, shows that airports such as Ronald Reagan Washington National Airport (KDCA) have a relatively low ROT (40s median ROT) while other airports such as Honolulu International Airport (PHNL) perform poorly in terms of ROT (57s median ROT). According to this figure, variability in Runway Occupancy Time is also observed within each airport. At Dallas Fort-Worth International airport (KDFW), for instance, Runway Occupancy Time ranges from 36s to 73s (95% of the values). The variability in Runway Occupancy Time, observed at several scales, is driven by multiple factors that collectively impact the braking deceleration of aircraft.

¹To analyze ROT, a very-conservative filtering of extreme ROT values was done by identifying landing observations in the database with an ROT more than 3 scaled Median-Absolute-Deviations (MAD) away from the median ROT per aircraft type and runway. This method is detailed in [23]. These extreme values representing less than 3% of the data correspond to abnormal braking behavior on the runway

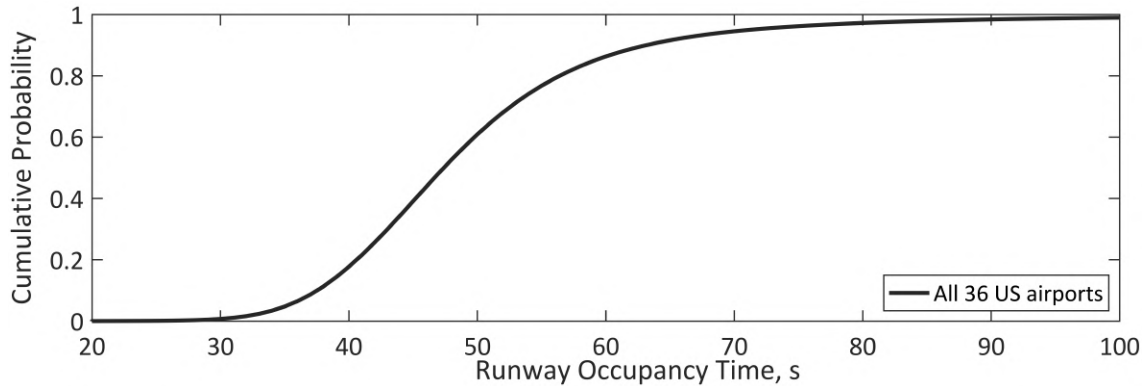


Figure 4-1: Cumulative distribution of ROT at the system level (36 US airports)

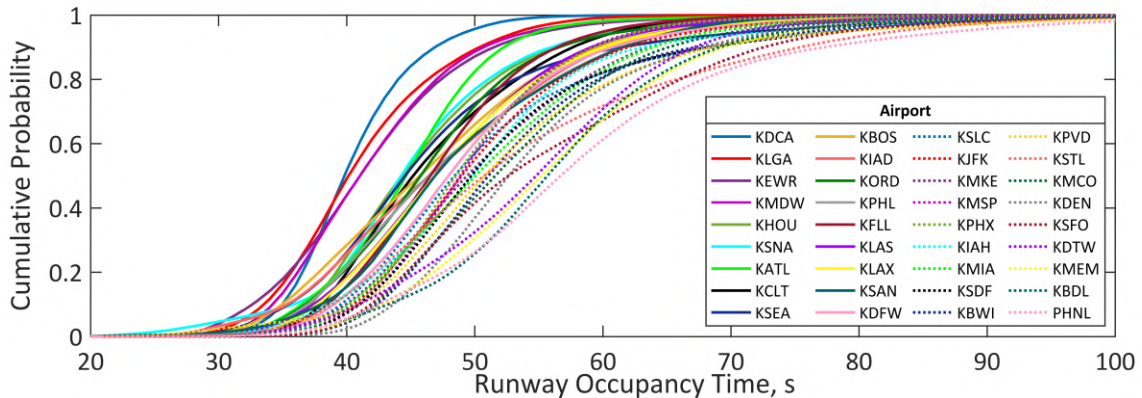


Figure 4-2: Cumulative distributions of ROT for the 36 US Airports

4.2 Identifying Factors Driving ROT using a Random Forest Algorithm

To identify the factors driving Runway Occupancy Time, a random-forest regression algorithm was trained to predict Runway Occupancy Time using the landing database. A random-forest is made of an ensemble of decision trees, trained to fulfill a regression or classification task. It usually provides a high predictive power while being relatively resilient to over-fitting and easy to tune. This supervised learning algorithm, if trained on a regression task, can provide a ranking of the importance of each input factor in explaining the variance of the predicted target variable in a dataset. This capability is often leveraged in data-science settings to identify the most important features to include in more complex predictive models (i.e. feature selection). The ranking is based on the relative appearance of the difference factors in the nodes of each decision tree and the ability of each node to reduce variance. By training a random-forest to predict ROT, a ranking of the different factors based on their ability to explain the variance of ROT can be therefore obtained.

4.2.1 Random Forest Models

The random-forest algorithm, first introduced in 1995 [24], is a bootstrap-aggregating (i.e. bagging) ensemble algorithm. Random-forest algorithms are used for both non-linear regression and classification tasks. They rely on building a forest of decision trees to fulfill a prediction task. In a regression setting, the different trees are trained using a dataset made of observed target values and potential predictors. The overall process used to build a random forest model is depicted in Figure 4-3. For each tree, the original dataset is resampled at random with replacement to create a bootstrapped dataset used to train the tree on the prediction task. The different trees are then used together to make collective predictions by averaging predictions. The different trees are weak-learners as they have seen only part of the original dataset. They have however a great prediction capability together and can account for a great proportion of the variance observed in target values.

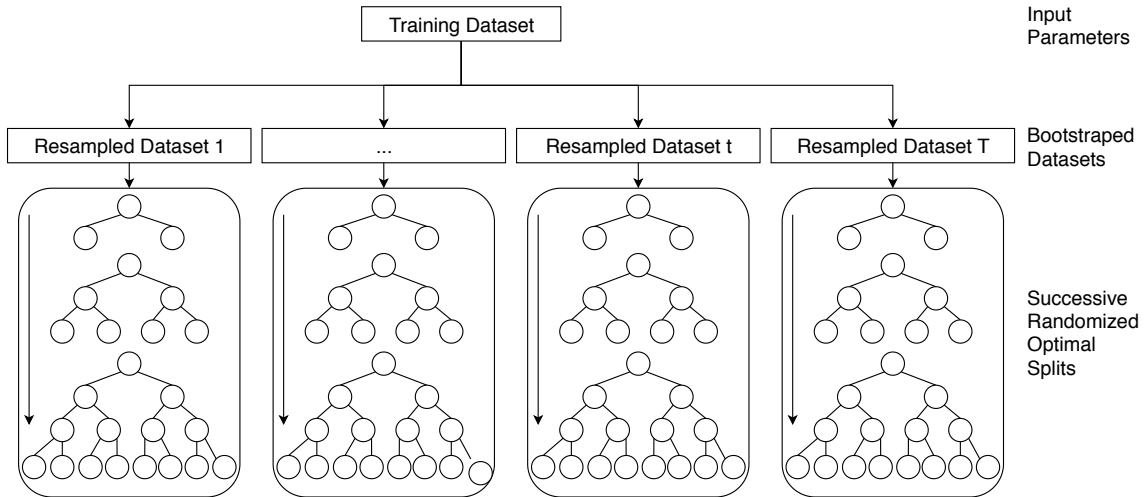


Figure 4-3: Training process of a random-forest algorithm

Each tree in the forest is made of nodes splitting the input data in two, based on the value of a decision factor. This decision factor can be either a categorical variable or a numerical variable. If the variable is categorical, the data is split in two by dividing the variable in two sets of categories. If the variable is numerical, the data is split in two using a splitting value. During the training process, these variables and splitting values or sets of categories are chosen for each node successively based on their ability to decrease the variance of target values for the created sub-datasets. An additional randomness is added in the training process by allowing the algorithm to choose the node variable from a restrained set of variables selected at random. Each tree is thus built progressively by making randomized optimal variable choices and splits.

To optimize the performance of a random-forest model, a set of hyper-parameters need to be tuned. These hyper-parameters encompass the number of trees in the forest and the maximum

depth of each tree. The performance of the model usually scales-up with the number of trees and is capped by computing power while the maximum depth has an impact on the complexity of each tree.

Once a random-forest algorithm has been trained to fulfill a regression task, a ranking of the different factors based on their ability to reduce the variance of the dataset can be computed. By looking at how much each node of each tree contributed to decrease the total variance of the dataset, a percentage of explained variance can be attributed to each factor. First, a decrease of variance can be attributed to each node of a tree based on equation [4.1](#).

$$\Delta Var(i) = Var(i) - p_l \cdot Var(i_l) - p_r \cdot Var(i_r) \quad (4.1)$$

with: $\Delta Var(i)$ the decrease in variance provided by node i
 $Var(i)$ the variance observed in the dataset split at node i
 $Var(i_l)$ the variance observed in the left dataset resulting from the split
 $Var(i_r)$ the variance observed in the right dataset resulting from the split
 p_l the proportion of the population of the left dataset resulting from the split
 p_r the proportion of the population of the right dataset resulting from the split

Second the contribution of each factor to the reduction of variance is computed using equation [4.2](#).

$$C(X) = \frac{1}{N_T} \sum_{t \in T} \sum_{i \in t | s(i)=X} p(i) \cdot \Delta Var(i) \quad (4.2)$$

with: $C(X)$ the contribution of factor X to the reduction of variance
 N_T the number of trees
 T the forest of trees
 t a given tree in the forest
 $\Delta Var(i)$ the decrease in variance provided by a node i in a tree t
 $p(i)$ the proportion of the population reaching node i
 $s(i)$ the factor used to split data at node i

The contribution of each factor can be then scaled and understood as the percentage of explained variance that can be attributed to a specific variable. Further details about random-forest algorithms and the ranking method are presented in [\[25\]](#). The following section explains how such a ranking can be obtained for Runway Occupancy Time.

4.2.2 Training a Random Forest Algorithm to Predict ROT

To obtain a ranking of the factors driving the variance of Runway Occupancy Time, a random-forest algorithm was trained to predict ROT using the landing data. A training set was first sampled from the filtered collected landing data and composed of 450,000 landing observations. These landing observations are described by the various recorded parameters, listed

in Table 3.2 (except parameters regarding the gate location, the airport, the runway used and the speed and deceleration profiles). The parameters describing each landing were used as predictors to train a random-forest model to predict ROT. No significant preprocessing of numerical features was required due to the flexibility of random-forest algorithms regarding standard-scaling. Categorical variables were encoded by mapping categories to integers. This enables the random-forest model to partition categorical variables into subsets of categories in the nodes. Categories with less than 20 observations were also pooled in a common single category (named "other") for each categorical feature for computational efficiency.

The training set was used to tune the hyper-parameters of the random-forest algorithm such as the number of trees and the maximum depth of each tree. These hyper-parameters were chosen in order to minimize the mean squared error (MSE) on the prediction of ROT using a 3-fold cross-validated grid-search. Random-forest models with 50 to 300 trees with a maximum depth ranging from 5 to 25 were tested. The maximum depth of each tree was found to have the most impact on the cross-validated mean-squared error while the number of trees had a minor impact. It was found that a forest made of 300 trees of maximum-depth 25 provided the best performance given the available amount of computing power. A model with these hyper-parameters was trained on the full training set and reached a $24s^2$ mean squared error (MSE) in the prediction of ROT on a testing dataset made of 50,000 other randomly selected landing observations. The open source python H2O package was used to train and build the random-forest algorithm [26]. A non-representative example of a tree built by the random-forest algorithm and truncated to a depth of 5 is depicted in Figure 4-4.

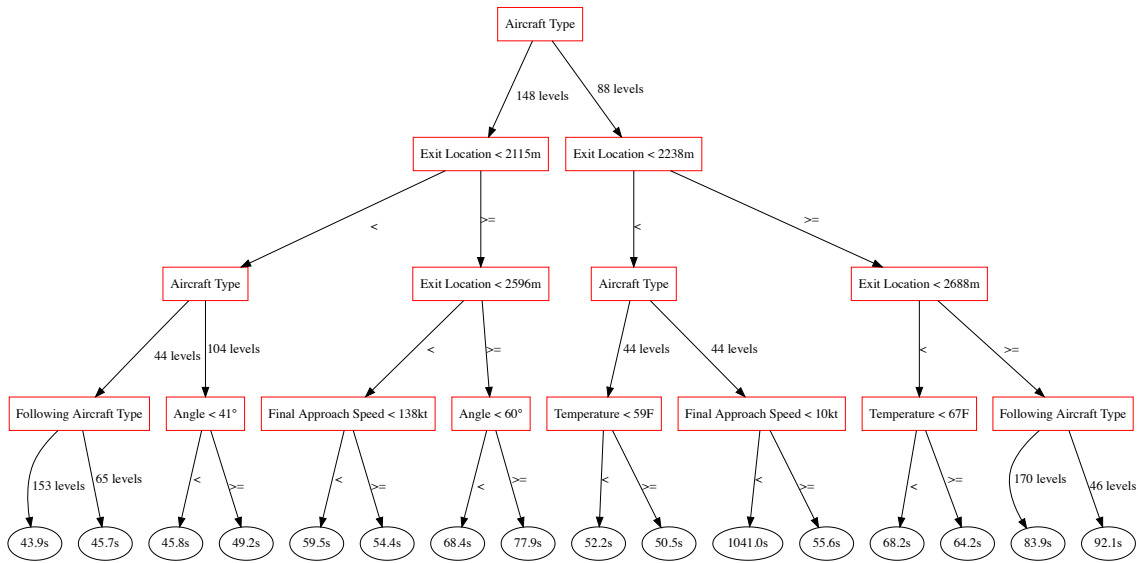


Figure 4-4: Example of a single random forest tree of depth 5

4.3 Ranking the Factors Driving ROT

By looking at how much each node of each tree of the random-forest model contributed to decrease the total variance of the training dataset, a ranking of the importance of each factor in the estimation of ROT was determined. This ranking, presented in Figure 4-5, lists the percentage of explained ROT variance that can be attributed to each factor.

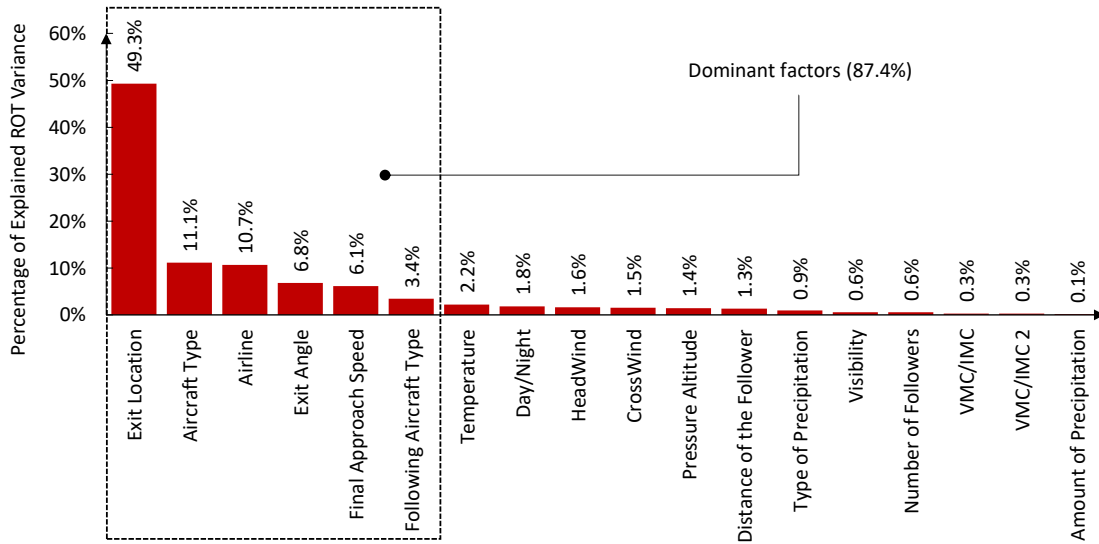


Figure 4-5: Ranking of the importance of ROT factors

In this ranking, the exit used by the landing aircraft to vacate the runway appears to be dominant and accounts for 56.1% of the explained variance of ROT. A runway exit can be characterized by its distance from the runway threshold, also called exit location (accounting for 49.3% of the variance) and by its angle with the runway axis (accounting for 6.8% of the variance). The aircraft type and final approach speed also appear to have a significant impact on ROT (accounting respectively for 11.1% and 6.1% of the variance). More surprisingly, the airline is the third most important ROT factor (accounting for 10.7% of the variance). This contradicts previous studies that did not observe significant differences in ROT between carriers [7]. The presence of one or more following aircraft on final approach also impacts ROT and accounts for 5.3% of the variance. Finally, weather factors appear to have less influence over ROT individually but account together for 10.7% of the ROT variance. It can be noted that some factors are correlated such as the airline and aircraft type. Their collective influence on ROT variance is usually divided evenly among the different factors thanks to the randomness implemented in the tree splits. Factors explaining more variance might get however an increased credit in some cases. In the end, 87.4% of the explained variance can be attributed to only 5 dominant factors. The impact of these dominant factors on Runway Occupancy Time needed to be understood and a detailed analysis of their relative influence is presented in the following section.

Chapter 5

Understanding the Impact of Dominant ROT Factors

The ranking of ROT factors provided by the random forest algorithm identified five dominant factors that account for 87.4% of the variance of Runway Occupancy Time. Indeed, the runway exit (location and angle), the airline, the aircraft type, the approach speed and the type of the following aircraft on approach almost completely explain the variance of ROT. An analysis of the impact of the five mentioned factors on ROT is presented in this section. This analysis was based on the same filtered landing data from 36 airports. The analysis focuses first on the general impact of aircraft type on ROT before analyzing the influence of the four other factors for the specific case of Airbus A320s.

5.1 Analysis of the Impact of Aircraft Type

According to the ranking of ROT factors, presented in Figure 4-5, the aircraft type accounts for 11.1% of the variance of ROT. Figure 5-1 shows the cumulative distributions of ROT for aircraft of each wake category ("Small", "Large", "757", "Heavy" and "Super Heavy"). It appears that the distributions of Runway Occupancy Time differ between legacy wake vortex categories and that aircraft belonging to categories with a higher maximum take-off weight (MTOW) have a higher Runway Occupancy Time on average.

Even within each wake category, specific aircraft models have different ROT distributions. This is illustrated in Figure 5-2 which shows the cumulative distributions of ROT for 6 common aircraft types belonging to the "Large" category. Within the B737 and A320 families, the largest aircraft variants (A321 and B737-900) have a higher Runway Occupancy Time compared to smaller versions. These larger aircraft variants differ not only by their heavier MTOW but also by their higher approach speeds due to tail clearance requirements. A higher MTOW and approach speed increases the momentum of the aircraft which results in higher ROT.

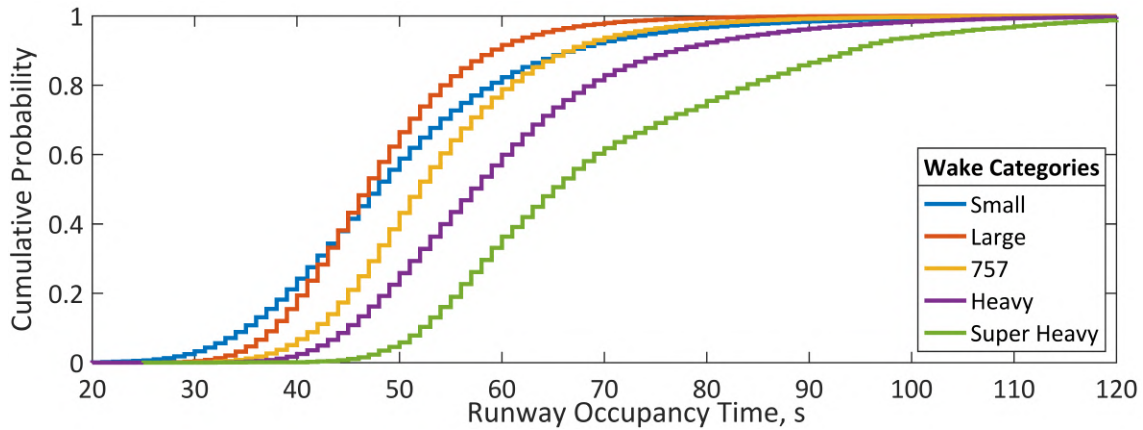


Figure 5-1: Cumulative distributions of ROT per wake category

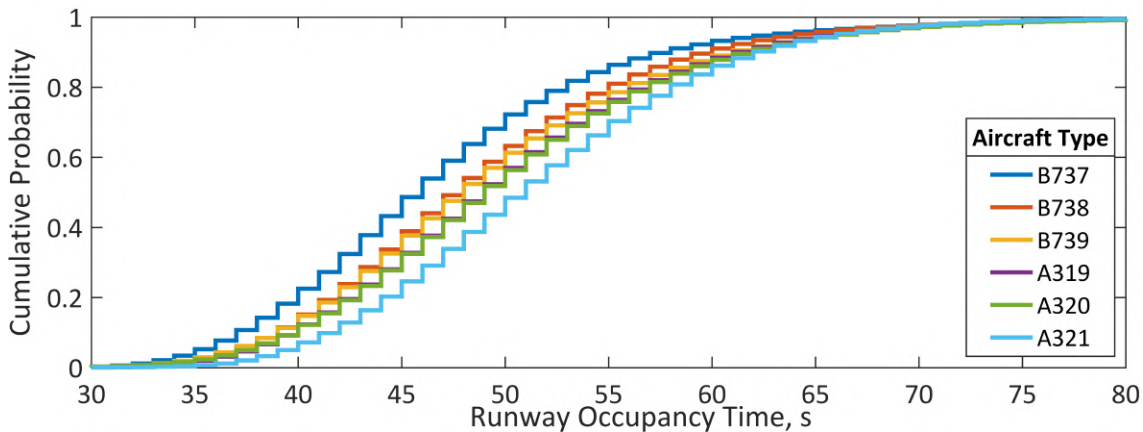


Figure 5-2: Cumulative distributions of ROT for 6 common “Large” aircraft types

Because of the high dependency of ROT with the type of aircraft, the influence of other factors on ROT must be analyzed by looking at specific aircraft types. This study presents a focused analysis on the A320 aircraft type, relatively well represented at each of the 36 studied airports with 255,376 extracted landings.

5.2 Analysis of the Impact of the Runway Exit Used

The runway exit that is used by an aircraft to vacate the runway accounts for 56.1% of the variance of ROT. The population of runway exits at US airports can be described by two parameters: the exit location that corresponds to the distance of the exit from the runway threshold and the angle of the exit with the runway axis that ranges from 0° to 180° . The most popular exit angles are 90° (right-angle exits) and 30° (high-speed exits). An example of the different kinds of exits is illustrated in Figure [5-3](#). The following study focuses on right-

angle (90°) and high-speed (30°) exits that are used in approximately 80% of the cases at the 36 considered airports. Exits displaying other angles were not specifically studied in this analysis.

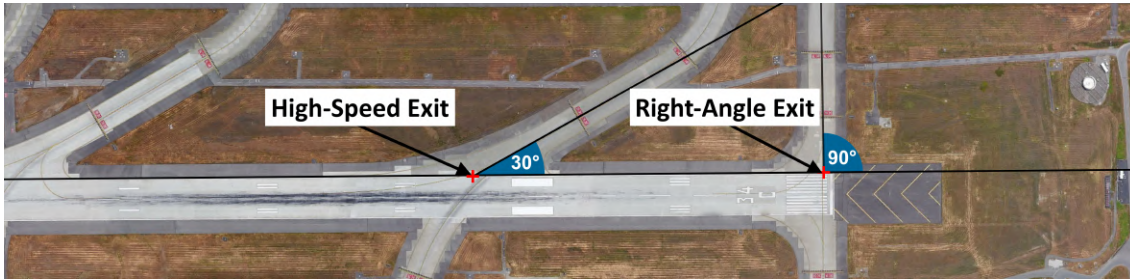


Figure 5-3: Example of the two most popular runway exit angles

5.2.1 Impact of the Runway Exit Location

The runway exit location is by far the most dominant ROT factor and accounts for 49.3% of the ROT variance. When looking at the overall impact of exit location on ROT for both right-angle (90°) and high-speed (30°) exits, Figure 5-4 demonstrates that ROT increases with the distance of the exit from the runway threshold, by approximately 0.019s/m to 0.022s/m for A320 aircraft. These values are consistent with the FAA AC 150/5300-13A which states that ROT increases on average by 0.025s/m [27]. This observation is linked to the fact that aircraft spend more time on the runway if they have to cover more distance before vacating the runway. Depending on its deceleration performance, an aircraft type can reach a broad range of exit locations and the location of the chosen exit for each landing will have a large influence on Runway Occupancy Time.

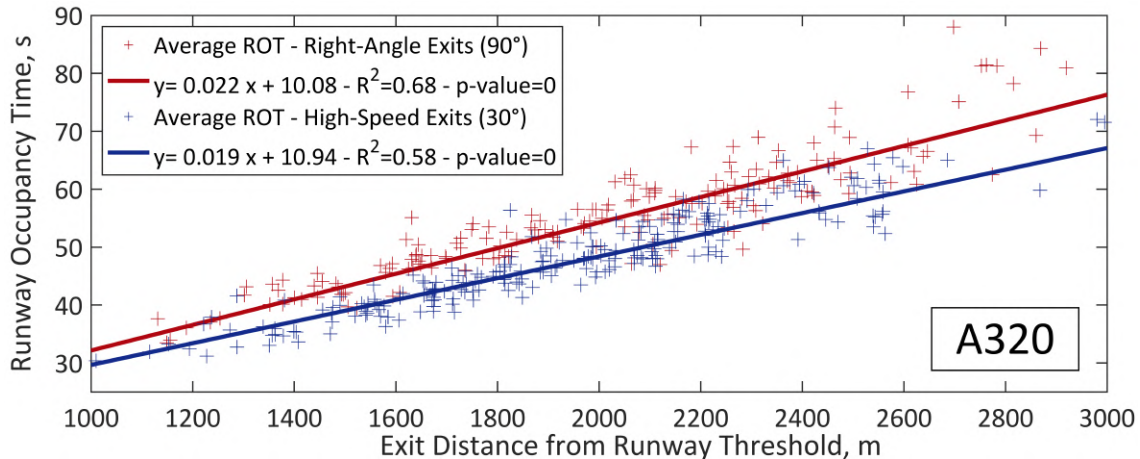


Figure 5-4: Evolution of A320 ROT depending on exit location and exit type

5.2.2 Impact of the Runway Exit Angle

The runway exit angle accounts for 6.8% of the ROT variance. Figure 5-5 exhibits the difference in cumulative distributions of ROT between high-speed (30°) and right-angle (90°) exits for the A320. According to Figure 5-4, high-speed exits (30°) reduce ROT of landing A320 by 4 to 10s on average compared to similarly located right-angle exits. The impact of exit angle on ROT can be explained by the fact that different exit angles enable different deceleration behaviors on the runway. First, different exit angles enable aircraft to vacate the runway at different speeds. High-speed exits (30°) are designed so that aircraft can exit the runway at higher speeds but can only be used in a single runway direction compared to right-angle exits (90°). This is shown in Figure 5-6 by the cumulative distributions of the exit speed of A320 for right-angle (90°) and high-speed (30°) exits.

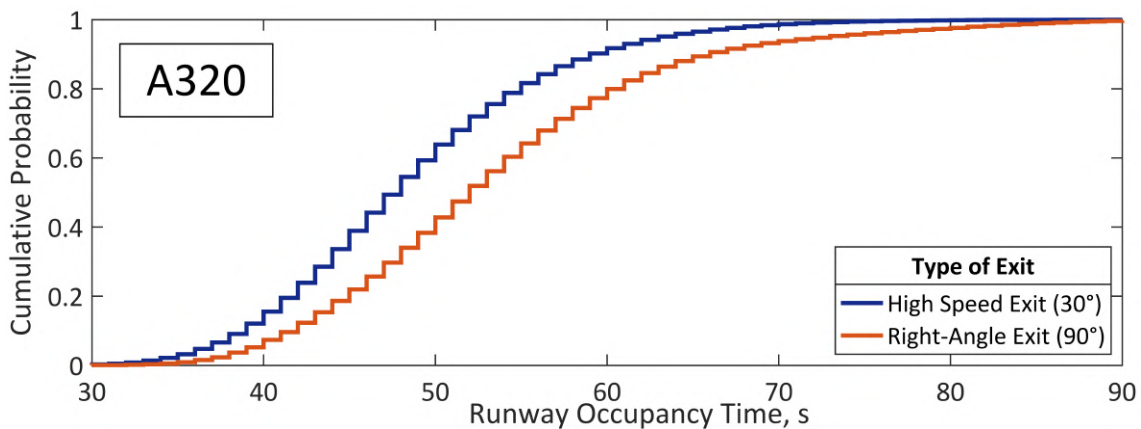


Figure 5-5: Cumulative distributions of A320 ROT depending on the type of exit

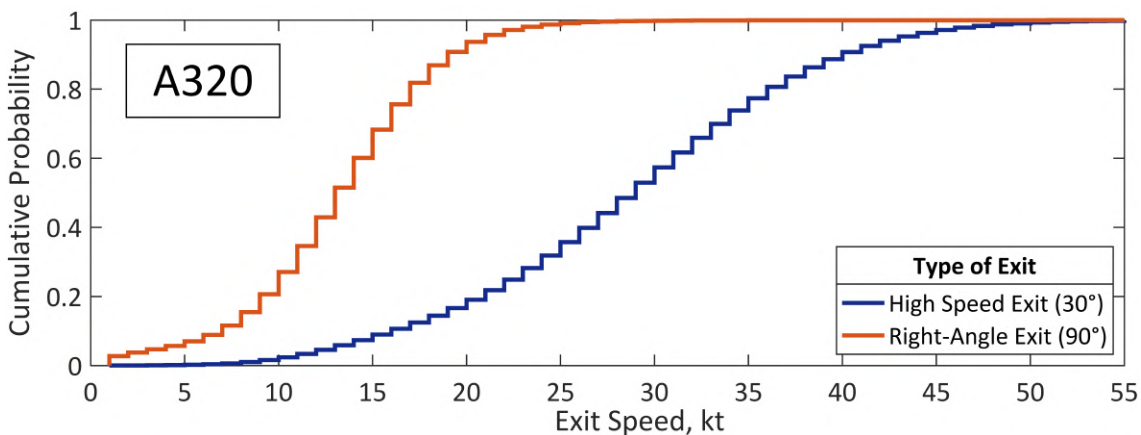


Figure 5-6: Cumulative distributions of A320 exit speed depending on the type of exit

These higher exit speeds, enabled by high-speed exits, are associated to higher average speeds on the runway as well, which results in a lower Runway Occupancy Time. This can be observed by comparing the average speed and deceleration profiles of A320 aircraft exiting at similarly located high-speed (30°) and right-angle (90°) exits. 350 pairs of right-angle (90°) and high-speed (30°) exits, located less than 30m apart and exhibiting similar average approach speed (less than 3kt difference) were identified in our dataset and average A320 speed and deceleration profiles were compared for these pairs. An example of such a pair of exits, made of exit E (runway 34L) at Seattle Tacoma International airport (KSEA) and exit A (runway 19) at Ronald Reagan Washington National airport (KDCA) is depicted in Figure 5-7. Both of these exits are located around 1900m away from the runway threshold and are used by A320 approaching with an average ground speed of 135kt.



Figure 5-7: Example of similarly located high-speed (30°) and right-angle (90°) exits

Figures 5-8 and 5-9 show the comparison of the average speed and deceleration profiles of A320s using these two exits. This case is representative of what was generally observed in the 350 comparisons. Although a large diversity of average deceleration profiles was seen in these comparisons, it was identified in approximately 62% of the cases that the average deceleration profiles were smoother for aircraft using high-speed exits (30°) with lower maximum deceleration rates. This difference in deceleration behaviors results in a higher average speed on the runway and a lower ROT for aircraft using high-speed exits (30°).

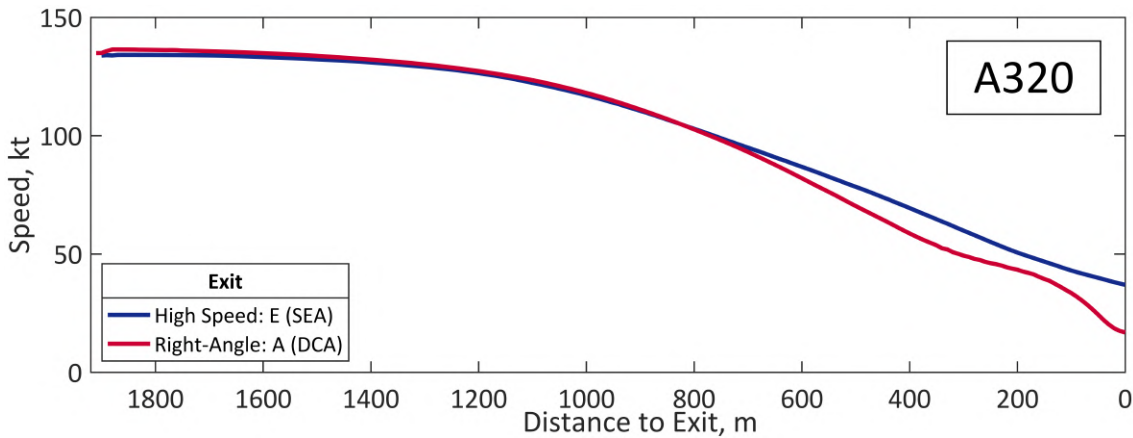


Figure 5-8: Example of comparison of average A320 speed profiles for two similarly located high-speed (30°) and right-angle (90°) exits

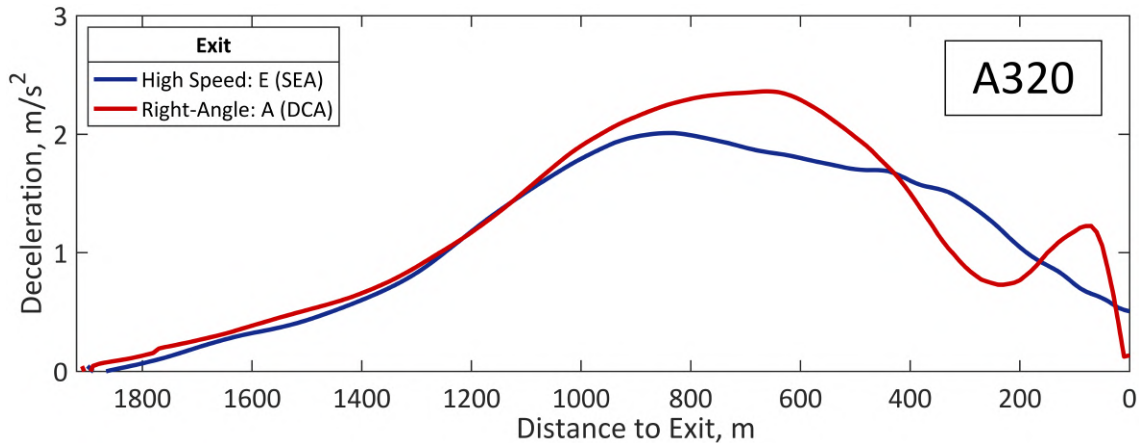


Figure 5-9: Example of comparison of average A320 deceleration profiles for two similarly located high-speed (30°) and right-angle (90°) exits

5.3 Analysis of the Impact of the Airline

The airline accounts for 10.7% of the Runway Occupancy Time variance. The large influence of this factor wasn't identified in previous studies [7] but is thought to be due to multiple facts. First, different airlines have different aircraft fleets and the airline factor is not statistically independent from the aircraft type factor. Second, pilots working for different airlines, received different pilot training and follow different operational procedures such as the use of different auto-brake settings. Their landing behaviors might consequently differ. The ROT distributions of 7 airlines extensively using A320 aircraft in the US are depicted in Figure 5-10 and exhibit noticeable differences at the system level.

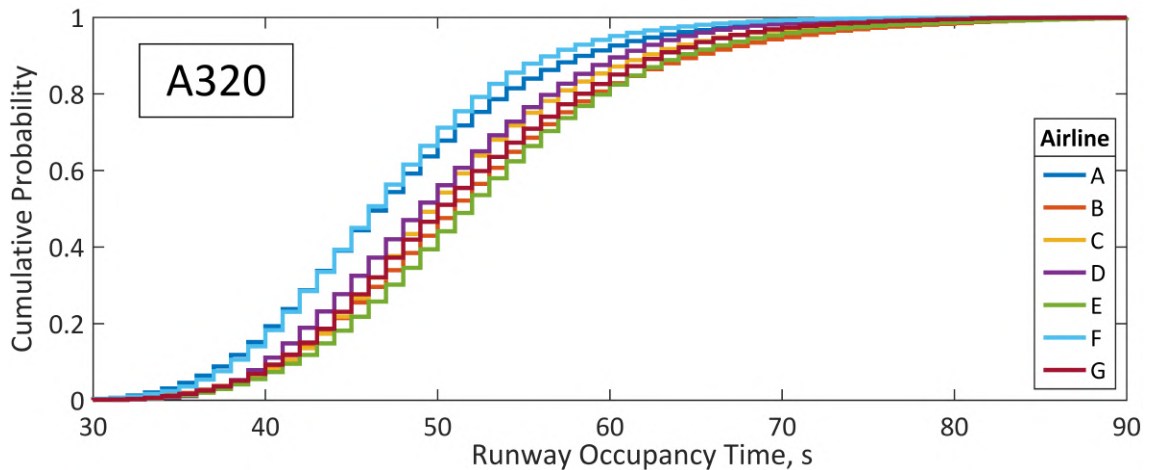


Figure 5-10: Cumulative distribution of A320 ROT depending on airline

At the airport level, pilots might be also incentivized to adapt their deceleration in order to vacate the runway at an exit minimizing the taxi-time to gate. The fact that different airlines usually have gates located in different terminals might trigger this impact. A comparison of the average ROT for A320 aircraft operated by these 7 carriers at 8 different airports where they all operate is depicted in Table 5.1 and demonstrates that the airline has an impact on Runway Occupancy Time at the airport level. This table also highlights the variability of ROT between different airports. These differences can be partly attributed to local airport characteristics. The very high average ROT observed for Denver International airport (KDEN) can be explained by the high elevation of the airport, leading aircraft to approach at higher speeds due to lower air density.

Table 5.1: Average A320 ROT for 7 airlines and 8 airports

Airport/Airline	DEN	FLL	LAS	LAX	LGA	MCO	ORD	SAN	36 Airports
A	58s	48s	48s	49s	46s	51s	47s	53s	48s
B	56s	48s	51s	47s	44s	54s	49s	50s	52s
C	54s	46s	50s	52s	43s	54s	48s	48s	51s
D	56s	46s	48s	49s	42s	50s	47s	52s	50s
E	56s	50s	51s	50s	44s	55s	49s	54s	53s
F	56s	50s	51s	48s	46s	56s	47s	55s	47s
G	53s	47s	48s	46s	41s	51s	47s	52s	51s
All Airlines	56s	47s	50s	48s	44s	52s	48s	53s	50s

5.4 Analysis of the Impact of the Final Approach Speed

The final approach speed of the landing aircraft accounts for 6.1% of the variance of ROT. Among the A320 observations, an important variability in the ground speed above the runway threshold is observed (99% between 115kt and 160kt). The correlation between final approach speed and Runway Occupancy Time is globally positive as shown in Figure 5-11 and each additional knot of approach speed results in 0.072s of additional ROT.

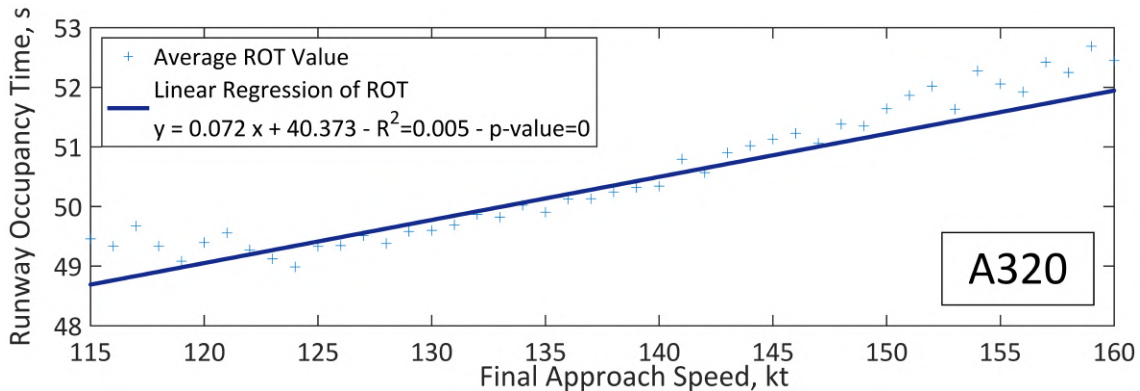


Figure 5-11: Observed A320 ROT depending on approach speed

A higher approach speed indeed forces the aircraft to exit further down on the runway due to its additional momentum and consequently increases its ROT. If aircraft having different final approach speeds are however able to vacate at the same exit location, the impact of final approach speed on ROT is reversed. An additional knot of final approach speed results in ROT being reduced by 0.13s to 0.49s for A320 for 90% of the exits with more than 100 observed landings (p-values were all measured below 0.05). This can be explained by the fact that aircraft approaching at higher speeds are running down the runway at higher average speeds which reduces their ROT. To observe this, the average deceleration profiles of A320 aircraft approaching at specific final approach speeds and exiting at the same location were compared for all exits located between 1000m and 3000m with more than 1000 landings (78 exits in total). An example of such a comparison is shown in Figure 5-12 and Figure 5-13 for exit K4 (runway 27R) at Philadelphia International airport.

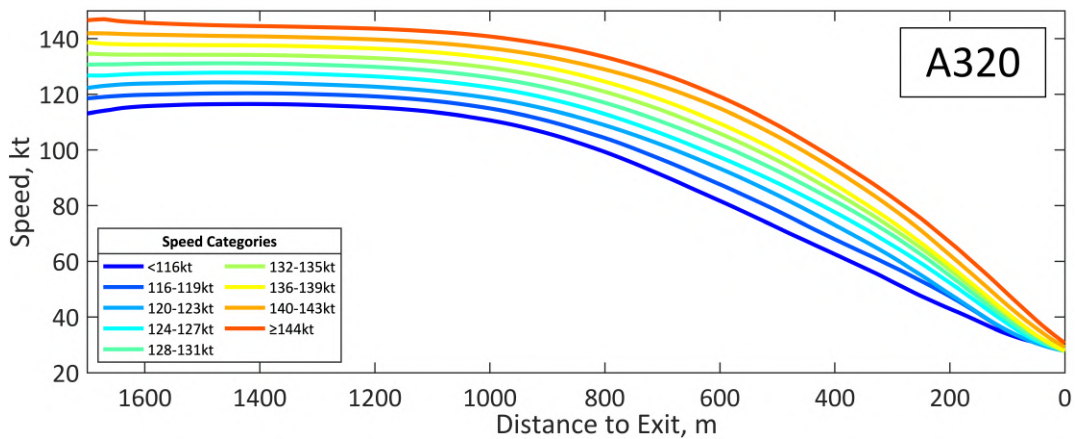


Figure 5-12: Example of comparison of average A320 speed profiles for different final approach speeds (exit K4, KPHL)

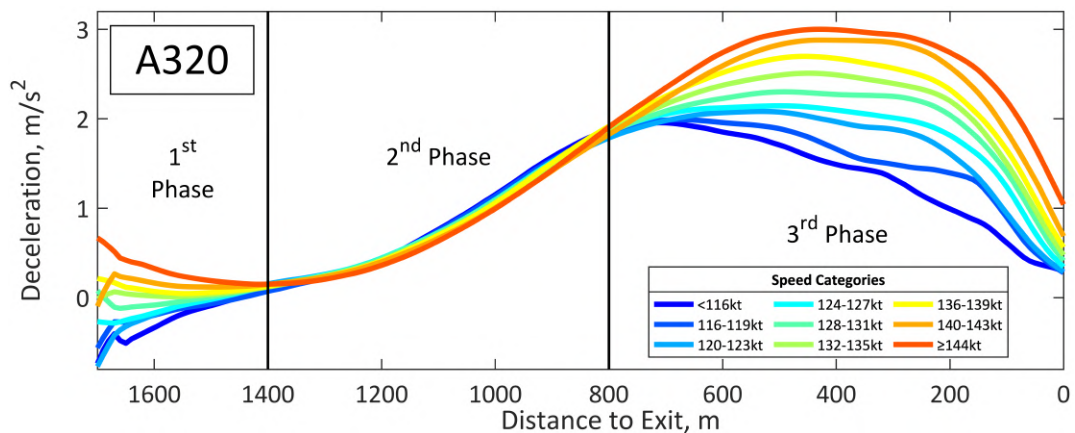


Figure 5-13: Example of comparison of average A320 deceleration profiles for different final approach speeds (exit K4, KPHL)

In these comparisons, it appears that aircraft with high approach speed are slightly decelerating during flare while slow approaching aircraft slightly accelerate. The average deceleration rates are then similar and increasing in a second phase of deceleration. These similar deceleration rates might be related to standardized braking procedures used by A320 pilots. These procedures can include the use of automated deceleration provided by autobrakes. On the A320, 3 autobrakes settings are available to pilots and correspond to three specific target deceleration rates to reach on the runway. The wheel braking actions of the aircraft are adapted automatically, given the amount of reverse thrust and spoilers used by the pilot, to reach the target deceleration rate. Autobrakes are commonly used by pilots to decelerate safely on the runway. In a third phase, however, faster approaching A320 are braking at higher average deceleration rates. Pilot seem to adapt their deceleration to reach a target exit speed and decelerate more if the speed of the aircraft is still relatively high. Autobrakes might be deactivated by pilots by either retracting spoilers, applying pressure on brake pedals or setting the autobrakes switch to off. The average speeds of fast approaching and slow approaching aircraft converge to a similar value only a few meters before the runway exit. Consequently, the Runway Occupancy Time is decreased with a higher final approach speed as the aircraft runs down the runway at a higher speed. This highlights the importance of building exits at optimal locations so that specific aircraft types can maintain a high average speed on the runway.

Two contour plots illustrating the overall impact of final approach speed on ROT and considering the exit location are presented in Figure 5-14 and Figure 5-15 for high-speed exits (30°) and right-angle exits (90°). They were built by first interpolating the observed average ROT values for non-observed values of approach speed and exit location and smoothing them using a moving average filter. The boundaries of the plots were defined using the convex-hull of the observations.

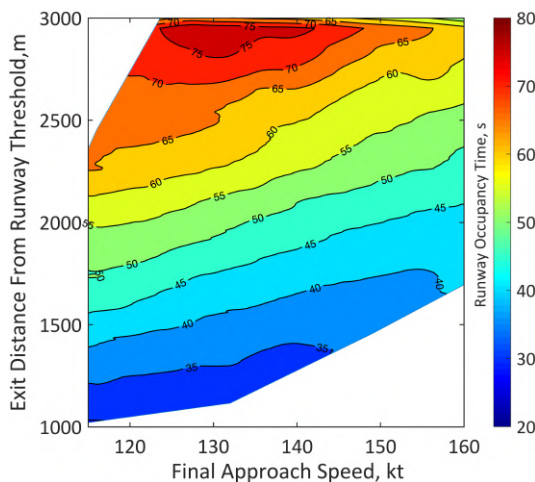


Figure 5-14: Contour plot of ROT depending on final approach speed and exit location for A320 using high-speed exits (30°)

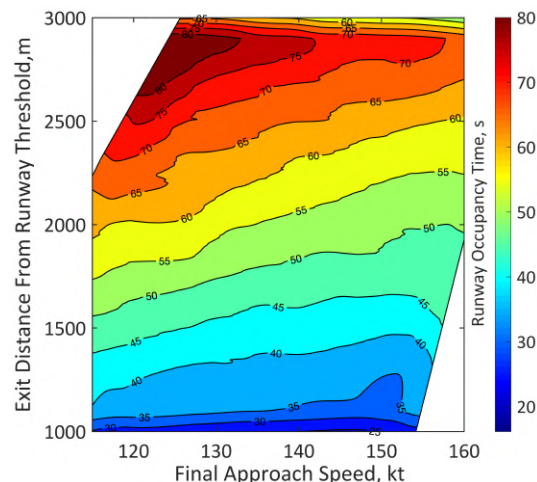


Figure 5-15: Contour plot of ROT depending on final approach speed and exit location for A320 using right-angle exits (90°)

These contour plots depict the combined effect of exit location and final approach speed on Runway Occupancy Time. First, the almost vertical gradient of ROT shows that the exit location has a much prominent impact on ROT compared to approach speed. Second, the boundaries of the contour plots show that a high approach speed forces aircraft to exit further down on the runway while slow approaching aircraft can vacate closer to the runway threshold. Third, for a constant exit location, the Runway Occupancy Time decreases with the approach speed, confirming the reverse effect of approach speed on ROT. Fourth, it can be noted that the impact of approach speed on ROT is increased for exits located very far from the runway threshold with a gradient of ROT becoming more horizontal. The ROT of aircraft vacating the runway far from the runway threshold depends more on the speed of the aircraft on the runway. This speed will be higher on average if the aircraft approaches faster. Finally, these two contour plots also highlight the significant reduction in ROT provided by high-speed exits compared to right-angle exits for a similar exit location and approach speed.

5.5 Analysis of the Impact of a Following Aircraft on Approach

As identified in the ranking of ROT factors, the proximity of another aircraft approaching behind the landing aircraft has an influence over the Runway Occupancy Time of a landing aircraft. The type of the following aircraft accounts for 3.4% of the variance of ROT and its distance from the landing aircraft accounts for 1.3% of the variance of ROT. To understand how the presence of a trailing aircraft impacts ROT, a pressure ratio defined as the number of wake vortex separation minima corresponding to the distance between the leading and trailing aircraft was computed for each A320 followed by another aircraft on approach. This ratio computed using Equation 5.1 gives information about how much traffic density was observed in the approach of a runway when an aircraft was landing. It can be lower than 100% when visual separation is applied between two approaching aircraft. With visual separation, the following aircraft is responsible of its separation with the leading aircraft and can break the separation minima if safety is assured.

$$\text{Pressure Ratio} = \frac{\text{Distance between Leading \& Trailing Aircraft}}{\text{Wake Vortex Separation Minimum}} \quad (5.1)$$

The wake turbulence separation minima that were used to compute the arrival pressure ratio are based on legacy wake turbulence minima for IFR approaches defined by order JO 7110.65X [2] for airports and time periods where RECAT Phase I wasn't implemented and on wake turbulence recategorization minima for IFR approaches defined by order JO 7110.659C [28] for airports and time periods where RECAT Phase I was implemented. Separation minima corresponding to more recent RECAT efforts (i.e. RECAT Phase II) were not implemented yet for the time span of the collected ASDE-X data at the 36 considered airports.

To easily assess the impact of a trailing aircraft on the ROT of a leading aircraft, landing flights were classified in three different categories based on the computed ratio. First, aircraft with a

ratio below 100%, corresponding to visual separation were gathered in a first category. Aircraft in this category are closely followed by the trailing aircraft and observe a very-high pressure of the trailing aircraft. The rest of the aircraft were divided in two other categories designed to correspond to a low pressure ("Low") and high pressure ("High") of the trailing aircraft. The "High" and "Low" pressure categories were designed to be airport-specific as the traffic density varies across airports. Some airports such as Laguardia airport are used to handle closely separated aircraft on final approach while other airports such as Fort Lauderdale International airport (KFL) separate aircraft more conservatively. To separate these two airport-specific categories, the distribution of pressure ratios was analyzed at each airport. The computed ratios were rounded to the closest decimal and the most observed rounded ratio was used as a threshold to distinguish aircraft observing a low pressure and high pressure at the specific airport. Figure 5-16 shows how the resulting three categories of arrival pressure were defined based on the distribution of arrival pressure ratio for Laguardia airport (KLGA). At Laguardia airport (KLGA), a ratio of 140% was used to distinguish a "High" arrival pressure from a "Low" arrival pressure.

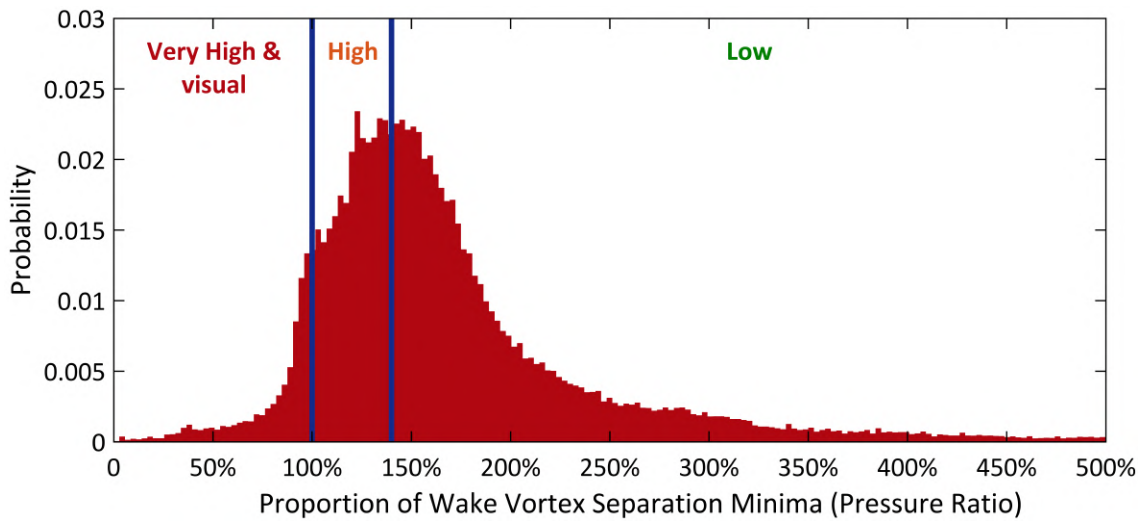


Figure 5-16: Example of arrival pressure categories at LaGuardia airport (KLGA)

The average values of Runway Occupancy Time and exit location for landing A320 operating in the three categories of arrival pressure were computed at each of the 36 airports. Based on these average values for 26 airports with more than 1000 observed A320 landings, it was found that the ROT and exit distance from the runway threshold generally decreases with a higher arrival pressure. The average values of ROT and exit location and 90% confidence interval per arrival pressure category for the 26 airports are listed in Table 5.2. According to this table, a "High" arrival pressure incentivizes the landing A320 to vacate the runway earlier compared to a "Low" arrival pressure which reduces ROT. Indeed, the leading aircraft is aware of the following traffic proximity via its communication with the air traffic control. To avoid a potential go-around of the following aircraft, the pilot of the leading aircraft is incentivized

to exit the runway earlier and quicker. Although the average ROT and exit location of aircraft of the "Very-High & Visual" category were found to be generally lower than those of the "High" category, the 90% confidence intervals of the mean estimates were usually overlapping with those of the "High" and "Low" categories due to the small number of observations. No formal conclusion was therefore made from the analysis of the "Very-High & Visual" arrival pressure category.

Table 5.2: Average A320 ROT and exit location depending on arrival pressure for 26 airports

Airport	Threshold	ROT, s (mean - 90% CI)			Exit Location, m (mean - 90% CI)		
		Visual	High	Low	Visual	High	Low
ATL	150%	42.6 ± 1.8	46.2±0.2	46.6±0.1	1781±125	1980 ± 6	1996 ± 3
BOS	160%	44.9 ± 0.8	45.8±0.3	47.7±0.2	1705 ± 22	1721 ± 7	1760 ± 4
BWI	190%	48.8±10.2	53.3±0.5	56.0±0.4	1754±358	1912±17	1983±13
CLT	160%	47.0 ± 1.9	46.6±0.2	49.1±0.2	1860 ± 63	1909 ± 7	1929 ± 6
DCA	180%	41.5 ± 1.9	41.4±0.3	42.1±0.2	1538±169	1502 ± 9	1519 ± 7
DEN	170%	49.5 ± 2.9	53.8±0.3	54.9±0.2	2345±111	2479±10	2525 ± 6
DFW	160%	49.4 ± 6.6	50.6±0.5	53.9±0.3	2022±307	2102±18	2200±11
DTW	150%	57.2 ± 5.2	53.9±0.5	56.5±0.3	1927±665	1945±21	2028±11
EWR	140%	41.1 ± 1.4	42.3±0.2	43.8±0.1	1552 ± 54	1696 ± 9	1740 ± 5
FLL	200%	46.2 ± 0.6	46.5±0.2	46.8±0.2	1823 ± 23	1817 ± 7	1830 ± 5
IAD	170%	50.0 ± 2.1	49.7±0.5	50.8±0.4	2051 ± 61	2000±18	2029±11
IAH	170%	49.8 ± 4.7	50.8±0.3	52.6±0.2	2156±180	2195±10	2231 ± 7
JFK	160%	44.8 ± 1.4	46.7±0.2	48.0±0.1	1655 ± 43	1723 ± 7	1765 ± 4
LAS	170%	45.3 ± 1.5	48.4±0.2	49.5±0.2	1989 ± 55	2106 ± 8	2126 ± 5
LAX	170%	44.3 ± 2.0	46.9±0.2	47.5±0.2	1824 ± 81	1916 ± 9	1946 ± 6
LGA	150%	40.6 ± 0.4	42.5±0.2	44.2±0.2	1440 ± 10	1516 ± 6	1531 ± 5
MCO	240%	51.5 ± 2.0	51.8±0.2	53.8±0.3	2106 ± 69	2089 ± 8	2115 ± 9
MIA	160%	45.4 ± 3.7	51.0±0.6	54.1±0.3	1896 ± 68	2041±22	2118±10
MSP	200%	48.7 ± 1.7	50.5±0.2	51.4±0.2	1860 ± 54	1885 ± 7	1886 ± 5
ORD	150%	46.7 ± 2.9	46.4±0.2	47.6±0.1	1835 ± 92	1873 ± 7	1907 ± 4
PHL	170%	46.1 ± 2.8	49.8±0.4	52.2±0.3	1883 ± 99	1967±14	2024 ± 9
PHX	150%	49.3 ± 0.9	49.6±0.3	51.0±0.1	1913 ± 31	1937±11	1999 ± 5
SAN	190%	49.5 ± 2.1	50.7±0.5	52.3±0.4	1873 ± 59	1882±13	1916 ± 9
SEA	150%	39.0 ± 3.5	44.3±0.4	45.5±0.2	1646±123	1862±11	1891 ± 7
SFO	190%	51.5 ± 1.7	51.1±0.3	51.9±0.3	1953 ± 42	1953 ± 9	2002 ± 9
SLC	170%	47.8 ± 1.4	48.9±0.4	51.7±0.3	2075 ± 41	2073±12	2100 ± 7

The better understanding of Runway Occupancy Time, that results from this analysis, opens the door to the development of new methods to estimate distributions of Runway Occupancy Time for specific runways. These methods can leverage recent machine learning models trained on large databases to predict ROT distributions based on the predictors identified in this study. Modifications to runway exit systems at capacity-constrained airports can be then proposed and their impact on ROT can be assessed using the developed models.

Chapter 6

Developing Predictive Models of Runway Occupancy Time

Based on the understanding of Runway Occupancy Time, predictive models of Runway Occupancy Time were developed using machine-learning algorithms. Recent machine-learning algorithms can model the collective influence of factors on Runway Occupancy Time based on observed data without any need to model the braking physics of a landing aircraft. The following section proposes an approach to predict the Runway Occupancy Time distribution of a given runway based on a combination of deep-learning algorithms. These deep-learning algorithms were designed to stochastically predict the Runway Occupancy Time of a given aircraft landing in very specific conditions and able to vacate the runway using a set of specified runway exits. By predicting ROT for thousands of landing aircraft, approaching in different conditions and representing the landing operations observed on a given runway, a probability distribution of Runway Occupancy Time can be predicted for the runway.

6.1 Overview of Predictive Models of Runway Occupancy Time

The overall strategy used to predict the ROT distribution of a runway consisted in developing models able to predict the ROT of an aircraft landing in specific conditions and using these models to predict ROT for thousands of landing flights representative of the landing operations before aggregating the predictions to come up with a ROT distribution. The parameters characterizing each landing aircraft can be either sampled randomly from distributions of parameters for the considered runway (Monte-Carlo simulation) or directly derived from observed landing observations on the runway. The later case is preferable due to the correlation of landing parameters and the assumption of independence between parameters used in the Monte-Carlo simulation. The several predictive models of ROT, presented in the following section were trained using the landing database, detailed in Chapter [3](#). The database was restrained to a

set of 105 popular landing aircraft representing 98% of the observations (3,378,783 landings in total). These aircraft are listed in appendix [A](#).

The models developed to predict the ROT of single landing aircraft were designed to be stochastic. This was motivated by the large variability of deceleration behavior observed for an aircraft landing in identical conditions on a runway described by a given set of available exits. The prediction of ROT is the result of a two-step process. A first model, based on Recurrent Neural Networks, predicts the probability of use of each runway exit available to the aircraft to vacate the runway. A second model, based on a set of Feed-Forward Neural Networks, predicts the average and variance of the time that the aircraft might take to vacate the runway using each of the available exits. By assuming that the ROT of an aircraft using a specific exit follows a normal distribution, this second prediction gives a probability distribution of ROT conditional to using a specific exit. By weighting these conditional probability distributions by the probability of use of each exit, a predicted gaussian-mixture probability distribution of ROT is finally obtained for the landing flight. The overall prediction process is illustrated in Figure [6-1](#).

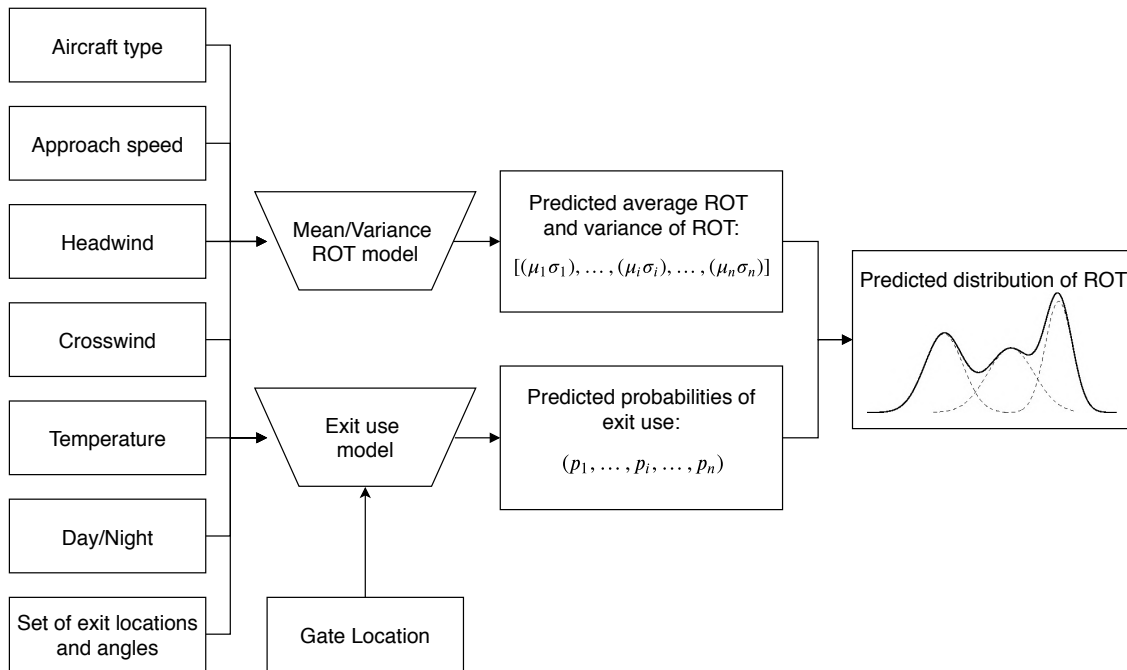


Figure 6-1: Overall prediction process of ROT

The developed predictive models use a specific set of parameters characterizing each landing flight to make predictions. These parameters are all included in the collected landing database and summarized in Table [6.1](#). This set of parameters includes most of the prominent factors driving ROT, identified in section [4](#). Each landing flight is characterized by its aircraft type, its final approach speed and the observed temperature, headwind, crosswind and day/night indicator. Some important factors are deliberately not considered as they would prevent

the models from being applied in more general situations. The airline, for example, is not considered as the resulting models would not be applicable to airports located outside of the US where different airlines operate. Additional parameters are used by the models to characterize the runway exits available to the landing aircraft. Each available exit is described by its distance from the runway threshold and its angle with the runway axis. Finally, the predictive model of exit use is fed with extra-information on the runway exit system. This information encompasses the distance of each runway exit to the gate location of the aircraft, its relative position to the runway axis and gate location and whether the exit is a crossing runway.

Table 6.1: Parameters used by predictive models

General Parameters	Parameters Specific to Exit Use Model
<ul style="list-style-type: none"> • Aircraft type • Approach speed • Day/night indicator • Temperature • Headwind • Crosswind • Locations of the runway exit • Angles of the runway exit 	<ul style="list-style-type: none"> • Distances between the runway exits and the final gate location • Relative positions of the runway exits with the runway axis and the final gate location • Exits identified as crossing runways

6.2 Predictive Modelling of Exit Use

To estimate the probability of use of each available exit on a runway by a landing aircraft, a predictive model based on a Recurrent Neural Network was developed. Recurrent neural networks are known for their ability to predict sequences of values associated to sequences of input data (i.e. sequence-to-sequence predictions). They are very popular for addressing Natural Language Processing (NLP) tasks such as machine translation or speech recognition. Applied in the estimation of exit use, they are chosen to predict a sequence of dependent exit use probabilities given an input sequence of available exits and given landing parameters.

6.2.1 Recurrent Neural Network Models

The functioning of a Recurrent Neural Network (RNN) [29] is depicted in Figure 6-2 and can be summarized as follow. A simple Recurrent Neural Network is a cell made of non-linear units and characterized by an internal state S . It is fed recursively with the different parameters

characterizing an element in the input sequence (i.e. step). At each step, the cell successively updates its internal state S with the information given at each step and outputs a prediction for the considered step using its current state. This internal state S can be considered as a memory of what has been successively observed by the cell along the sequence of input. The predictions made by the Recurrent Neural networks are thus highly dependent of the information it has observed so far. These predictions as well as the updated internal state of the RNN are the result of a collection of calculations using predefined non-linear functions embedded in the cell units and weights connecting the different units. The sequence of predictions given by the RNN can be post-processed in some cases using an activation function to obtain predictions compliant with the desired output characteristics.

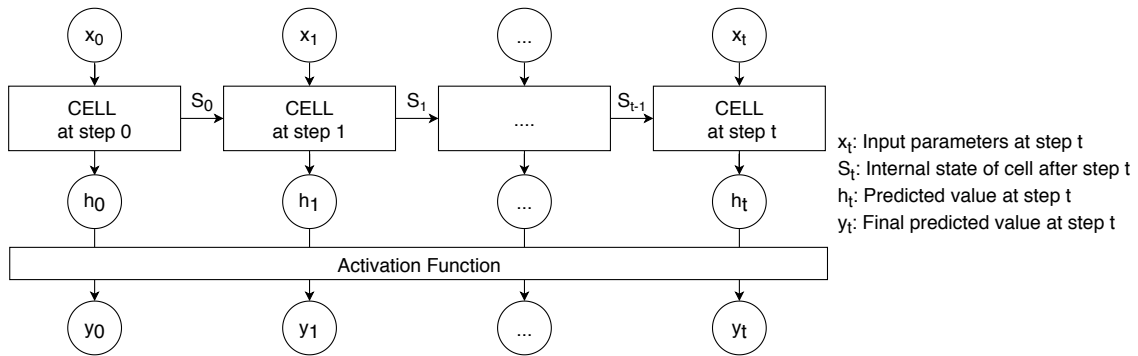


Figure 6-2: Simplified functioning of a recurrent neural network

The architecture of Recurrent Neural Networks is greatly flexible and multiple parameters can be tuned in order to reach a desired level of performance on a given modelling problem. Among these parameters, the number of hidden recurrent units within each cell can be tuned and the type of non-linear activation functions can be chosen. Multiple layers of Recurrent Neural Network cells can be stacked on top of each other as well to increase the capability of the model to predict results of very complex phenomena. These hyper-parameters need to be chosen wisely to create a well-performing model. Different memory processes (i.e. computations of the internal state S) can be also implemented in the Recurrent Neural Network cells. The most popular memory cells are Gated-Recurrent Units (GRU) [29] and Long-Short-Term Memory units (LSTM) [29] that can remember long-term dependencies with long sequences of input.

In order to be functional, the weights used by the Recurrent Neural Networks during the predictions are obtained by training the model on observed sequences of input and target sequences of output. During training, the algorithm gives predictions on the observed sequences of input, compares its predictions with the target outputs, computes a comparative loss and updates its weights in order to reduce the loss (using gradient back-propagation). By observing a large number of sequences, the algorithm usually converges to an optimal configuration of weights minimizing the loss on the observed data. Further details about Recurrent Neural Networks can be found in [29].

6.2.2 Training Recurrent Neural Networks to Predict Exit Use

To create Recurrent Neural Networks able to predict the probability of use by a landing aircraft for each exit on a runway, a Recurrent Neural Network model was trained with the collected landing database. A significant pre-processing of the landing data was required. For each of the 3,378,783 landings included in the collected database, the numerical parameters were scaled and standardized and categorical parameters were one-hot encoded. Such processing is standard in Machine Learning settings and prevents the introduction of a bias between parameters during the training process. Second, sequences of input data corresponding to the different available exits were created for each flight. For a given landing aircraft, each step of the sequence corresponds to a runway exit available to the aircraft. The data characterizing each step includes the characteristics of the exit and the landing parameters of the aircraft. The created steps for each sequence were then sorted in an ascending order, using the distance of the exits to the runway threshold. Because different runways have different numbers of exits, the created sequences have different lengths. For efficient training (i.e. training with batches of sequences), the sequences were padded with additional steps filled with a singular value (i.e. 1000) to reach a constant length of 36. These additional steps are masked automatically in the predictions. Third, sequences of target probabilities were created. They correspond to sequences of zeros with a single one located at the index corresponding to the runway exit actually used to vacate the runway in the observation. An example of a sequence of input without the standard scaling and one-hot encoding is given in Table 6.2 for an aircraft landing on runway 34L at Salt Lake City International airport (KSLC).

Table 6.2: Example of sequence of input for an aircraft landing on runway 34L (KSLC)

Exit #	0	1	2	3	4	5	6	7	8	9	10
Location, m	40	114	790	1188	1519	1671	2083	2446	2815	3540	3622
Angle, °	90	90	145	145	145	35	35	35	35	90	90
Runway Side	1	1	1	1	1	1	1	1	1	1	1
Distance to Gate, m	1602	1534	1028	850	828	861	1062	1322	1628	2283	2360
Aircraft	A320	A320	A320	A320	A320	A320	A320	A320	A320	A320	A320
Approach Speed, kt	150	150	150	150	150	150	150	150	150	150	150
HeadWind, kt	6	6	6	6	6	6	6	6	6	6	6
CrossWind, kt	4	4	4	4	4	4	4	4	4	4	4
Temperature, F	29	29	29	29	29	29	29	29	29	29	29
Day/Night	Day	Day	Day	Day	Day	Day	Day	Day	Day	Day	Day
Crossing Runway	No	No	No	No	No	No	No	No	No	No	No

The 3,378,783 processed sequences were then divided in three sub-datasets. A training set encompassing 64% of the sequences and a validation set encompassing 16% of the sequences were randomly selected and were used to find the optimal hyperparameters of the model. They were then combined to train the final model with the chosen hyper-parameters. A testing set including the remaining 20% of the data was also created and used to assess the performance of the final trained model.

To find the optimal design of the predictive model, a general architecture of the RNN model was first laid-out. Long-Short-Term Memory units (LSTM) were chosen as memory cells based on their recognized efficiency to deal with long input sequences. Rectified Linear units (Relu) [29] were also chosen as non-linear activation functions and hard-sigmoid [29] functions were used for the recurrent activation inside the LSTM cells. Finally, a time-distributed dense linear function followed by a non time-distributed softmax activation function [29] were added to post-process the RNN predictions to obtain a sequence of output probabilities summing-up to one. This general architecture was inspired by the Pointer Networks architecture (Ptr- Nets) presented in 2015 [30]. The Pointer Networks model is one of the first deep-learning models to use an attention mechanism to predict a sequence of outputs where each element is part of the sequence of inputs. The Pointer Networks model was initially designed to address geometrical problems and uses an encoder-decoder architecture. For each input in a given sequence, the Pointer Networks model points back at another input in the form of a probability distribution over the inputs using an encoder-decoder architecture. It later inspired simpler models with no decoder such as the Attention Sum Reader Network used to address question-answering problems based on a context document [31]. Compared to the Pointer Networks model, this model would point back only once at the input using a probability distribution over the inputs as well. The designed predictive model of exit use is simpler than the Pointer Networks model [30] and the Attention Sum Reader Network model [31]. Similarly to the Attention Sum Reader Network, it is only based on an encoder RNN but differs by using directly the successive hidden-states provided by the RNN as weights that are normalized to form a probability distribution over the input. These hidden-states are not merged in any way with external data. The architecture of the predictive model is shown in Figure 6-3.

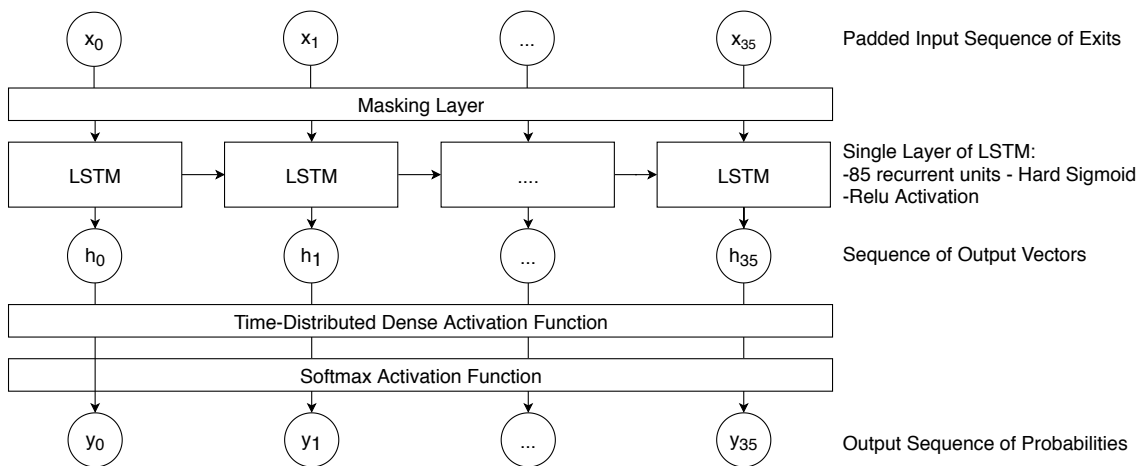


Figure 6-3: Final architecture of the predictive model of exit use

The general architecture of the exit use model was refined by finding the set of optimal number of recurrent units and number of LSTM layers giving the greatest model performance. The model performance was assessed using a categorical cross-entropy loss function, given in

Equation 6.1. This loss function was also used in the training process to update the weights of the RNN cell using mini-batch stochastic gradient-descent with batches of 200 sequences.

$$L = - \sum_{i=0}^t p_i \cdot \log(y_i) \quad (6.1)$$

with: L the categorical crossentropy loss
 y_i the predicted probability of use of exit i
 p_i the observed probability of use of exit i

To find the optimal set of hyper-parameters, a grid-search was done using the training and validation sets. The configuration giving the lowest validation loss in the grid-search results was chosen. A single layer of Long-Short-Term Memory units (LSTM) was picked as multiple layers did not help improve the validation loss and increased the complexity of the model. Regarding the number of recurrent units, a configuration with 85 units was found to provide the lowest validation loss. This number of units resulted in a validation loss of 0.774 as per Figure 6-4. The detailed final architecture of the predictive model is shown in Figure 6-3. The development of the recurrent neural networks model was done using the open-source python package Keras [32].

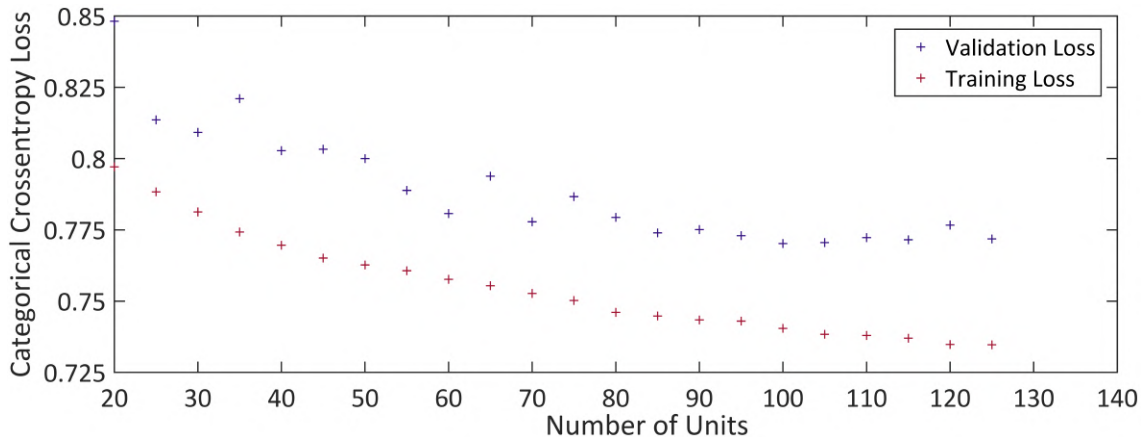


Figure 6-4: RNN training and validation loss depending on number of units

A model with the optimal configuration of hyper-parameters found was finally trained on the combination of validation set and training set, using batches of 200 sequences and a total of 34 epochs of data. The model reaches a 0.78 categorical crossentropy loss on the testing set. This corresponds to a prediction of the true exit used to vacate the runway in 69.5% of the cases. The detailed performance of the predictive model of exit use, broken-down per runway, for 218 runways with more than 100 landing observations in the testing set, is presented in Appendix B. This performance is fairly good regarding the complexity of the predictive task at hand and is capped for multiple reasons.

First, for identical landing conditions, a pilot might choose multiple exits to vacate the runway and the model will never be able to predict with confidence a single exit due to uncertain pilot behavior. The accuracy of the model therefore depends on the number of exits on a runway and on their relative popularity from a pilot standpoint. Second, the predictive model of exit use was designed to be generally applicable to multiple runways with different exit systems. Its predictive power on a per runway basis is therefore limited compared to runway-specific models aiming at predicting real-time exit use probabilities. Indeed, each runway has its own characteristics regarding for instance the taxiway system connecting the runway to the airport terminal and pilot behaviour might vary as well from one airport to another as specific airlines with various pilot policies might operate locally. For these reasons, predicting exit use probabilities for various runways with a single model is a challenging task. The predictive model of exit use provides predictions reflecting the average exit choice behavior that was observed across the 284 runways of the 36 US airports.

More complex RNNs architectures using bidirectional LSTMs [29] were investigated as well and didn't showcase any performance improvement. Future work could focus on exploring other RNN architectures that might provide better performance in the exit use prediction problem. Other factors driving exit choice and pilot behavior on the runway could be investigated as well in the future.

In the end, the developed model enables the prediction of probabilities of exit use for unseen configurations of runway exit systems by understanding how the different exit characteristics and landing parameters drive the exit decisions of pilots. More than modelling the braking performance of the aircraft, this data-driven model bases its predictions on previously observed pilot behaviors.

6.3 Predictive Modelling of Mean/Variance of ROT

Once estimates of exit use probabilities have been obtained for the landing aircraft, predictions of Runway Occupancy Time associated to each exit need to be computed. For each exit on the runway, it is assumed that the aircraft is vacating the runway using that specific exit and estimates of its average ROT and variance of ROT were predicted. By assuming that the Runway Occupancy Time of an aircraft is normally distributed, these predictions of mean ROT and variance of ROT can be used to construct a predicted normal probability distribution of ROT for the landing aircraft.

6.3.1 Neural Network Models

To predict average and variance values of ROT, a set of predictive Neural Networks models was trained. Feed-Forward Neural-Networks [29] are popular models in Machine-Learning able to estimate the results of complex-non linear phenomena. They can be used for both regression and classification purposes. Similarly to Recurrent Neural Networks, they are made of layers of units, characterized by non-linear functions and connected by weights. These layers

of units process the input data by transforming them in successive multidimensional feature spaces before computing the final desired prediction. The number of layers, units and types of non-linear functions need to be chosen in a relevant way to guarantee the model performance while keeping it simple. To be functional, the different weights of a Neural Network need to be trained by observing input data and bench-marking its predictions with actual target data. The weights are updated to reduce a custom loss function, adapted to the specific prediction setting. Further details about Neural Networks can be found in [29].

6.3.2 Prediction Process of Mean/Variance Estimates of ROT

A set of Neural-Networks was trained on the collected landing database to predict the average and variance values of ROT of aircraft using a specific exit. For each landing flight in the database, the different parameters listed in the first column of Table 6.1 were pre-processed by standard-scaling the numerical variables and one-hot encoding [29] categorical variables. The 3,378,783 processed landing flights were then divided between a training set, validation set and testing set using the same split used for the predictive model of exit use. Landing flights with extreme-values of ROT above 200s were considered as outliers and dismissed from the different datasets as significantly penalizing models during training. The different datasets were used to optimize, train and assess two types of Neural Networks.

First, B Neural Networks with identical architectures were trained on B different datasets $D_{b=1}^B$ resampled with replacement from the combination of the training and validation sets and downsized to half the number of observations of the original sets. These "bootstrapped" Neural Networks are all designed to predict the average Runway Occupancy Time of a landing aircraft. These B Neural Networks predict B average values of Runway Occupancy Time $ROT_{i,b}$ for a landing aircraft i . A final prediction of the average ROT of the aircraft is obtained by averaging these B estimates as per Equation 6.2.

$$\widehat{ROT}_i = \frac{1}{B} \sum_{b=1}^B ROT_{i,b} \quad (6.2)$$

Second, predictions of the variance of ROT for the landing aircraft are computed. The variance of ROT σ_i^2 for the landing aircraft i was broken-down in two components as per Equation 6.3.

$$\sigma_i^2 = \sigma_{\widehat{ROT}_i}^2 + \sigma_{Y_i}^2 \quad (6.3)$$

The first component of the variance $\sigma_{\widehat{ROT}_i}^2$ is associated to the misspecification of the B models. If the final average ROT estimate is considered as exact, the B models have predicted relatively inaccurate intermediary predictions for the average ROT. This is due to the misspecification of the weights of the models. These weights are very different among models because of different

weight initializations and different data observed during training. This model misspecification variance is estimated using Equation 6.4.

$$\sigma_{\widehat{ROT}_i}^2 = \frac{1}{B-1} \sum_{b=1}^B (\widehat{ROT}_i - ROT_{i,b})^2 \tag{6.4}$$

The second component of the variance of ROT $\sigma_{y_i}^2$ is due to the stochasticity of ROT. The Runway Occupancy Time of an aircraft landing with specific parameters and using a specific runway exit is variable and depends on the braking behavior of the aircraft and pilot. This second component of the variance of ROT is estimated using a second type of Neural Network. This additional neural network was trained to predict this second variance using the same set of parameters characterizing the landing and the runway exit used and using a new target variable corresponding to the squared residuals of the average ROT predictions r_i^2 . These squared residual values are computed using Equation 6.5 and based on the observed target Runway Occupancy Time values t_i .

$$r_i^2 = \max((\widehat{ROT}_i - t_i)^2 - \sigma_{\widehat{ROT}_i}^2, 0) \tag{6.5}$$

The overall process used to obtain estimates of the mean and variance of ROT for a landing flight is depicted in Figure 6-5. More details about the bootstrap method used to predict mean and variance estimates are given in [33].

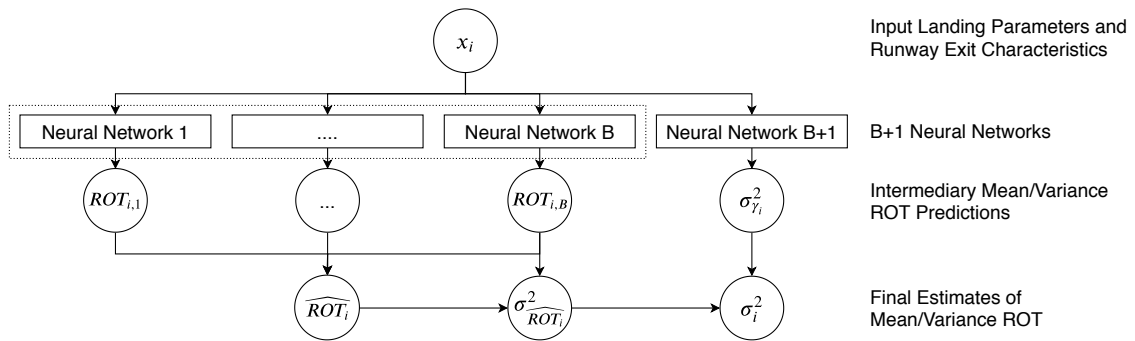


Figure 6-5: General predictive process of mean/variance of ROT

6.3.3 Training Neural Networks to Predict Mean/Variance Estimates of ROT

To put the predictive framework at work, multiple neural networks configurations were tested. The architectures and training processes of the $B+1$ neural networks are explained in the following part.

Regarding the first type of neural network, the optimal hyper-parameters shared by the neural

networks were found based on a grid-search conducted on the training and validation sets. The models were trained and assessed using a standard mean squared Error (MSE) loss. The generic formula of this loss is presented in Equation [6.6]. Two different non-linear functions, hyperbolic tangents (Tanh) [29] and Rectified Linear Unit (Relu) [29], were first tested. It was found that hyperbolic tangents functions outperformed Relu in all cases. Models with one or two layers with a number of Tanh units on each layer ranging from 50 to 1000 were then trained and assessed and their performance is displayed on Figure [6-6]. An optimal configuration with 2 layers with 700 Tanh units on each layer was found to provide good validation performance while keeping the computational cost low.

$$L = \frac{1}{n} \sum_{i=1}^n (y_i - p_i)^2 \quad (6.6)$$

with: L the mean squared error loss

y_i the predicted value for observation i

p_i the observed value for observation i

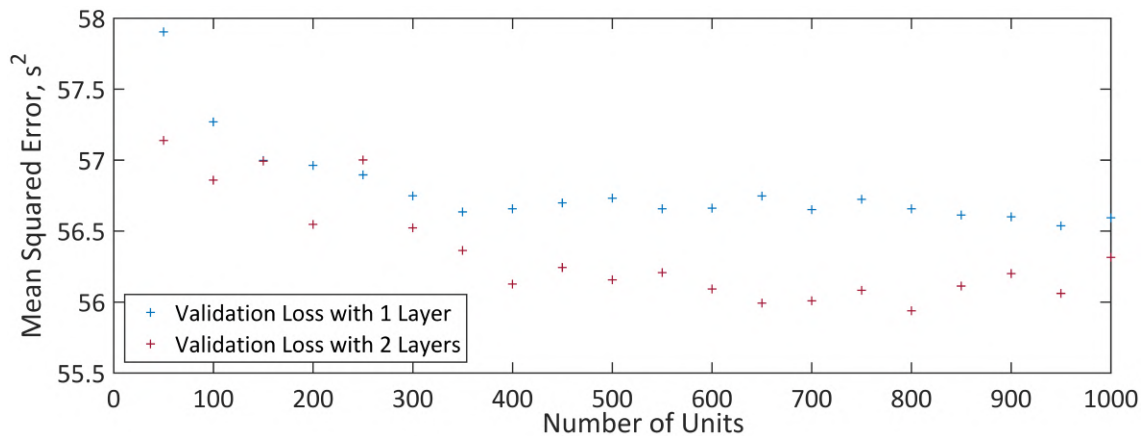


Figure 6-6: Validation loss of average ROT predictive model depending on number of units

Finally, 1000 Neural Networks with this architecture were trained on 1000 datasets resampled with replacement from the training and validation sets and downsized to half the number of observations of the original sets. 1000 was chosen as a value for B to provide stable enough ROT predictions. The development of these 1000 neural networks model was done using the open-source python package Keras [32]. These models, combined, reach a $57.8s^2$ mean-squared error in the prediction of average ROT on the test set. While this average loss is high, the distribution of the squared error on the testing set shows that for 90% of the flights, the error is lower than $60s^2$. The distribution of the loss on the testing set is depicted in Figure [6-7].

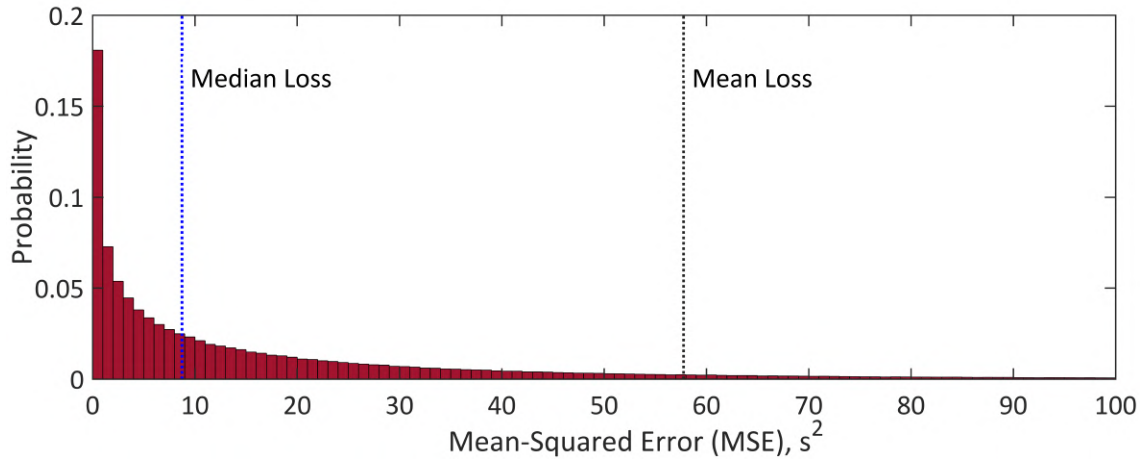


Figure 6-7: Distribution of mean squared error in the prediction of average ROT on testing dataset

The presence of some outliers in the collected ROT pollutes the average performance score of the models but doesn't affect the actual performance of the models. Outliers associated with very high squared-error usually correspond to abnormal behavior on the runway such as slow movement on the runway surface after a significant deceleration. The recorded speed and position for several landing flights, associated to a high squared error in predicted ROT and selected randomly were analyzed. These landing flights were all characterized by a very slow movement of the aircraft on the runway after a significant deceleration. These cases do not correspond to normal operations with aircraft pressured to vacate the runway quickly. For these cases, the models usually underestimate the Runway Occupancy Time. A metric less sensitive to outliers is the median-squared error, equal to $8.7s^2$. This metric is truly representative of the performance of the model to predict Runway Occupancy Time for aircraft landing in dense traffic conditions and pressured to vacate the runway.

The detailed performance of the predictive models of average ROT, broken-down per runway, for 218 runways with more than 100 landing observations in the testing set, is presented in Appendix [C](#).

In order to train the second type of Neural Network, another type of target data needed to be computed first for the existing training, validation and testing datasets. Using the 1000 trained neural networks, predictions of average ROT and model misspecification ROT variance for each landing flight were computed and a target variable made of prediction squared residuals was derived using Equation [6.5](#). To predict $\sigma_{y_i}^2$ using these squared residuals as target data, a custom loss, presented in Equation [6.7](#) was used. This loss forces the neural network to predict a variance maximizing the likelihood of a normal distribution given the observed residuals. A special exponential activation layer was added as well at the end of the network to guarantee the positive sign of the prediction.

$$L = \frac{1}{2}(\ln(\sigma_{y_i}^2) + \frac{r_i^2}{\sigma_{y_i}^2}) \quad (6.7)$$

with: L the custom likelihood loss

$\sigma_{y_i}^2$ the predicted variance of errors

r_i^2 the observed squared residuals in the prediction of ROT

The optimal hyperparameters of the second Neural Network were obtained using a grid-search approach similar to the one used for the B Neural Networks. Multiple architectures with several layers of hyperbolic tangent (Tanh) [29] and Rectified Linear Units (Relu) [29] were tested using the training and validation sets. A configuration with 120 relu units, distributed over one layer was found to minimize the validation loss. The final model, using the optimal architecture found, was then trained on the combination of training and validation sets and reaches a loss of 2.026 on the testing set. The development of this last neural network model was done using the open-source python package Keras [32].

It was found that the model was overestimating the overall predicted variance. This is due to the fact that maximum likelihood estimators of variance are not robust to outliers. The presence of very high squared residuals in the data used for training affects the model performance. Improvements of the model performance could result from the development of a detailed methodology to identify and dismiss outliers at the data-collection level. It can be noted here that both predictive models of average ROT and variance of ROT were trained using the same data (i.e. combination of training and validation sets). This might introduce bias in the prediction of variance and underestimate the actual variance. However because of the large amount of data (more than 2 million observations) used for training, it was assumed that predictive models of average ROT were not overfitting. Therefore squared residuals used for training the variance model were not underestimated. Further improvements of the models could include the use of a separate additional dataset of observations to train the variance model.

6.4 Predicting the ROT Distribution for a Landing Aircraft

The three different types of models presented in the previous sections provide together stochastic predictions of Runway Occupancy Time for an aircraft landing with specific parameters on a runway with a given set of exits. The predictions of the three types of models are combined using the process described in Figure 6-1. The gaussian ROT distributions predicted for each exit are weighted by the probabilities of exit use to obtain a gaussian-mixture probability distribution of ROT for the landing aircraft. An example of such a stochastic prediction of ROT is presented in Figure 6-8 and Table 6.5. The landing parameters and runway exit system used for the prediction are listed in Tables 6.3 and 6.4.

Table 6.3: Example of parameters of aircraft landing on runway 34L (KSLC)

Aircraft	Approach Speed	HeadWind	CrossWind	Temperature	Day/Night
A320	150kt	6kt	4kt	29°F	Day

Table 6.4: Example of runway exit system of runway 34L (KSLC)

Exit #	0	1	2	3	4	5	6	7	8	9	10
Location, m	40	114	790	1188	1519	1671	2083	2446	2815	3540	3622
Angle, °	90	90	145	145	145	35	35	35	35	90	90
Distance to Gate, m	1602	1534	1028	850	828	861	1062	1322	1628	2283	2360
Crossing Runway	No	No	No	No	No	No	No	No	No	No	No

Table 6.5: Example of exit use and ROT predictions for aircraft landing on runway 34L (KSLC)

Exit #	0	1	2	3	4	5	6	7	8	9	10
Probability of Use, %	0.1	0.0	0.0	0.2	0.6	5.4	60.9	31.0	1.6	0.1	0.0
Average Predicted ROT, s	501	53	91	97	48	41	45	54	64	97	100
Misspecification Variance, s^2	62	65	126	48	29	2	4	1	0	2	10
Variance of Errors, s^2	1860	1777	1194	749	402	70	27	33	52	272	292

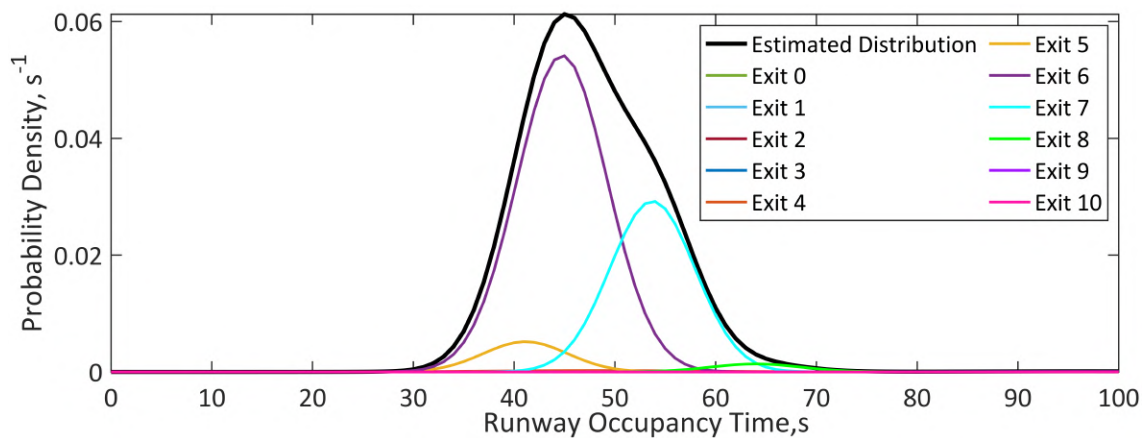


Figure 6-8: Example of predicted ROT distribution and weighted components per exit for an aircraft landing on runway 34L (KSLC)

6.5 Predicting ROT Distributions by Runway

By repeating such stochastic predictions of ROT for multiple aircraft landing on a same runway in different conditions, the Runway Occupancy Time distribution of a runway can be obtained. This distribution is computed by weighting the different gaussian mixture distributions of the different landing flights with uniform weights. The computed distribution is itself a gaussian mixture distribution with $N_1 \cdot N_2$ components (N_1 being the number of exits on the runway and N_2 the number of predicted landing operations).

In order to predict a representative ROT distribution for a studied runway, the different simulated landing operations must be however representative of the operations seen on the runway. Multiple approaches can be used to replicate these operations. If detailed data is available on specific aircraft landing in specific conditions on the studied runway, this data can be used directly as an input by the predictive models. This is the case for the multiple runways of the 36 studied airports in the US where landing parameters were collected for thousands of landings. An example of a Runway Occupancy Time distribution predicted for runway 25L at Phoenix Sky Harbor International airport (KPHX) is depicted in Figure 6-9. For this prediction, the input data that was used corresponds to the landings observed on runway 25L at KPHX included in the database and gathered in the testing dataset.

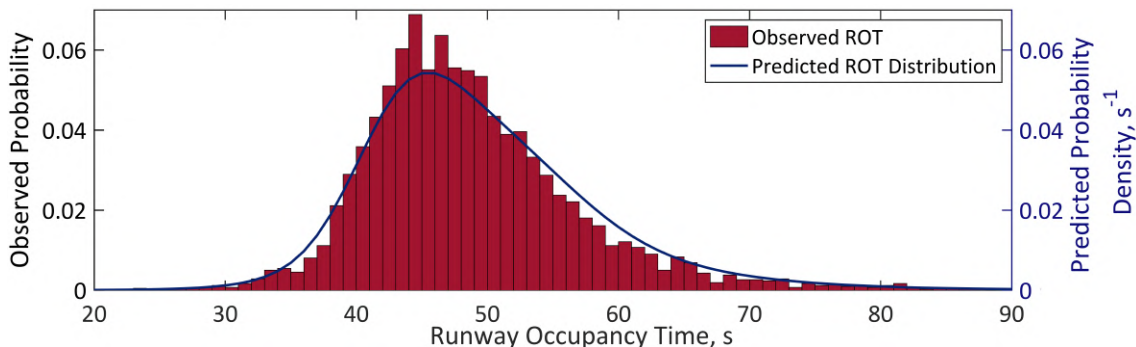


Figure 6-9: Predicted ROT distribution for runway 25L at Phoenix Sky Harbor International airport (KPHX)

For some runways around the world, however, detailed landing data is not available and only aggregated information on landing operations is accessible. This aggregated information can encompass the fleet-mix of aircraft operating on the runway, general distributions of weather parameters and final approach speeds per aircraft as well as general information on gate locations. Information on the runway exit system can be also extracted using airport diagrams and Google-Earth. Using this aggregated information, landing operations can be simulated by sampling at random aircraft from the fleet-mix and landing parameters from the different distributions. Although some landing parameters are correlated (e.g. headwind and approach speed), it can be assumed as a first order that parameters are statistically independent and can be sampled independently. The number of simulated landings is chosen so as to guarantee

the convergence of the predicted ROT distribution. This convergence can be assessed by computing statistical distances between the successive predicted distributions corresponding to an increasing number of simulated operations.

6.6 Performance of Models in Predicting ROT Distributions by Runway

The different predictive models, presented in the previous sections, were trained and assessed to predict the ROT distribution of a single landing flight using simple loss metrics. The final objective of the models is however to jointly predict the total Runway Occupancy Time distribution of a runway. The performance of the models in fulfilling this task was assessed by comparing predicted ROT distributions for different runways at the 36 US airports with actual observed distributions. For each runway with more than 100 landing observations in the testing set, a gaussian mixture ROT distribution was predicted and a dataset of 10,000 ROT values sampled at random from the distribution was created. This dataset was compared with the observed ROT values included in the testing dataset for each considered runway. The Kullback–Leibler divergence served as a first performance metric to compare predicted and observed ROT distributions. The formula of this metric is presented in Equation [6.8](#).

$$D_{\text{KL}}(P, Q) = \sum P(x) \ln \left(\frac{P(x)}{Q(x)} \right) \quad (6.8)$$

with $D_{\text{KL}}(P, Q)$ the Kullback–Leibler divergence of distribution Q relative to distribution P
 x the studied random variable

The Kullback-Leibler divergence is a non-negative asymmetric metric assessing the amount of information lost by modelling an observed distribution using a predicted distribution. If this divergence is close to zero then the observed distribution is well approximated by the estimated distribution. This metric can take very large non-bounded values if the approximation is poor. While the Kullback-Leibler divergence is defined objectively, its interpretation is however somewhat subjective. No threshold divergence value exists in the literature to affirm that an observed probability distribution can be approximated with confidence by a predicted distribution. This metric was however used to get a sense of the performance of the models and the presented results can serve as a benchmark for further studies aiming at predicting ROT distributions. The values of this metric for 211 runways with more than 100 landing observations in the testing set are presented in Appendix [D](#). The Kullback–Leibler divergence was found to be on average equal to 0.11 nats, relatively close to zero and demonstrating a small loss of information. The average divergence drops to 0.05 nats for runways with more than 1000 observations in the testing set. This seems to indicate a good overall performance of the models in estimating Runway Occupancy Time distributions by runway.

A more meaningful way to assess the performance of predictive models consists in comparing

simple parameters characterizing the observed and predicted ROT distributions. The mean ROT values were compared to assess the performance of the models in replicating the location of the distribution. The average absolute difference between means of the distributions was equal to 1.6s. This average value drops to 1.3s for runways with more than 1000 observations in the testing set. These absolute differences are small relatively to the precision of ROT measurements from ASDE-X data and demonstrate the good performance of the model in predicting accurate locations for ROT distributions.

The Median-Absolute-Deviation (MAD) was used to assess the fidelity of the models in replicating the scale of the distribution. This metric was used instead of the variance as more robust to extreme ROT values observed in the testing dataset. The average ratio between median absolute deviations of the distributions is equal to 1.1. This highlights the good performance of the model in predicting an accurate scale for ROT distributions although the models slightly overestimate the spread of the distribution. This can be seen in some predicted distributions, showing larger tails than in the observed distributions. These larger tails are due to the overestimation of the variance of ROT, mentioned in section 6.3. An example of a predicted Runway Occupancy Time showcasing a larger left tail is depicted in Figure 6-10 for runway 17 at Philadelphia International airport (KPHL). Further improvements in the models could focus on predicting better estimates of variance of ROT for a given landing flight by filtering extreme values of ROT in the collected data first or using more robust estimators of scale. The values of the predicted and observed mean and Median-Absolute-Deviation of ROT for 211 runways with more than 100 landing observations in the testing set are presented in Appendix D.

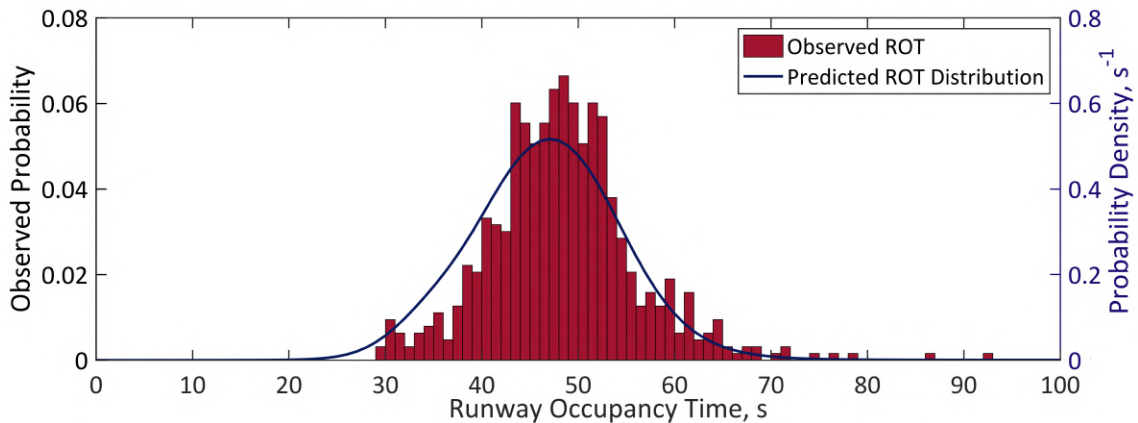


Figure 6-10: Predicted ROT distribution with larger left tail for runway 17 at Philadelphia International airport (KPHL)

THIS PAGE INTENTIONALLY LEFT BLANK

Chapter 7

Case Study - Reducing ROT at Keflavík Airport

The predictive models of Runway Occupancy Time, presented in the previous chapter, were used to assess potential ways to reduce Runway Occupancy Time at Keflavík airport in Iceland. Keflavík airport is the major international airport of Reykjavik and currently has two long crossing runways. The observed Runway Occupancy Time on these runways is very high and the airport operator seeks to recover additional capacity for the different runways by reducing ROT. As mentioned in Chapter 5, the design of runway exits available to a landing aircraft to vacate the runway is the main leverage airport operators have to reduce Runway Occupancy Time. The runway exit system needs to be optimized for the expected landing operations by implementing exits located at appropriate distances from the runway threshold. It used to be common for these decisions to be empirical or based on general cumulative distributions of exit use per aircraft category [27]. These distributions do not account for the specific landing conditions and detailed fleet-mix observed at the airport. The predictive models of ROT can provide runway-specific guidance to airport operators about where to locate optimal runway exits. Guidance on the optimal changes to current exits and the design of new exits was provided to the airport operator (ISAVIA) using the developed predictive models of ROT. The detailed study aiming at reducing ROT at Keflavík airport is presented in the following section.

7.1 Understanding Current Landing Operations at Keflavík Airport

Keflavík International airport (BIKF) is the international airport of Reykjavik, Iceland, located 50 kilometers away from the city. The airport was built during the second world war by the US military and is now the main hub of several airlines. The traffic of the airport has increased dramatically from 2009 to 2018 with +200% movements a year and is driven by tourism and demand for transatlantic flights. In 2018, the traffic at Keflavík airport was estimated at

approximately 68000 movements a year, putting high pressure on the infrastructure of the airport [34]. The runways are reaching their maximum capacity and the airport operator is seeking to recover additional movements for the existing runways by reducing Runway Occupancy Time. According to ROT measurements derived from ADS-B data collected in 2018 and presented in section 7.1.1, the average ROT at Keflavík airport was equal to 80s in 2018. This contrasts with the average 49s observed at the 36 US airports. Keflavík airport has two 3060m-long perpendicular crossing runways, aligned north-south (i.e. runway 01-19) and east-west (i.e. runway 10-28) respectively. These runways are depicted in Figure 7-1. According to Table 7.1, the average ROT ranges from 65 to 90s on a per runway basis. This highlights the overall poor Runway Occupancy Time performance of each runway.

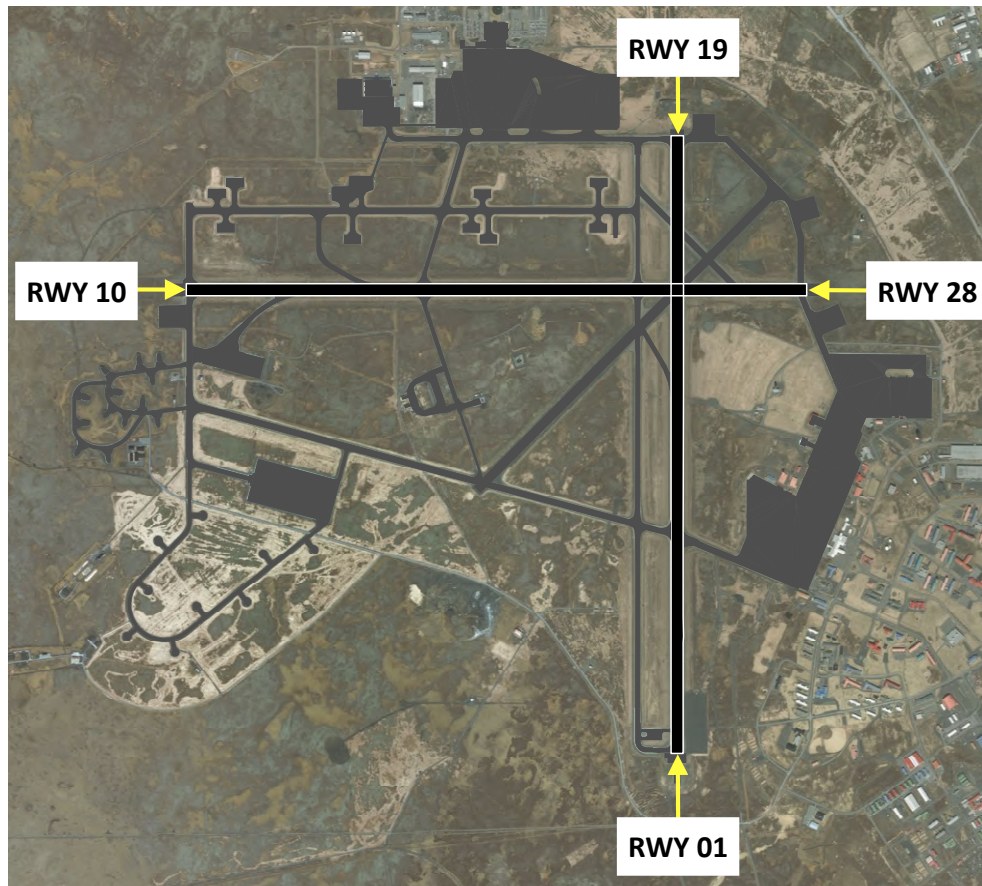


Figure 7-1: Runway configuration of Keflavík airport (BIKF)

Table 7.1: Average Runway Occupancy Time for each runway at Keflavík airport (BIKF)

Runway	01	10	19	28	Total
Average ROT, s	94	82	66	68	80

The overall diagram of the airport is depicted in Figure 7-2 and presents the current configuration of the airport and details regarding the exit system.

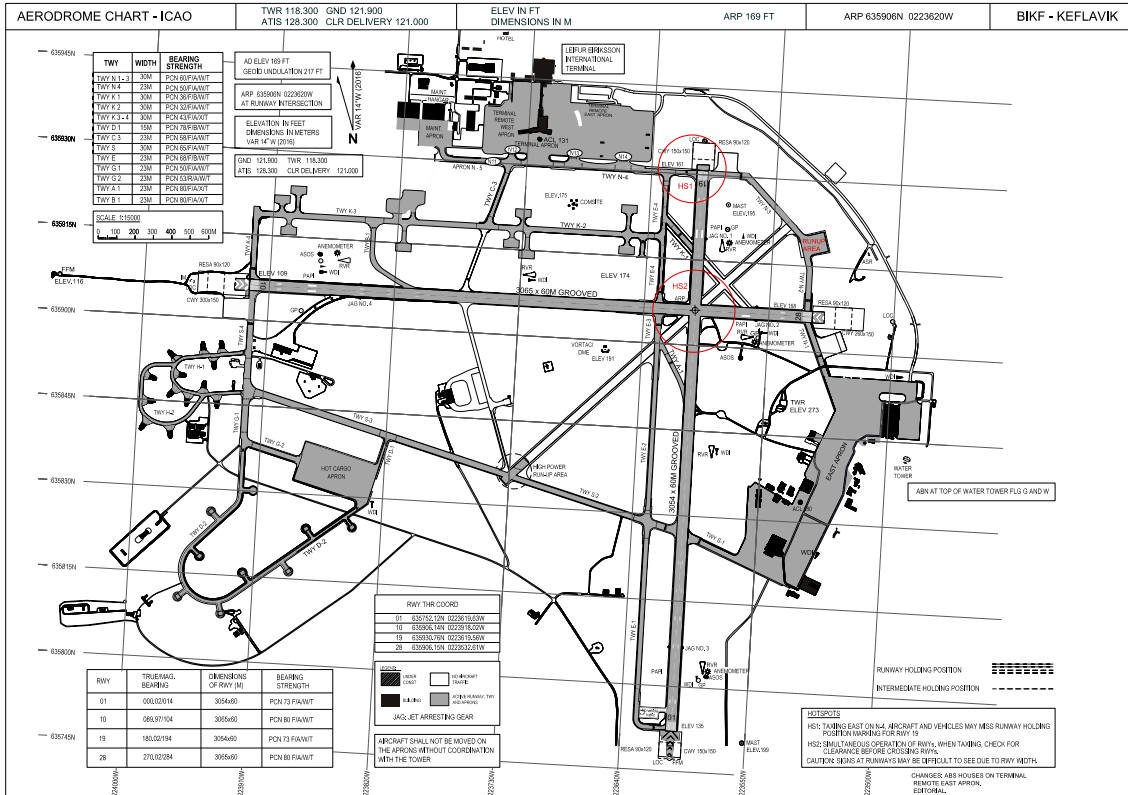


Figure 7-2: Aerodrome chart of Keflavík airport (BIKF)

7.1.1 Collecting ROT Measurements and Landing Data

To reduce Runway Occupancy Time at Keflavík airport, a good understanding of the current landing operations and Runway Occupancy Time performance of the airport was needed. To analyze this performance, data regarding landing operations observed in 2018 was collected using the same process used to build the landing database at the 36 studied US airports. This process, presented in Chapter 3.1, was applied to data coming from different local sources.

Flight tracks around Keflavík airport were collected using the Automatic Dependent Surveillance-Broadcast (ADS-B) system. This system is installed on most modern jetliners and broadcasts the identification of the aircraft, its ground speed and its GPS coordinates every second. ADS-B data was collected by ISAVIA around Keflavík airport for 2018, using ground-based antennas and presents a similar quality to ASDE-X data. The flight tracks included in the ADS-B data were used to identify flights landing at Keflavík airport in 2018. An example of some ADS-B flight tracks and identified landing aircraft observed on a given day around Keflavík airport is shown in Figure 7-3.

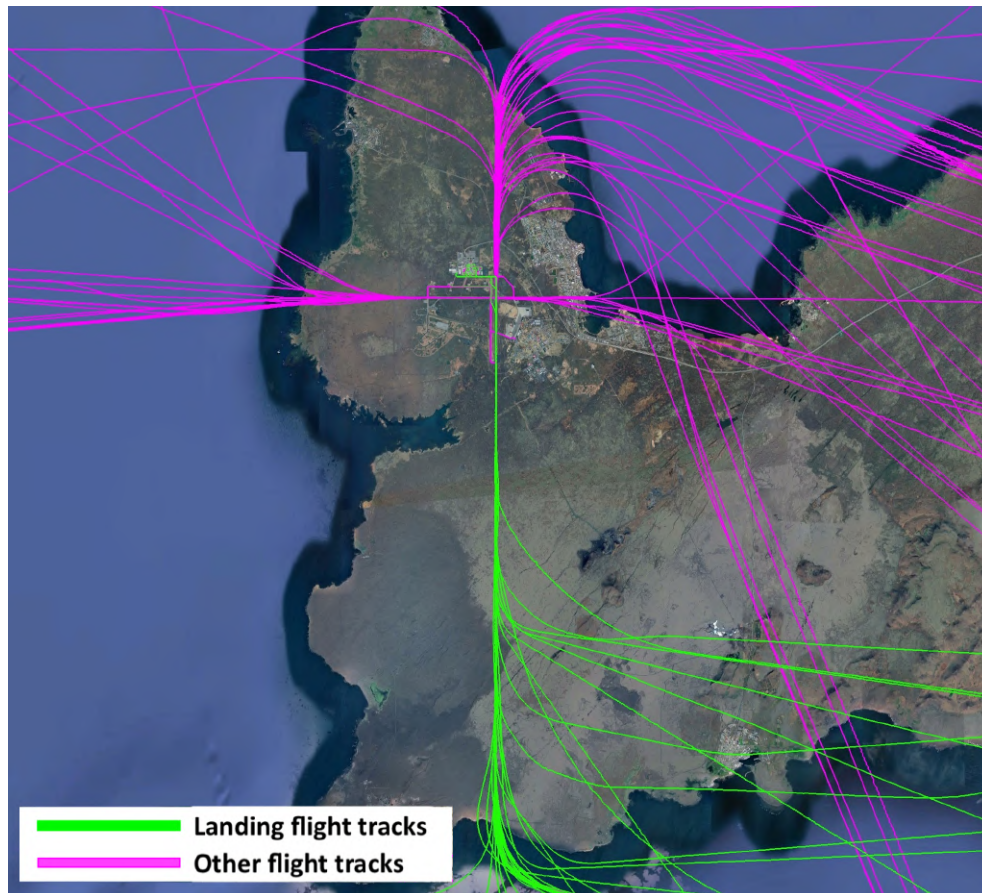


Figure 7-3: Example of flight tracks at Keflavík airport (BIKF on 01-01-2018)

Second, geometry data was collected for the four runways and 18 runway exits of the airport. This geometry data was measured using a detailed map of the airport provided by ISAVIA. It enables the identification of the runway and runway exit used by each landing aircraft in the flight tracks. Figure 7-4 shows the runway threshold and runway exit identified for a given landing flight at Keflavík airport (BIKF). Runway Occupancy Time can be then measured for the landing flight.



Figure 7-4: Example of the runway threshold and runway exit identified for a landing flight at Keflavík airport (BIKF)

For each landing aircraft, the aircraft type, airline, final approach ground speed and gate location were identified. Additional data regarding weather parameters was derived from Meteorological Aerodrome Reports (METAR). These reports are available at Keflavík airport and published every 30 minutes. Published information includes temperature, wind speed and direction, pressure altitude, visibility, and type and amount of precipitation. In the end, the collected database is composed of 22,869 aircraft landing observations at Keflavík airport, described by 16 discrete parameters, listed in Table 7.2.

Table 7.2: Collected landing data, airport data and weather data at Keflavík airport (BIKF)

Landing data	airport data	Weather data
<ul style="list-style-type: none"> • Runway Occupancy Time • Aircraft type • Airline • Approach speed 	<ul style="list-style-type: none"> • Runway used • Location of the runway exit used • Angle of the runway exit used • Distance between the runway exit used and the final gate location • Relative position of the runway exit used with the runway axis and the final gate location 	<ul style="list-style-type: none"> • Temperature • Headwind • Crosswind • Type of precipitation • Amount of precipitation • Pressure altitude • Visibility

7.1.2 Understanding the Characteristics of Landing Operations

The landing data was used to analyze the landing operations at Keflavík airport. Among the 22,869 landing aircraft identified in the database, it was observed that aircraft landed mainly on runways 01, 10 and 19. These runways are each used by approximately 30% of the landing aircraft while runway 28 is only used in 10% of the cases. This runway usage is driven by the distribution of wind direction observed at Keflavík. This wind primarily comes from the north-east and south-east of the airport. More generally, the weather observed during landing operations is windy and cold with an average temperature of 42°F and average wind speed of 13kt. The observed distributions of wind and temperature are shown in Figures 7-5 and 7-6.

The types of aircraft operating at Keflavík are relatively homogeneous with 97% of the aircraft belonging to the "Large" and "Heavy" FAA legacy wake categories. The observed fleet-mix mainly encompasses members of the A320, B737, B757, A330 and B767 families. It can be noted that very recent aircraft types such as the A320/A321 NEO and B737 MAX 8/9 are observed in 2018 at Keflavík airport. The remaining 3% of the fleet mix are made of 96 different aircraft types, mostly general aviation aircraft and Bombardier Q-Series aircraft operating within Iceland. The detailed fleet-mix of aircraft landing at Keflavík airport is presented in Figure 7-7.

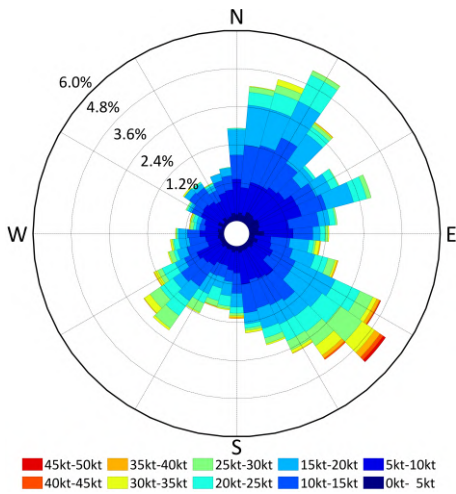


Figure 7-5: Distribution of wind at Keflavík airport (BIKF)

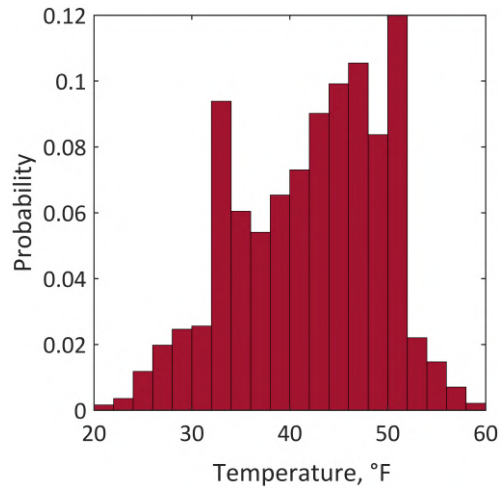


Figure 7-6: Distribution of temperature at Keflavík airport(BIKF)

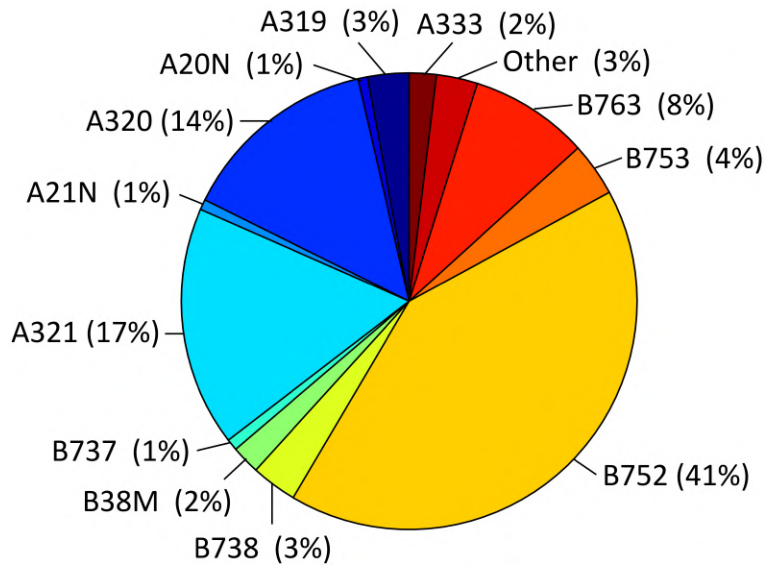


Figure 7-7: Observed fleet-mix of landing aircraft at Keflavík airport (BIKF)

While the observed fleet mix is homogeneous, landing operations are not evenly distributed over the day. Two peaks of operations, characterized by an above-average number of landings per 10 minute interval, can be identified. The first peak, from 4:20AM to 6:50AM, corresponds to east-bound traffic coming from North America. The second peak from 1:30PM to 4:20PM corresponds to west-bound traffic coming from Europe. These two peaks of operations, representing 58% of the landings, are depicted in Figure 7-8 and correspond to an increased pressure on runway throughput.

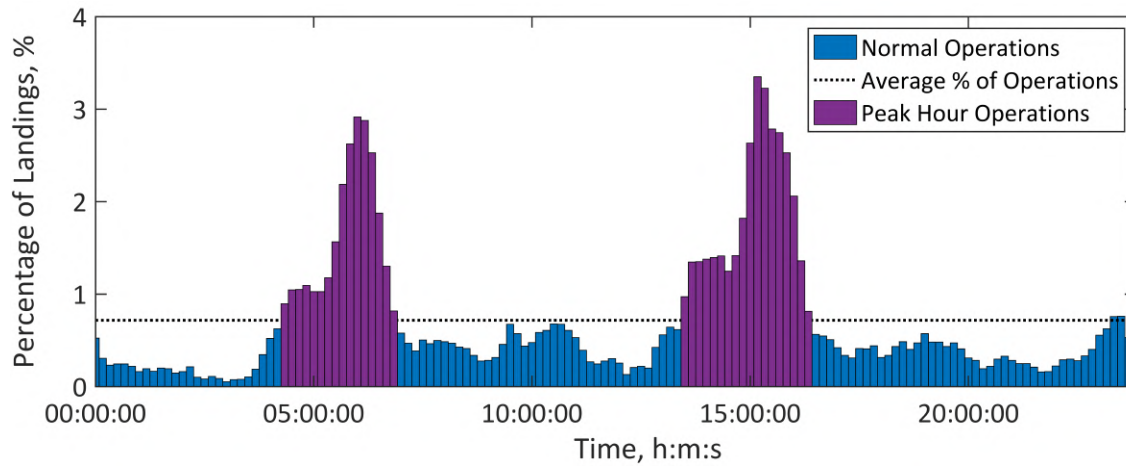


Figure 7-8: Average daily distribution of landings at Keflavík airport (BIKF)

Finally, most landing aircraft are taxiing to the same terminal after vacating the runway. This terminal, located in the north of the airport, corresponds to the gates of commercial aircraft. In rare occasions, aircraft taxi to the east apron, corresponding to the cargo terminal. The observed gate locations of landing aircraft at Keflavík airport are depicted in Figure [7-9](#).

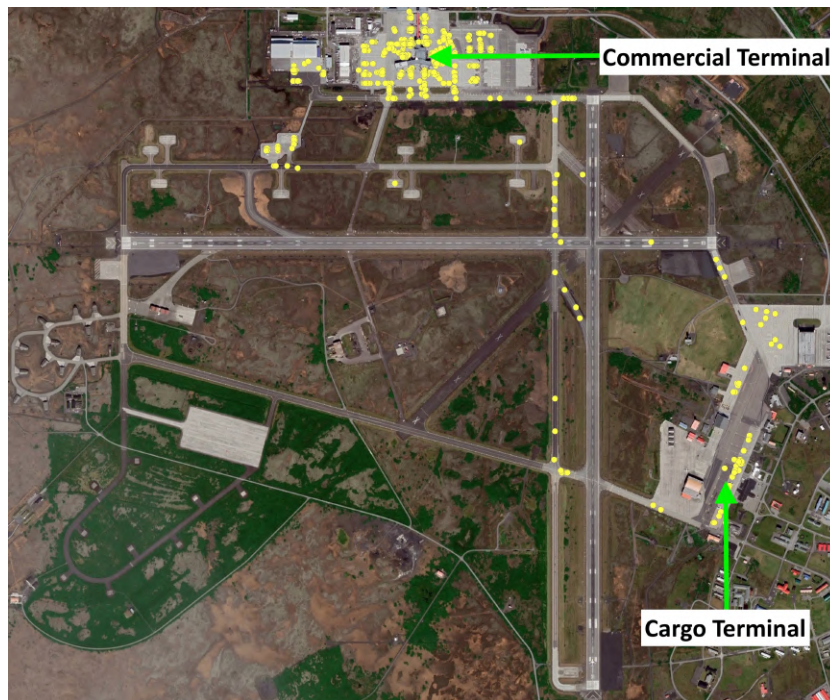


Figure 7-9: Terminal locations for aircraft landing at Keflavík airport (BIKF)

7.1.3 Assessing the Current Runway Occupancy Time performance

While the characteristics of landing operations observed at Keflavík airport are not atypical, the associated Runway Occupancy Time measurements are abnormally high compared to what is observed at US airports. During peak-hours, the average measured Runway Occupancy Time is equal to 77s. This average ROT is significantly higher than the 49s average ROT observed at the 36 US airports studied. Figure 7-10 shows the cumulative distribution of ROT at the 36 US airports and during peak-hours at Keflavík airport.

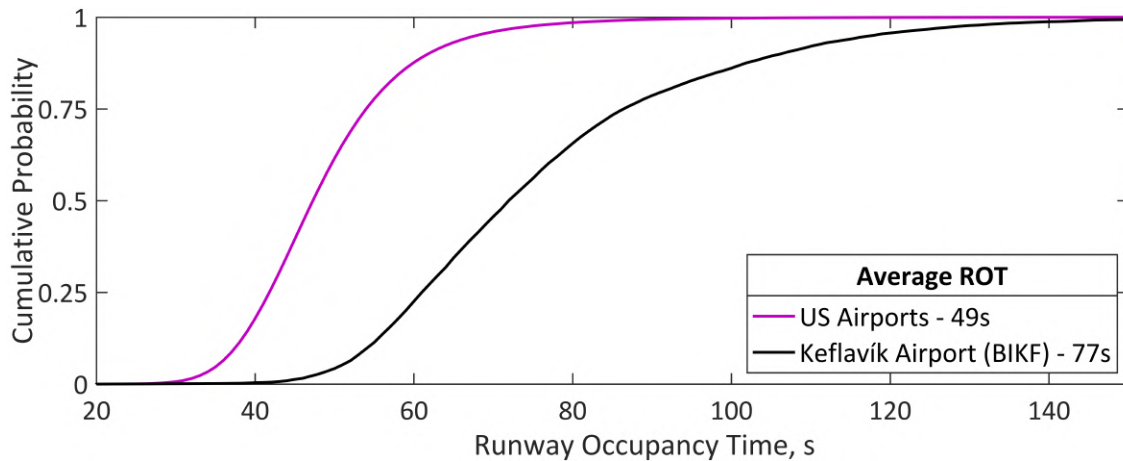


Figure 7-10: Runway Occupancy Time distribution at US airports and during peak-hours at Keflavík airport (BIKF)

This average Runway Occupancy Time can be broken down per runway. Table 7.3 shows the average ROT during peak-hours for each runway at Keflavík airport. According to this table, it appears that all runways have a high Runway Occupancy Time with runways 01 and 10 under-performing even more relatively to runways 19 and 28.

Table 7.3: Average Runway Occupancy Time during peak-hours for each runway at Keflavík airport (BIKF)

Runway	01	10	19	28	Total
Average ROT, s	90	80	65	65	77

The poor Runway Occupancy Time performance observed at Keflavík airport considerably limits the throughput of runways for several reasons. First, with a high Runway Occupancy Time, Air Traffic Controllers are incentivized to add significant buffers when separating aircraft on final approach to prevent go-arounds. Aircraft on final approach are thus separated with distances significantly greater than the wake vortex separation minima in use. Keflavík airport currently operates with conservative legacy ICAO wake vortex separation minima on final approach, presented in Table 7.5 for IFR operations. These minima concern four categories of aircraft, detailed in Table 7.4.

Second, the high Runway Occupancy Time is a bottleneck for runway capacity that needs to be solved before proposing other solutions to increase runway throughput. Because of a constraining Runway Occupancy Time, the impact of potential future reductions of Wake Vortex Separation minima (RECAT) on runway throughput might be very limited at Keflavík airport for instance.

Table 7.4: Legacy ICAO aircraft wake categories - ICAO DOC 4444

	Light	Medium	Heavy	Super
MTOW (lb)	MTOW ≤ 15,500	15,500 < MTOW < 300,000	MTOW ≥ 300,000	A380, AN225

Table 7.5: Final approach wake turbulence separation minima (IFR) - ICAO DOC 4444

Separation Minimum (NM)		Following Aircraft			
		Super	Heavy	Medium	Light
Leading Aircraft	Super	MRS*	6	7	8
	Heavy	MRS*	4	5	6
	Medium	MRS*	MRS*	MRS*	5
	Light	MRS*	MRS*	MRS*	MRS*

*Minimum Radar Separation (2.5, 3 or 5 NM - 3 NM at Keflavík)

Finally, the high Runway Occupancy Time observed at Keflavík prevents the airport operator to further reduce the Minimum Radar Separation between aircraft on final approach, according to ICAO PANS-ATM (Procedures for Air Navigation Services related to Air Traffic Management) [4]. The current Minimum Radar Separation is equal to 3NM at Keflavík airport thanks to the existing radar, ADS-B and multilateration detection capabilities of the airport. To reduce the Minimum Radar Separation to 2.5NM, airport operators must comply with multiple requirements established by ICAO, including the reduction of the average Runway Occupancy Time below 50s for each runway.

For the reasons mentioned above, reducing Runway Occupancy Time for each runway could help increase runway throughput at Keflavík airport in the short and long term. The following section provides guidance to the operator of Keflavík airport on how to reduce Runway Occupancy Time.

7.2 Reducing Runway Occupancy Time at Keflavík Airport

As mentioned in Chapter 5, the operator of Keflavík airport could reduce Runway Occupancy Time by modifying the runway exit system of the airport. Potential changes to the runway exit system include the construction of new runway exits. The predictive models of ROT, presented in Chapter 6, were used to assess the impact of these changes on ROT and drive optimal decisions. These predictive models were fed with the landing data observed at Keflavík airport during peak-hours and used the fleet-mix, weather conditions and gate locations observed in 2018 to assess potential changes.

To reduce the average Runway Occupancy Time during peak-hours, the characteristics of the current exit system of each runway were analyzed first. The current use and average Runway Occupancy Time of each available runway exit were measured during peak-hours using the database at Keflavík airport. These results were used to identify potential vectors of improvement to the runway exit system.

Second, the performance of the models in predicting the average use and Runway Occupancy Time for each exit in the current exit system was evaluated. The models were fed with landing data observed at Keflavík airport during peak-hours and predicted successively the exit use and Runway Occupancy Time per exit for each landing aircraft. Each landing operation was described by its aircraft type, approach speed, headwind, crosswind and temperature. The predicted values were then averaged over each exit and compared with actual observed data. This enabled the identification of potential discrepancies between predictions and observations. Any significant difference was then investigated by understanding what specificity of the operations at Keflavík airport was at the root of the discrepancy. This insight was sometimes provided by subject-matter experts such as air-traffic controllers, pilots and airport operators from Keflavík.

Third, a set of potential modifications to the runway exit system was developed using the understanding of the performance of the current exit system and the modifications envisioned by the airport operator. These changes include the implementation of new high-speed exits located to provide the most reduction in ROT and the implementation of exits corresponding to future taxiways planned by the airport operators. The locations of high-speed exits providing the most reduction in ROT were found by testing a range of potential locations. It was observed at US airports that high-speed exits were not located closer than 200m apart from each other and this constraint was used during the investigation of potential high-speed exit locations. To assess the impact of potential changes to the exit system, modified runway exit systems were fed to the predictive models. The models then predicted the exit use and Runway Occupancy Time per exit for each aircraft landing during peak-hours and included in the database. Average values of exit use and Runway Occupancy Time were aggregated for each modified exit system and compared to identify the modification providing the best reduction in ROT for the runway.

This process is detailed in the following four sections for each runway of Keflavík airport.

7.3 Reducing Runway Occupancy Time for Runway 28

7.3.1 Assessing the Performance of the Current Runway 28 Exit System

Runway 28 is a 3065m-long runway with an observed average Runway Occupancy Time of 65s during peak-hours. According to Figure 7-11, the exit system of this runway is composed of 3 different exits located at 828m (exit E), 2178m (exit B) and 3032m (exit K). While exits E and K are both right-angle exits (90°) enabling aircraft to vacate the runway on both sides of the runway, exit B is a high-speed exit leading the aircraft towards the main terminal.

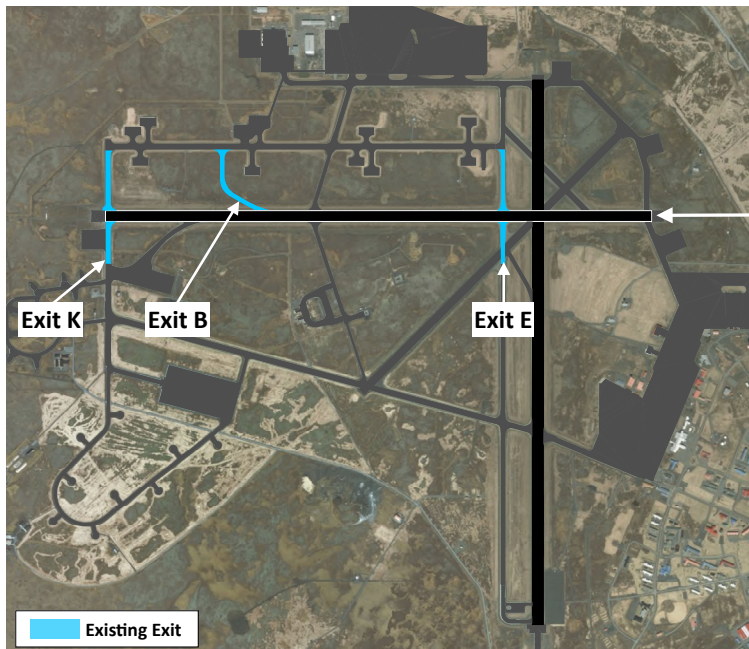


Figure 7-11: Exit system of runway 28

The landing data for runway 28 during peak-hours is made of 1245 landing observations. As shown in Table 7.6, aircraft use exit B in 96.1% of the cases while exits E and K are used in 0.7% and 3.2% respectively. The average Runway Occupancy Time measured for aircraft using exit B is 63s while aircraft using exit K have a 116s average ROT. The average Runway Occupancy Time value for exit E was not provided due to the small quantity of data available.

Table 7.6: Average exit use and Runway Occupancy Time observed for each exit of runway 28

Runway exit	Exit location, m	Exit angle, °	Exit use, %	Average ROT, s
E	828	90	0.7	-
B	2178	30	96.1	63
K	3032	90	3.2	116
				Total: 65

The use of exit B by the majority of landing aircraft indicates that some aircraft might be able to vacate the runway before exit B from a braking performance standpoint. The construction of high-speed exits located before exit B could help reduce the average Runway Occupancy Time.

7.3.2 Assessing the Performance of Predictive Models for Runway 28

To assess the validity of the predictive models for runway 28, exit use and average ROT predictions were computed for runway 28 in its current configuration using the landing data observed during peak-hour operations. As shown in Table 7.7, the predicted average Runway Occupancy Time of the runway was 61s which is close to the measured 65s. The predicted exit use and Runway Occupancy Time for each exit are consistent with the observations with exit B predicted to be used in 98.1% of the cases with an average Runway Occupancy Time of 60s. The use of exit E and K is also predicted to be very low with 1.0% exit use and 0.9% exit use respectively. The predicted average exit use and Runway Occupancy Time for each exit were used as reference values when assessing potential modifications of the exit system.

Table 7.7: Average exit use and Runway Occupancy Time predicted for each exit of runway 28

Runway exit	Exit location, m	Exit angle, °	Exit use, %		Average ROT, s	
			Observed	Predicted	Observed	Predicted
E	828	90	0.7	1.0	-	68
B	2178	30	96.1	98.1	63	60
K	3032	90	3.2	0.9	116	96
					Total: 65	Total: 61

The consistency of predicted results with actual observations proves the ability of the model to give reliable exit use and Runway Occupancy Time predictions for runway 28. The predictive models can be used with confidence in assessing the impact of runway exit system modifications on Runway Occupancy Time for runway 28.

7.3.3 Evaluating Modifications to the Current Runway 28 Exit System

To reduce the average Runway Occupancy Time of runway 28, the construction of high-speed exits (30°) was evaluated. Additional high-speed exits on runway 28 would potentially capture part of the traffic currently using exit B while providing a lower ROT.

Impact of an Additional High-Speed Exit

The location of a high-speed exit providing the best reduction in ROT was evaluated. Potential exits can be built between the current exit E and exit K as exits located before exit E would never be used. 40 evenly-separated potential exit locations were identified. In 7 cases, these locations are closer than 200m from the current high-speed exit B and a total of 33 feasible exit locations, depicted in Figure 7-12, ended-up being tested.

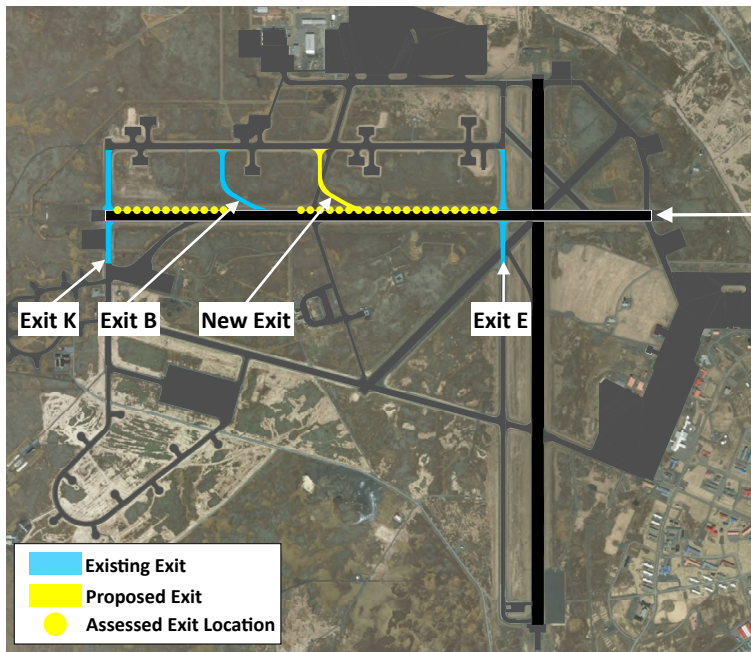


Figure 7-12: Potential new exit system for runway 28

For each location, a new runway exit system was fed to the predictive models and predictions of exit use and Runway Occupancy Time were made. The average Runway Occupancy Time of the runway was computed for each modified runway exit system. As shown in Figure 7-13, depicting the evolution of the average ROT of the runway depending on the location of the new high-speed exit, a new high-speed exit located around 1635m would provide the most ROT reduction with an 11s decrease.

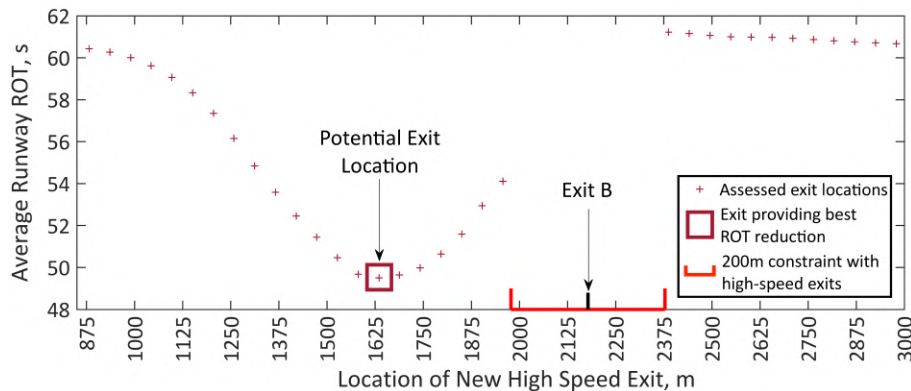


Figure 7-13: Average Runway Occupancy Time of runway 28 depending on new high-speed exit location

This location, depicted in Figure 7-12, is the result of a trade-off between how much traffic is able to use the exit and how low the Runway Occupancy Time provided by the new exit is.

As shown in Table 7.8, assuming the new high-speed exit, the traffic is now split between the current exit B, capturing 33.2% of the traffic and the new exit, capturing 65.5% of the traffic. The traffic using the new exit has however a lower Runway Occupancy Time compared to aircraft using exit B with a 45s average ROT, versus a 58s average ROT for exit B. This reduces the overall Runway Occupancy Time of the runway.

Table 7.8: Average exit use and Runway Occupancy Time predicted for each exit of runway 28 with additional high-speed exit

Runway exit	Exit location, m	Exit angle, °	Exit use, %		Average ROT, s	
			Old	New	Old	New
E	828	90	1.0	0.6	68	66
New exit	1635	30	-	65.5	-	45
B	2178	30	98.1	33.2	60	58
K	3032	90	0.9	0.7	96	90
					Total: 61	Total: 50

Impact of Two Additional High-Speed Exits

While an additional high-speed exit provides a significant reduction in Runway Occupancy Time, implementing a second additional high-speed exit may reduce the average Runway Occupancy Time of runway 28 even more. The location of the first additional high-speed exit was frozen at 1635m and the ROT impact of a second new high-speed exit (30°) on top was assessed.

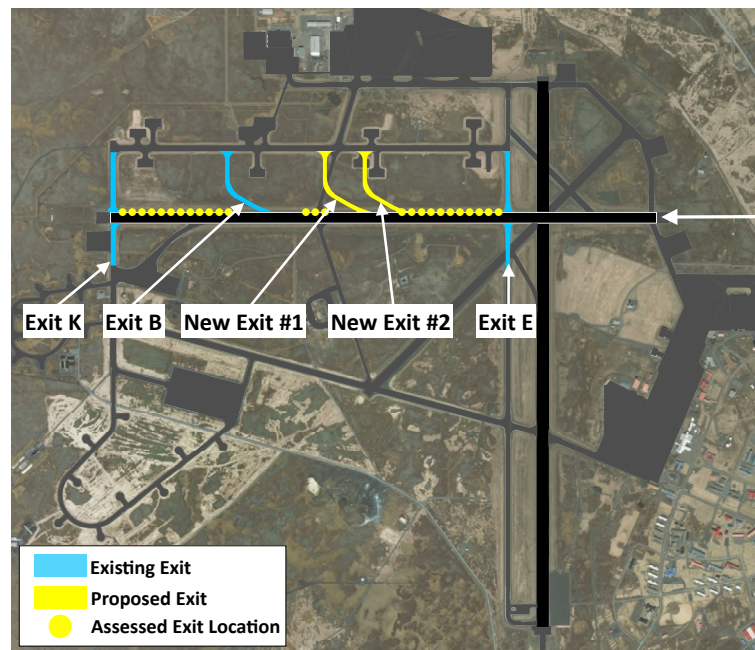


Figure 7-14: Potential new exit system for runway 28

The location of this second high-speed exit needed to be optimized as well and a set of 40 potential locations between exit E and exit K was designed. It was restrained to 26 locations located more than 200m away from the two assumed high-speed exits, depicted in Figure 7-14.

The average Runway Occupancy Time of the runway was predicted for each modified runway exit system and the exit location providing the best reduction in average ROT was identified around 1420m. According to Figure 7-15, this new exit would provide a total 15s decrease in Runway Occupancy Time.

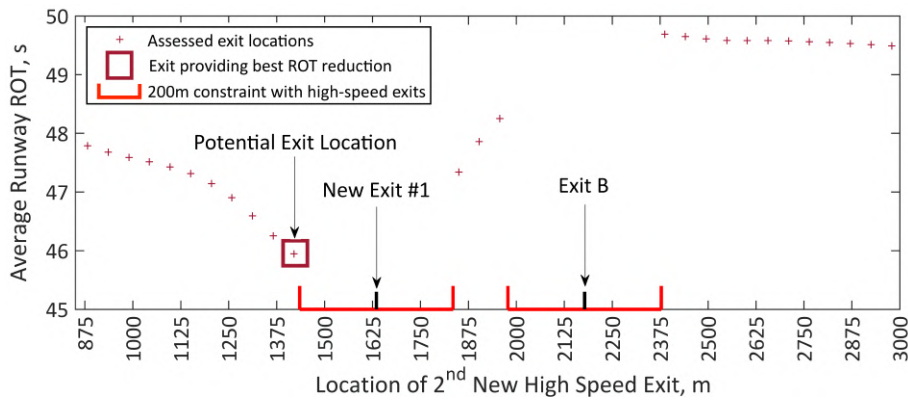


Figure 7-15: Average ROT of runway 28 depending on 2nd new high-speed exit location

When looking at the distribution of exit use, presented in Table 7.9, it was observed that the two new designed high-speed exits are used by a total of 80.5% of the aircraft while exit B now only captures 17.8% of the traffic in this configuration. These exits also provide a lower Runway Occupancy Time which decreases the average Runway Occupancy Time of the runway.

Table 7.9: Average exit use and Runway Occupancy Time predicted for each exit of runway 28 with a 2nd additional high-speed exit

Runway exit	Exit location, m	Exit angle, °	Exit use, %		Average ROT, s	
			Old	New	Old	New
E	828	90	1.0	0.5	68	61
New exit 2	1420	30	-	21.0	-	40
New exit 1	1635	30	-	59.5	-	44
B	2178	30	98.1	17.8	60	56
K	3032	90	0.9	1.2	96	95
					Total: 61	Total: 46

It is noted that the locations of the two new high-speed exits mentioned previously were successively optimized. A simultaneous optimization of the two exit locations was also tested and provided very similar locations for the two additional high-speed exits. These would have been located at 1366m and 1581m respectively and would provide an average Runway Occupancy Time of 45.7s for the runway according to Table 7.10.

Table 7.10: Average exit use and Runway Occupancy Time predicted for each exit of runway 28 with two simultaneously optimized additional high-speed exits

Runway exit	Exit location, m	Exit angle, °	Exit use, %		Average ROT, s	
			Old	New	Old	New
E	828	90	1.0	0.5	68	61
New exit	1366	30	-	15.2	-	38
New exit	1581	30	-	62.0	-	42
B	2178	30	98.1	20.9	60	57
K	3032	90	0.9	1.5	96	95
					Total: 61	Total: 45.7

7.4 Reducing Runway Occupancy Time for Runway 19

7.4.1 Assessing the Performance of the Current Runway 19 Exit System

Runway 19 is a 3054m-long runway with an observed average Runway Occupancy Time of 65s. According to Figure 7-16, the exit system of this runway is made of 4 different exits located at 765m (RWY 10/28), 1214m (exit A), 1963m (exit S) and 3028m (exit E). While RWY10/28 and exit E both make a 90° angle with the runway axis, exit S has a 105° angle towards the west and a 75° towards the east and exit A is an opposite high-speed exit (150°).

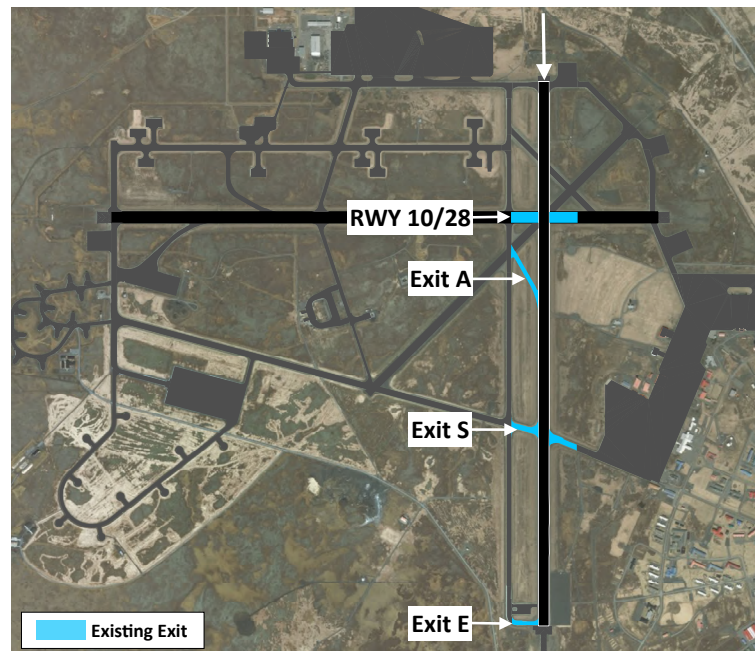


Figure 7-16: Exit system of runway 19

The landing data for runway 19 during peak-hours consists of 3967 landing observations. As

shown in Table 7.11, 98.2% of aircraft use exit S while exits A, E and RWY10/28 are rarely used. The average Runway Occupancy Time measured for aircraft using exit S was 63s while aircraft vacating the runway using exit E had a 110s average ROT. The average Runway Occupancy Time values for exit A and for runway 10/28 were not provided because of limited data.

Table 7.11: Average exit use and Runway Occupancy Time observed for each exit of runway 19

Runway exit	Exit location, m	Exit angle, °	Exit use, %	Average ROT, s
10/28	765	90	0.2	-
A	1214	150	0.2	-
S	1963	105/75	98.2	63
E	3028	90	1.4	110
				Total: 65

The use of exit S by the majority of landing aircraft indicates that some aircraft are able to vacate the runway before exit S from a braking performance standpoint. The construction of new high-speed exits located before exit S could help reduce the average ROT.

7.4.2 Assessing the Performance of Predictive Models for Runway 19

To assess the validity of the predictive models for runway 19, exit use and average ROT predictions were computed for runway 19 in its current configuration using the landing data observed during peak-hour operations. As shown in Table 7.12, the predicted average ROT of the runway was 61s which is close to the measured 65s. The average use and ROT for each runway exit were aggregated and compared to the actual observed values. According to Table 7.12, the predicted distribution of exit use does not match the observed distribution.

Table 7.12: Average exit use and Runway Occupancy Time predicted for each exit of runway 19

Runway exit	Exit location, m	Exit angle, °	Exit use, %			Average ROT, s		
			Observed	Predicted		Observed	Predicted	
				w/ A	w/o A		w/ A	w/o A
10/28	765	90	0.2	1.5	0.6	-	76	58
A	1214	150	0.2	13.1	0	-	52	-
S	1963	105/75	98.2	84.6	98.5	63	62	62
E	3028	90	1.4	0.8	0.9	110	89	95
						65	61	62

The main discrepancy concerns exit A, capturing 13.1% of the aircraft in the predictions while gathering 0.2% of the use in the observations. This discrepancy between the model predictions and the observations can be explained by local pilot behavior regarding the use of high angle runway exits (above 90°). These high angle runway exits are sometimes used in the US to vacate the runway while pilots prefer not to use them at Keflavík airport, according to pilots from a major airline operating at Keflavík. To account for this local behavior, exit A was removed

from the exit system fed to the predictive models and a new set of predictions was computed. According to Table 7.12, this new set of predictions was this time consistent with the observed exit use and average Runway Occupancy Time for each exit. The average ROT predicted by the models for runway 19 with exit A dismissed from the exit system is equal to 62s.

The consistency of predicted results, obtained by ignoring exit A, with actual observations proves the ability of the model to give reliable exit use and ROT predictions for runway 19. The predictive models can be used with confidence to assess the impact of runway exit system modifications on ROT and exit A was removed from all runway exit systems assessed later.

7.4.3 Evaluating Modifications to the Current Runway 19 Exit System

Exit S currently captures the majority of the traffic vacating runway 19 but provides a high ROT due to its large exit angle. A reduction in ROT could be achieved by building new high-speed exits to share the traffic with the current exit S while providing lower ROT.

Impact of an Additional High-Speed Exit

Implementing an additional high-speed exit could help reduce the Runway Occupancy Time of runway 19. A set of 40 evenly-separated potential exit locations, ranging from RWY10/28 to exit E, was identified and is depicted in Figure 7-17.

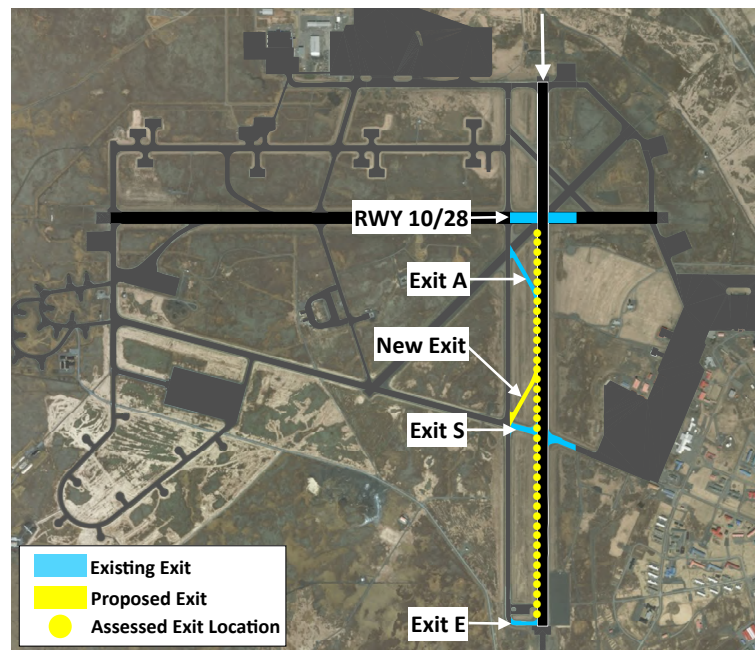


Figure 7-17: Potential new exit system for runway 19

These locations do not conflict with any existing high-speed exit (200m constraint) and the predictive models were used to assess the 40 resulting modified exit systems. According to Figure 7-18, an exit location providing the best ROT reduction was found at 1609m.

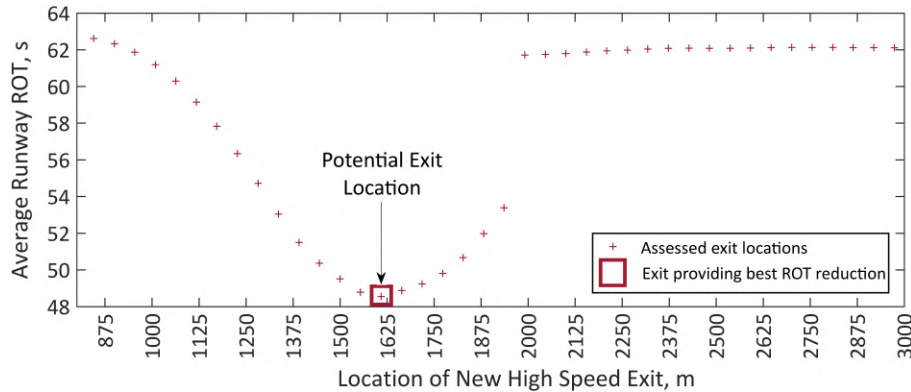


Figure 7-18: Average Runway Occupancy Time of runway 19 depending on new high-speed exit location

This new high-speed exit, depicted in Figure 7-17, would provide a 13s decrease in Runway Occupancy Time. According to Table 7.13, this exit would capture 72.4% of the traffic while exit S would be used by 26.4% of the aircraft.

Table 7.13: Average exit use and Runway Occupancy Time predicted for each exit of runway 19 with an additional high-speed exit

Runway exit	Exit location, m	Exit angle, °	Exit use, %		Average ROT, s	
			Old	New	Old	New
10/19	765	90	0.6	0.4	58	58
A	1214	150	0	0	-	-
New exit	1609	30	-	72.4	-	44
S	1963	105/75	98.5	26.4	62	60
E	3028	90	0.9	0.8	95	92
					Total: 62	Total: 49

7.5 Reducing Runway Occupancy Time for Runway 01

7.5.1 Assessing the Performance of the Current Runway 01 Exit System

Runway 01 is a 3054m-long runway with an observed average Runway Occupancy Time of 90s. According to Figure 7-19, the current exit system of this runway is made of 5 different exits located at 1079m (exit S), 1828m (exit A), 2277m (RWY10/28), 2611m (exit K) and 3021m (exit N). While RWY10/28 and exit N both make a 90° angle with the runway axis, exit S has a 75° angle towards the west and a 105° towards the east. Exit A is a high-speed exit (30°) and exit K has a 45° angle.

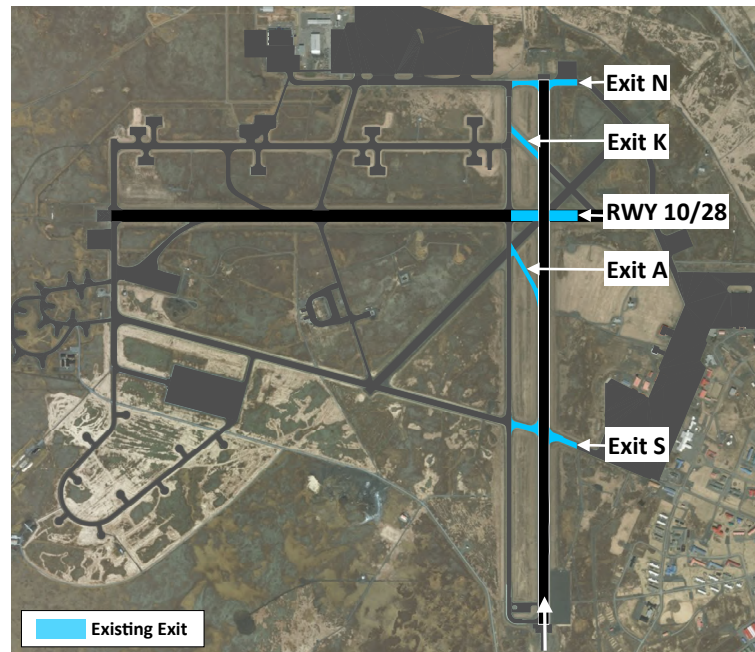


Figure 7-19: Exit system of runway 01

The landing data for runway 01 during peak-hours consists of 3982 landing observations. As shown in Table 7.14, the exit use observed on runway 01 is very singular with traffic mainly split between exit A (20.7%), exit K (24.4%) and exit N (50.7%).

Table 7.14: Average exit use and Runway Occupancy Time observed for each exit of runway 01

Runway exit	Exit location, m	Exit angle, °	Exit use, %	Average ROT, s
S	1079	75/105	0.7	-
A	1828	30	20.7	52
10/28	2277	90	3.5	77
K	2611	45	24.4	83
N	3021	90	50.7	109
				Total: 90

Exit A seems to be underused according to its characteristics while exit N and K are overused based on their locations. This can be explained by two main factors. First, exit K and exit N provide good connection and lower taxi-time to the main terminal location. Aircraft might be incentivized to run further down the runway and use exits K and N to minimize their taxi-time to gate. Second, the use of exit A is restrained by some taxiing flow pattern observed at Keflavík. According to the airport operator, when runway 01 is active, it is simultaneously used for take-offs and landings. Departing aircraft use the parallel taxiway to taxi down to the threshold of

runway 01 and prevent landing aircraft from using exit A and in some cases exit K. Reducing the interaction between departing and arriving aircraft through taxiway modifications may increase the use of exits A and K and reduce the overall ROT of runway 01. Extra modifications of the runway exit system could be envisioned as well to reduce Runway Occupancy Time such as the implementation of additional high-speed exits.

7.5.2 Assessing the Performance of Predictive Models for Runway 01

To assess the validity of the predictive models for runway 01, exit use and average ROT predictions were computed for runway 01 in its current configuration using the landing data observed during peak-hour. As shown in Table 7.15, the predicted average Runway Occupancy Time of the runway was 63s which is very different from the measured 90s. The predicted average use and Runway Occupancy Time for each exit are also different from the observations.

Table 7.15: Average exit use and Runway Occupancy Time predicted for each exit of runway 01

Runway exit	Exit location, m	Exit angle, °	Exit use, %		Average ROT, s	
			Observed	Predicted	Observed	Predicted
S	1079	75/105	0.7	1.1	-	44
A	1828	30	20.7	46.7	52	51
10/28	2277	90	3.5	3.7	77	73
K	2611	45	24.4	47.2	83	73
N	3021	90	50.7	1.3	109	99
					Total: 90	Total: 63

First exit A is predicted to be used in 46.7% of the cases, compared to the 20.7% observed in real-life operations. This discrepancy is expected as the predictive models are not aware of the interaction between departing and arriving aircraft on the adjacent taxiway, restraining the use of exit A.

The predictive models however capture the high use of exits located close to the gates and predict exit K to be used in 47.2% of the cases as providing a fast-connection to the terminal. This is not happening in the observations because exit K is constrained as well by the departing aircraft and landing aircraft use exit N instead.

The predicted average exit use and Runway Occupancy Time values, listed in Table 7.15, can be considered as representative of what would be observed on runway 01 if the use of exits A and K wasn't constrained by departing aircraft taxiing to the threshold.

7.5.3 Evaluating Modifications to the Current Runway 01 Exit System

As mentioned in the previous section, reducing the interaction between departing and arriving aircraft when runway 01 is active may increase the use of exit A and K and reduce ROT. This can be done by implementing a bypassing taxiway, parallel to the current taxiway E. The impact of implementing such a bypassing taxiway is first assessed in the following section. Assuming that

the bypassing taxiway is built, the influence on ROT of other modifications to the runway exit system, such as the implementation of additional high-speed exits, is then evaluated.

Impact of a Bypassing Taxiway

To prevent departing aircraft, taxiing towards the threshold of runway 01, from interacting with landing aircraft willing to vacate the runway using exit A or exit K, the implementation of a bypassing taxiway, parallel to taxiway E is considered by the airport operators. This alternative taxiway is depicted in Figure 7-20 and would be used by departing aircraft. The objective of implementing this taxiway is to significantly increase the use of exit A which currently has a lower average Runway Occupancy Time compared to exit K and N. This would reduce the overall Runway Occupancy Time of runway 01.

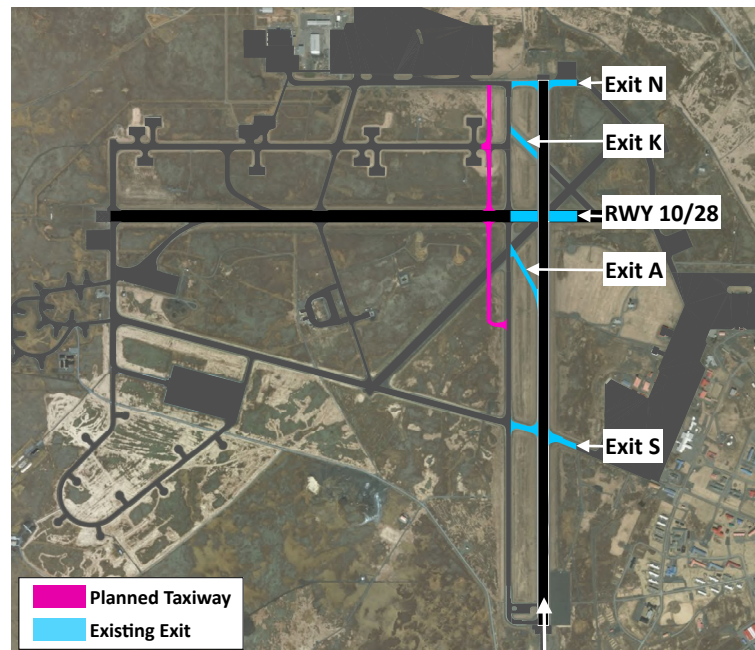


Figure 7-20: Exit system of runway 01 with planned taxiway

It can be assumed that the previously predicted values of exit use and average ROT for each exit are representative of what would be observed on runway 01 with a bypassing taxiway implemented. According to the model predictions, presented in Table 7.16, the average Runway Occupancy Time would be decreased by 27s. This significant decrease would be due to an increase use of exit A (46.7%) and exit K (47.2%). Exit N on the other side would be used less than observed currently.

By assuming that this bypassing taxiway is implemented, additional modifications to the current exit system can be proposed to further reduce the ROT of runway 01.

Table 7.16: Average exit use and Runway Occupancy Time predicted for each exit of runway 01 with a bypassing taxiway

Runway exit	Exit location, m	Exit angle, °	Exit use, %		Average ROT, s	
			Old	New	Old	New
S	1079	75/105	0.7	1.1	-	44
A	1828	30	20.7	46.7	52	51
10/28	2277	90	3.5	3.7	77	73
K	2611	45	24.4	47.2	83	73
N	3021	90	50.7	1.3	109	99
					Total: 90	Total: 63

Impact of an Additional High-Speed Exit

Implementing an additional high-speed exit may further reduce the Runway Occupancy Time of runway 01. A set of 40 evenly-separated potential exit locations, ranging from exit S to exit N, was identified. This set was restrained to 31 feasible exits, given the the 200m separation constraint with the existing high-speed exit A. These exits are depicted in Figure 7-21.

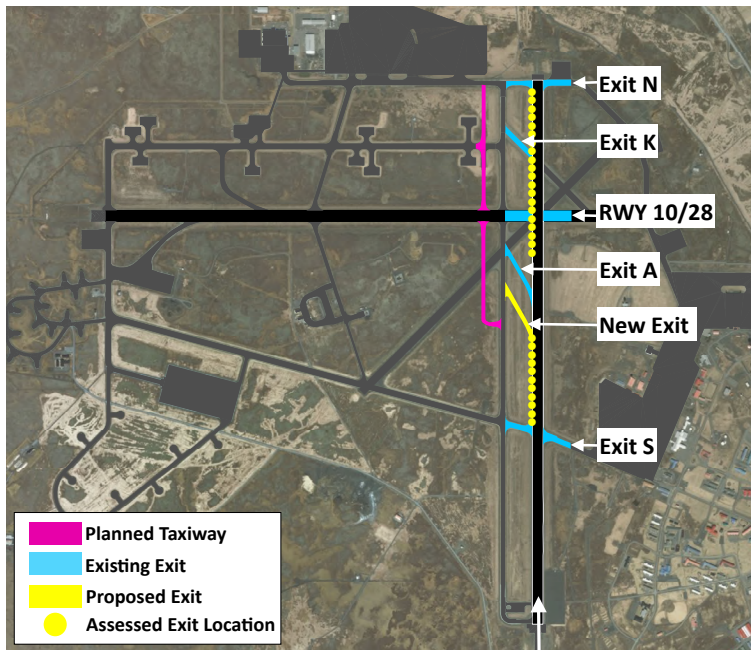


Figure 7-21: Potential new exit system for runway 01

The predictive models were used to assess the 31 resulting runway exit systems. According to Figure 7-22, an exit located at 1600m would provide the best reduction in average ROT.

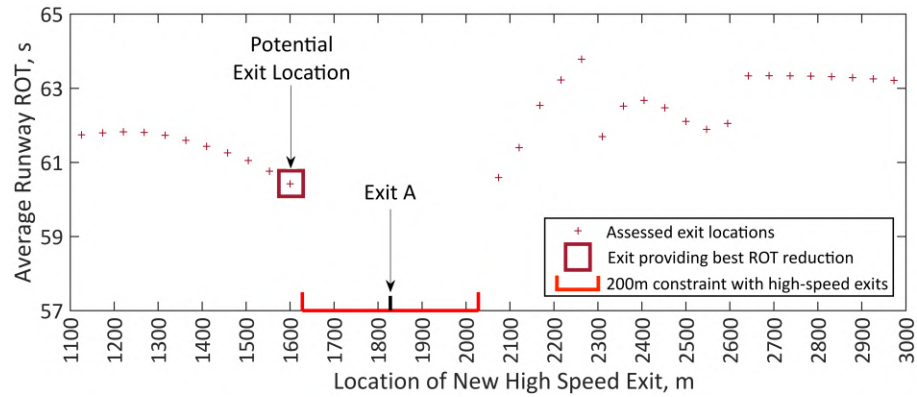


Figure 7-22: Average Runway Occupancy Time of runway 01 depending on new high-speed exit location

This new high-speed exit, depicted in Figure 7-21, would provide a total 30s decrease in average Runway Occupancy Time. According to Table 7.17, this exit would capture only 11.3% of the traffic while exit A would be used by 41.1% of the aircraft and 41.2% of the aircraft would use exit K.

Table 7.17: Average exit use and Runway Occupancy Time predicted for each exit of runway 01 with new high-speed exit

Runway exit	Exit location, m	Exit angle, °	Exit use, %		Average ROT, s	
			Old	New	Old	New
S	1079	75/105	0.7	0.7	-	45
New exit	1600	30	-	11.3	-	45
A	1828	30	20.7	41.1	52	50
10/28	2277	90	3.5	4.7	77	73
K	2611	45	24.4	41.2	83	73
N	3021	90	50.7	1.0	109	98
					Total: 90	Total: 60

This additional low reduction in ROT, compared to the sole implementation of a bypassing taxiway, is due to the low incentive for pilots to vacate the runway as soon as possible. Even though well-located exits are available and could be used by aircraft from a braking performance standpoint, pilots are willing to use the exits minimizing their taxi-time to gate. For runway 01, these exits are exit N and exit K. A change in pilot behavior at Keflavík airport may provide significant Runway Occupancy Time reduction and the predictive models were used to demonstrate this.

Impact of a Pilot Incentive to Vacate the Runway Early

A better incentive for pilots to vacate runway 01 as soon as possible can be simulated by creating a virtual gate location at the midpoint of the runway as per Figure 7-23. With this gate location, pilots would be motivated to exit earlier and not keep on running down the runway.

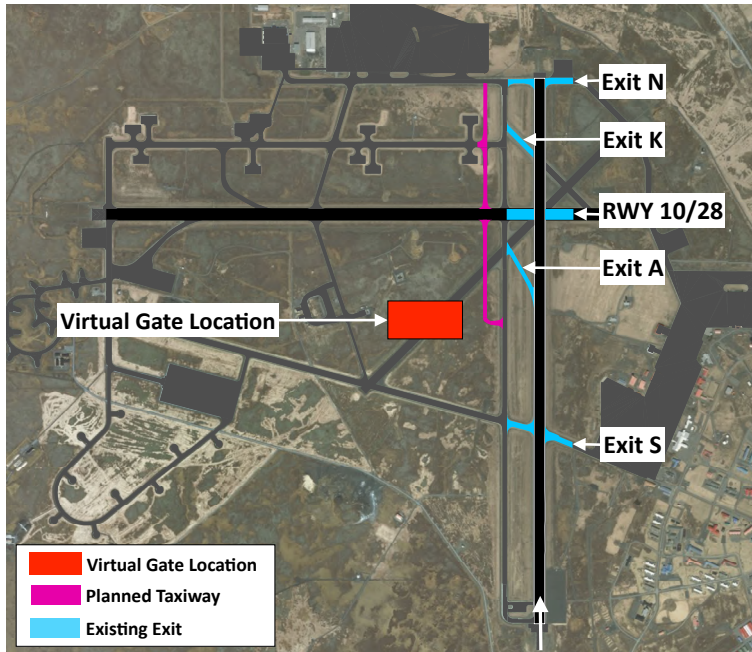


Figure 7-23: Exit system of runway 01 with pilot incentive to exit early

The predictive models were used to predict the exit use and ROT of each exit of the current exit system with aircraft virtually going to the simulated gate. The presence of the bypassing taxiway was still assumed in this case. According to Table 7.18, the predicted ROT for runway 01 with an incentive to vacate the runway early is equal to 51s. This is 39s lower than the currently observed ROT. With an incentive to vacate early, pilot would use exit A in 91.6% with a Runway Occupancy Time of 50s.

Table 7.18: Average exit use and Runway Occupancy Time predicted for each exit of runway 19 with pilot incentive to vacate the runway early

Runway exit	Exit location, m	Exit angle, °	Exit use, %		Average ROT, s	
			Old	New	Old	New
S	1079	75/105	0.7	0.6	-	45
A	1828	30	20.7	91.6	52	50
10/28	2277	90	3.5	3.1	77	68
K	2611	45	24.4	4.4	83	69
N	3021	90	50.7	0.3	109	94
					Total: 90	Total: 51

Impact of an Additional High-Speed Exit with a Pilot Incentive to Vacate Early

The average ROT of runway 01 may be significantly reduced by incentivizing pilot to exit as early as possible. With this incentive, adding another high-speed exit on runway 01 may further reduce Runway Occupancy Time. The same process of testing 31 different high-speed exit locations, presented in Section 7.5.3 was repeated with the incentive to exit the runway early. This incentive was still simulated with the presence of a virtual gate location. According to Figure 7-24, a high-speed exit located at 1553m would provide the best ROT reduction. Assuming the implementation of this new exit and of the bypassing taxiway and a pilot incentive to exit early, the average ROT would be decreased to 48s, down by 42s compared to the current measured ROT.

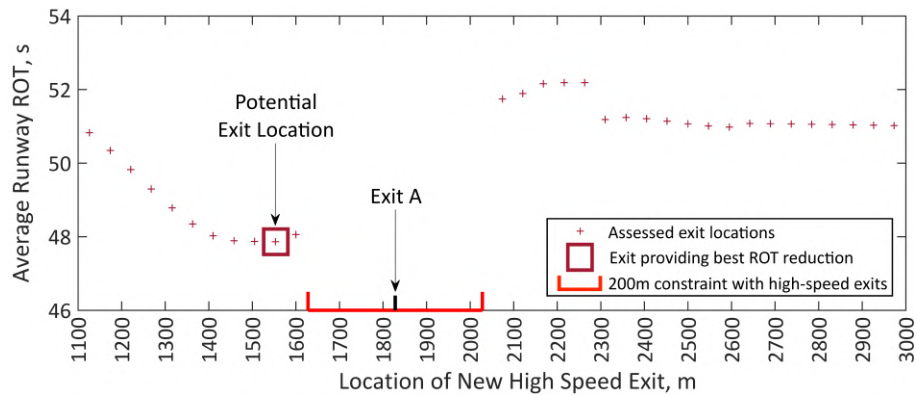


Figure 7-24: Average Runway Occupancy Time of runway 01 depending on new high-speed exit location with pilot incentive to vacate the runway early

As shown in Table 7.19, the new exit would capture 41.3% of the traffic while exit A would be used by 50.3% of the aircraft. This is significantly more than in the previous parametric test.

Table 7.19: Average exit use and Runway Occupancy Time predicted for each exit of runway 01 with new high-speed exit and pilot incentive

Runway exit	Exit location, m	Exit angle, °	Exit use, %		Average ROT, s	
			Old	New	Old	New
S	1079	75/105	0.7	0.3	-	45
New exit	1553	30	-	41.3	-	44
A	1828	30	20.7	50.3	52	48
10/28	2277	90	3.5	1.9	77	67
K	2611	45	24.4	5.9	83	71
N	3021	90	50.7	2.7	109	92
					Total: 90	Total: 48

7.6 Reducing Runway Occupancy Time for Runway 10

7.6.1 Assessing the Performance of the Current Runway 10 Exit System

Runway 10 is a 3065m-long runway with an observed average Runway Occupancy Time of 80s. As depicted in Figure 7-25, the exit system of this runway is made of 3 different right-angle exits located at 2200m (exit E), 2412m (RWY 01/19) and 3019m (exit N).

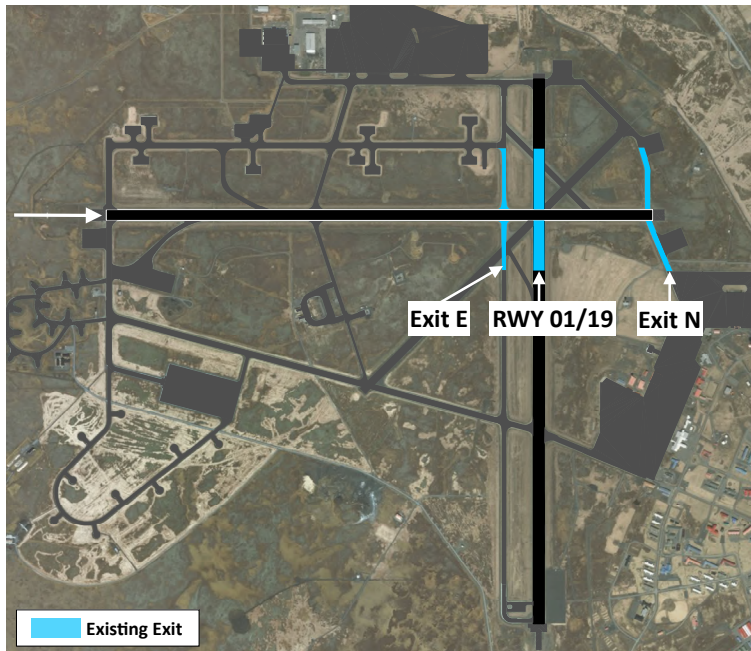


Figure 7-25: Exit system of runway 10

The landing data for runway 10 during peak-hours is made of 4092 landing observations. As show in Table 7.20, 95.5% of the aircraft use exit E to vacate the runway while exits N and RWY 01/19 are rarely used. These three exits have however a high average ROT , above 70s, due to their location and 90° angle.

Table 7.20: Average exit use and Runway Occupancy Time observed for each exit of runway 10

Runway exit	Exit location, m	Exit angle, °	Exit use, %	Average ROT, s
E	2220m	90	95.5	79
01/19	2412m	90	2.7	84
N	3019	90/70	1.8	123
				Total: 80

The use of exit E by the majority of aircraft indicates that some aircraft are able to vacate the runway before E from a braking performance perspective. The construction of high-speed

exits before exit E could capture part of the traffic currently using E while reducing the ROT of landing aircraft.

7.6.2 Assessing the Performance of Predictive Models for Runway 10

To assess the validity of the predictive models for runway 10, exit use and average ROT predictions were computed for runway 10 in its current configuration using the landing data observed during peak-hour operations. As shown in Table 7.21, the predicted average Runway Occupancy Time of the runway was 71s which is slightly lower than the measured 80s. The predicted exit use are however very consistent with the observed values.

Table 7.21: Average exit use and Runway Occupancy Time predicted for each exit of runway 10

Runway exit	Exit location, m	Exit angle, °	Exit use, %		Average ROT, s	
			Observed	Predicted	Observed	Predicted
E	2220m	90	95.5	94.8	79	70
01/19	2412m	90	2.7	2.7	84	74
N	3019	90/70	1.8	2.5	123	96
					Total: 80	Total: 71

The lower ROT values predicted by the model are not concerning as they are associated to exits located far from the runway threshold. A large variability in braking behavior can be observed for aircraft reaching these exits and predicting precise average ROT for these exits is hard. The predicted values of exit use and average ROT were used as reference values and the impact of potential modifications to the exit system was assessed relatively to them.

7.6.3 Evaluating Modifications to the Current Runway 10 Exit System

As mentioned in Section 7.5.1, a potential additional taxiway, parallel to runway 01/19 is planned by the operator of Keflavík airport to alleviate taxiing conflicts between aircraft departing and arriving when runway 01 is active. This taxiway, depicted in pink in Figure 7-20, would represent an additional right-angle exit for runway 10, located just before the current exit E. The impact on ROT of this modification to the runway exit system was assessed first. Assuming this new right-angle exit, the implementation of additional high-speed exits were then evaluated.

Impact of a New Exit Corresponding to the Bypassing Taxiway for Runway 01

As shown in Figure 7-26, the bypassing taxiway for runway 01 would correspond to a right-angle exit located at 2110m just before exit E.

According to the predictive models, such a taxiway would reduce the average ROT by 4s. As detailed in Table 7.22, this new exit would capture most of the traffic (91.2%) while exit E would be used in 4.4% of the cases. Because the new exit would be located earlier compared to exit E, its average ROT would be 3s lower, decreasing the overall ROT of the runway.

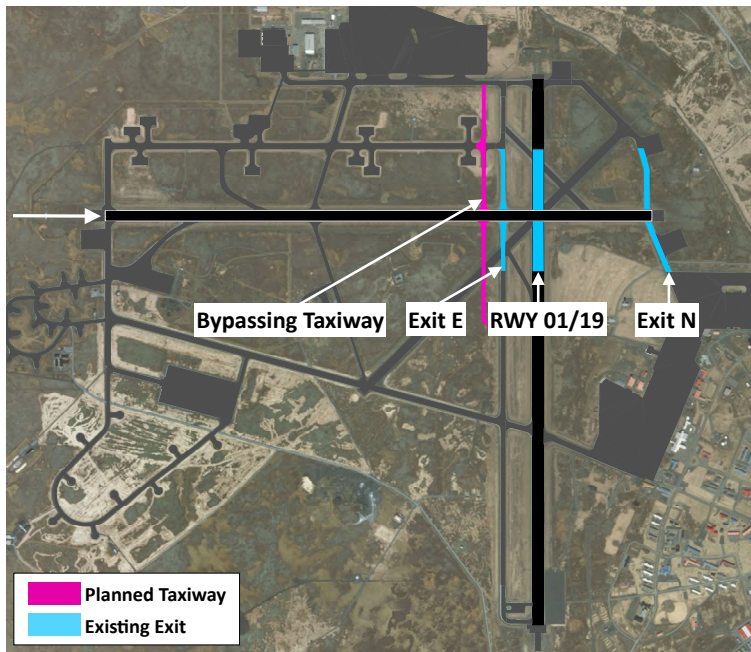


Figure 7-26: Potential new exit system for runway 10

Table 7.22: Average exit use and Runway Occupancy Time predicted for each exit of runway 10 with new right-angle exit

Runway exit	Exit location, m	Exit angle, °	Exit use, %		Average ROT, s	
			Old	New	Old	New
New taxiway	2110m	90	-	91.2	-	66
E	2220m	90	94.8	4.4	70	69
01/19	2412m	90	2.7	3.3	74	79
N	3019	90/70	2.5	1.1	96	98
					Total: 71	Total: 67

This modification of the current exit system reduces the average ROT of runway 10 marginally. Adding an additional high-speed exit could help further reduce ROT.

Impact of a New High-Speed Exit in Addition to the Planned Taxiway

To find the location of a new high-speed exit that would provide the lowest average ROT for runway 10, a set of 22 evenly-spaced locations, ranging from exit B to the new taxiway was identified. These locations are depicted in Figure 7-27 and do not conflict with any existing high-speed exit (200m constraint). Assuming that the bypassing taxiway was implemented, the resulting modified exit systems were assessed using the predictive models.

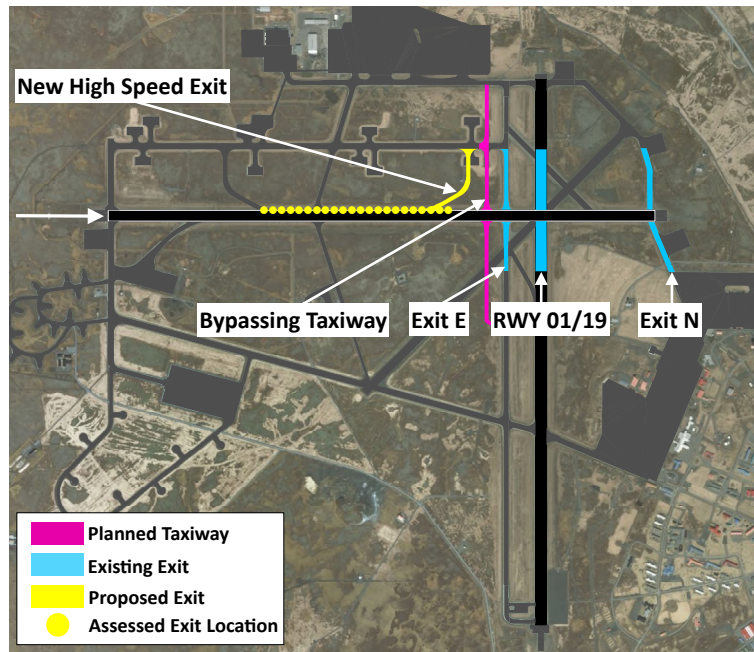


Figure 7-27: Potential new exit system for runway 10

According to Figure 7-28, a high-speed exit located at 1800m would provide the best ROT reduction with a 17s decrease in average ROT.

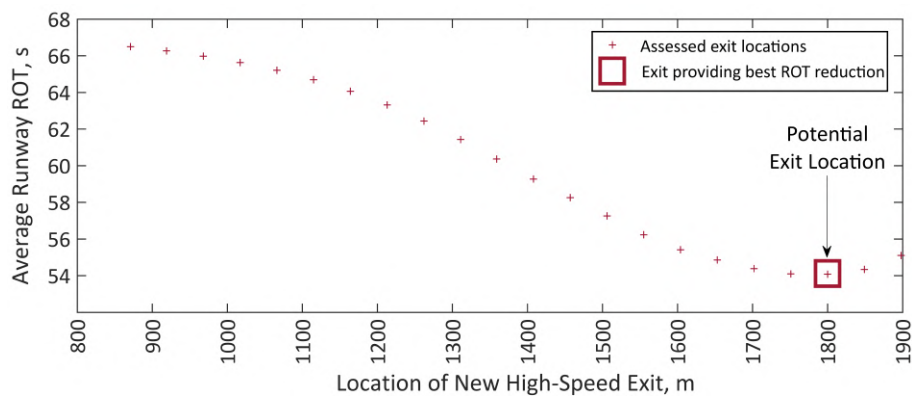


Figure 7-28: Average Runway Occupancy Time of runway 10 depending on new high-speed exit location

According to Table 7.23, in this scenario, the new high-speed exit would capture 72.3% of the traffic with an ROT of 49s while the two following exits would capture 24.1% of the traffic combined with an average ROT around 65-67s.

Table 7.23: Average exit use and Runway Occupancy Time predicted for each exit of runway 10 with new taxiway and additional high-speed exit

Runway exit	Exit location, m	Exit angle, °	Exit use, %		Average ROT, s	
			Old	New	Old	New
New exit	1800m	30	-	72.3	-	49
New taxiway	2110m	90	-	14.4	-	65
E	2220m	90	94.8	9.7	70	67
01/19	2412m	90	2.7	2.3	74	75
N	3019	90/70	2.5	1.3	96	98
					Total: 71	Total: 54

As per Figure 7-28, the average predicted ROT is not very sensitive to exit location in the surroundings of the best location found. A high-speed exit located between 1650m and 1900m would provide a decrease of 16 to 17s in overall ROT. This gives flexibility to the airport operator to locate the high-speed exit closer to the planned taxiway. Having the high-speed exit and the new taxiway directly connected would simplify the runway exit system. If airport operators were to add a new high-speed exit coupled to the planned taxiway, this exit would be located at 1890m, depicted in Figure 7-29.

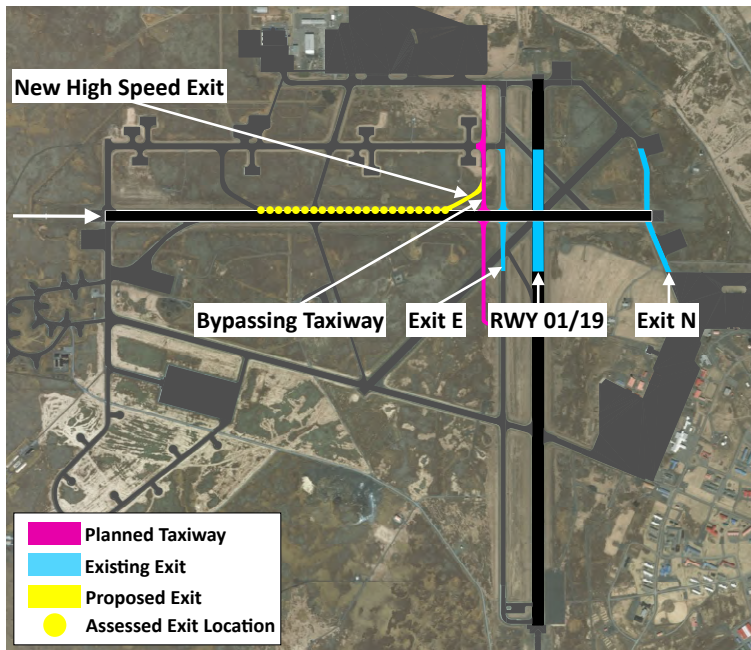


Figure 7-29: Potential new exit system for runway 10

Adding this coupled high-speed exit would reduce the average ROT of the runway by 16s according to predictive models. As detailed in Table 7.24, in this scenario, the new high-speed exit would capture 79.1% of the traffic with an ROT of 51s while the two following exits would capture 17.9% of the traffic combined with an average ROT around 65-67s.

Table 7.24: Average exit use and Runway Occupancy Time predicted for each exit of runway 10 with new taxiway and coupled high-speed exit

Runway exit	Exit location, m	Exit angle, °	Exit use, %		Average ROT, s	
			Old	New	Old	New
New exit	1890m	30	-	79.1	-	51
New taxiway	2110m	90	-	10.7	-	65
E	2220m	90	94.8	7.2	70	67
o1/19	2412m	90	2.7	1.8	74	76
N	3019	90/70	2.5	1.2	96	98
					Total: 71	Total: 55

This new runway exit system configuration with both the new taxiway and a coupled high-speed exit provides a relatively good reduction of ROT for runway 10.

7.7 Summary of Potential Modifications to the Exit System

The impact on ROT of several modifications to the exit system of each runway was evaluated in the previous sections. Table 7.25 summarizes the potential modifications that were assessed and presents their impact on the average ROT.

Table 7.25: Predicted reductions in average ROT with potential modifications

Runway	Modification	Average ROT, s	ROT reduction, s
28	Current exit system	61	-
	Adding a high-speed exit	50	-11
	Two successively optimized high-speed exits	46	-15
	Two simultaneously optimized high-speed exits	45.7	-15.3
19	Current exit system	62	-
	Adding a high-speed exit	49	-13
o1	Current exit system	90	-
	Current exit system with additional bypassing taxiway	63	-27
	Adding a high-speed exit and a bypassing taxiway	60	-30
	Incentivizing pilots to exit earlier and adding a bypassing taxiway	51	-39
	Incentivizing pilots to exit earlier, adding a bypassing taxiway and a high-speed exit	48	-42
10	Current exit system	71	-
	Adding an exit corresponding to the bypassing taxiway	67	-4
	Adding an exit corresponding to the bypassing taxiway and a high-speed exit	54	-17
	Adding an exit corresponding to the bypassing taxiway and a coupled high-speed exit	55	-16

For runway 28, three different modifications to the runway exit system were assessed. According to Table 7.25, adding two additional high-speed exits offers the best reduction in Runway Occupancy Time with a total 15s reduction. Optimizing the locations of these two additional high-speed exits successively or simultaneously is equivalent and result in similar exit locations. This 15s total ROT reduction is slightly more than the 11s reduction provided by adding only one high-speed exit.

For runway 19, a single modification to the runway exit system was assessed. As shown in Table 7.25, adding an additional high-speed exit at a good location appears to be a feasible solution providing a 13s reduction in ROT.

For runway 01, the impact of four changes to the exit system and pilot behavior were assessed. According to Table 7.25, adding the planned bypassing taxiway would reduce ROT from 90s to 63s. Adding another high-speed exit on top would provide little additional ROT reduction. Incentivizing pilots to exit as early as possible on runway 01 may on the other hand provide better ROT reduction with a 12s additional decrease in average ROT. Once pilots show more willingness to vacate early, the airport operator could envision adding an optimal high-speed exit, which would provide an additional 3s ROT reduction.

For runway 10, the impact of three changes to the exit system were assessed. According to Table 7.25, adding an exit corresponding to the bypassing taxiway of runway 01 will marginally reduce ROT. Adding an additional high-speed exit could help further reduce ROT by a total of 16 to 17s. This high-speed exit can be located at a location providing the best ROT reduction or coupled with the bypassing taxiway. These two different options provide almost the same ROT reduction and correspond to very similar locations for the additional high-speed exit.

A summary of the modifications of the exit system providing the best ROT reduction for each runway of Keflavík airport is depicted in Figure 7-30. The proposed modifications are described by their associated reduction in average Runway Occupancy Time for each considered runway. The proposed changes may reduce the average ROT below 50s for runway 19 and runway 28. For runway 01, they should be associated with a greater incentive for pilots to vacate the runway early to provide a significant reduction of ROT. With these modifications, the predicted average Runway Occupancy Time during peak hours for Keflavík airport would be reduced by 23s and dropped to 50s.

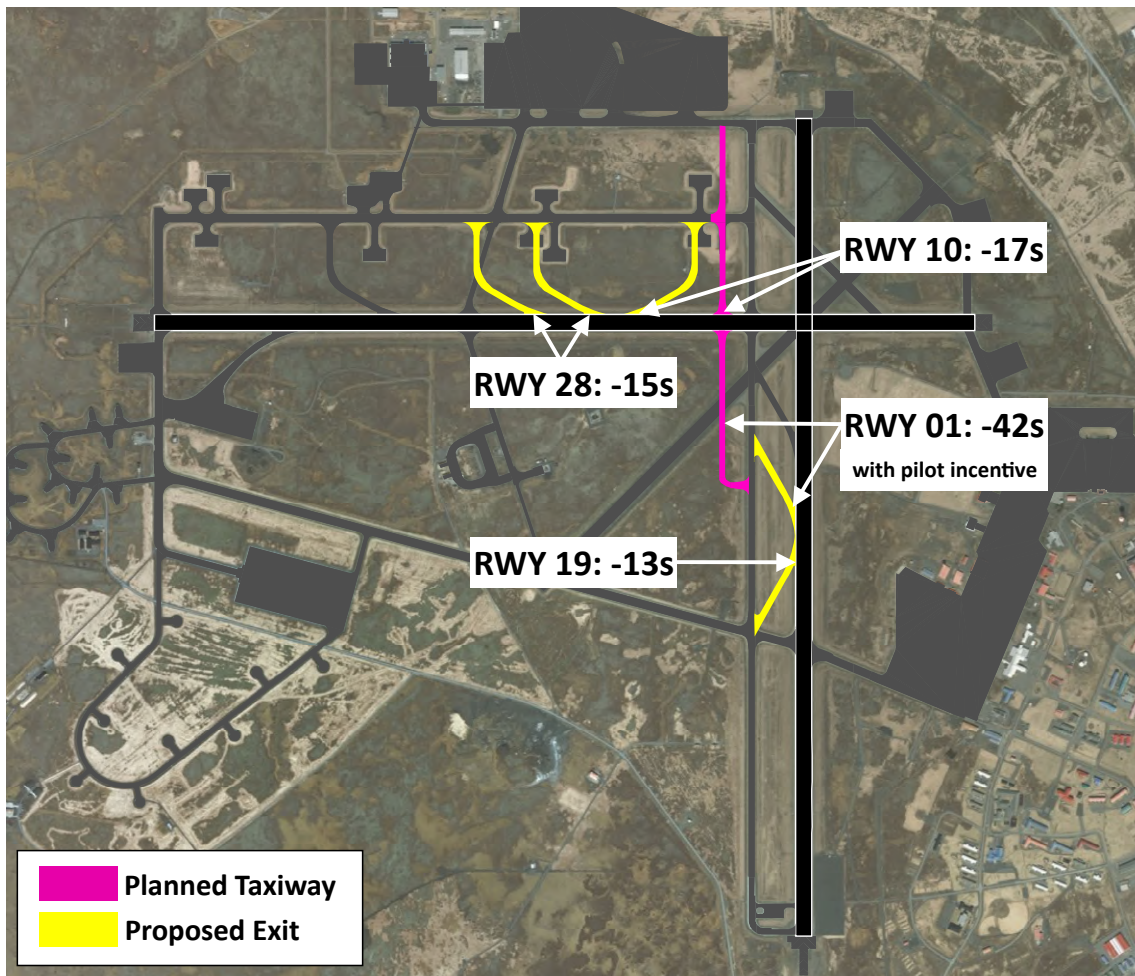


Figure 7-30: Summary of potential modifications to the exit system

Chapter 8

Conclusion

This thesis presented a data driven approach to reducing Runway Occupancy Time by identifying and understanding factors driving ROT and developing predictive models to optimize runway exit systems at capacity constrained airports. A detailed analysis of Runway Occupancy Time first provided a ranking of the main factors driving Runway Occupancy Time based on an exhaustive list of potential ROT precursors. This ranking, derived by a random-forest algorithm, gives a first comprehensive picture of the factors affecting Runway Occupancy Time, compared to previous studies. It was found that a total of 5 dominant factors explain approximately 90% of the variance of ROT. These factors include the aircraft type, the final approach speed, the characteristics of the exit used to vacate the runway, the airline and the presence of a following aircraft in final approach. These various factors demonstrate that ROT is both driven by the aircraft braking performance and pilot behaviour.

The impact of these 5 dominant factors on ROT was studied in details by comparing ROT distributions and deceleration profiles of aircraft on the runway. First, it was observed that Runway Occupancy Time highly depends on the type of the landing aircraft and that heavier aircraft had higher average ROT in general due to their high landing momentum requiring increased braking forces. The impact of the 4 other dominant factors was then studied by looking at A320 landing observations. This analysis showed that the exit system available to a landing aircraft to vacate the runway had a major impact on ROT. The use of exits located far down on the runway highly increases ROT while vacating the runway through high-speed exits provides a significant reduction in ROT. Differences in ROT distributions were observed between A320s operated by different carriers at the same airport. This highlights the impact of human behavior on ROT. The choice of the exit used to vacate the runway is influenced by the airline specific braking procedures and a willingness to minimize the aircraft taxi-time to gate, impacting ROT. The final approach speed of landing aircraft was found to have a dual impact on ROT. Fast approaching aircraft land with a higher momentum and are forced to exit further down the runway, resulting in an increased ROT but have a higher average speed on the runway resulting in a reduced ROT compared to slow approaching aircraft using the

same exit. Finally, the presence of a trailing aircraft close behind in final approach was found to incentivize pilots to vacate the runway earlier and reduces ROT on average. This detailed analysis provided a comprehensive picture of how multiple dominant factors influence Runway Occupancy Time. It was notably identified that the runway exit system available to a landing aircraft was the main leverage airport operators have to reduce ROT. By designing runway exits adapted to the expected landing observations on a runway, airport operators can reduce the Runway Occupancy Time of a specific runway. Optimal exits need to be implemented at locations driven by both aircraft braking performance and pilot behavior.

This thesis then introduced predictive models of Runway Occupancy Time, built based on the identified dominant ROT factors. Compared to existing methods used to predict ROT, these models were based on recent Machine Learning algorithms specifically designed and tuned to predict stochastically the Runway Occupancy Time of a landing aircraft. These models were trained using millions of landing observations and account for previously observed pilot behaviour at US airports. The developed models contrast with existing predictive methods of ROT that aim at replicating the braking deceleration of aircraft on the runway, requiring significant complex assumptions. The developed predictive models overcame this difficulty by using self-learning algorithms, able to predict the outcome of non-linear phenomena. By predicting ROT for several landing operations observed on a runway, these models are able to predict the general distribution of ROT for a runway. The developed models demonstrated an overall good performance in predicting ROT distributions while being highly flexible and adaptable to various landing environments. This opens the door to further use of deep-learning algorithms to model complex aerospace operational phenomenon based on available data. The developed models however lack interpretability compared to existing methods. Further improvements of the models could include the ability to explain what factors drove specific predictions. Recent advances in machine-learning (e.g. shapley values, Local Interpretable Model-agnostic Explanations (LIME)) could provide such capability without penalizing the accuracy of the models. Further improvement in the predictive power of the models could be explored as well by testing other Machine-Learning architectures. Predicting reliable exit use probabilities appeared to be the most challenging part of the modelling due to the diversity of the runway exit systems in the US, the number and proximity of exits on runways and the variability of pilot behavior. An increased predictive performance might be provided by using more complex RNN models and by accounting for other factors that influence pilot behavior.

Finally, this thesis showed how these models could be used to assess potential changes to existing runway exit systems. By assessing the impact of modifications on the average ROT of a runway, airport operators are able to design exits adapted to the local specificities of the landing operations. A case-study aiming at optimizing the runway exit system of Keflavík airport in Iceland, using the developed predictive models, was presented. The ROT performance of each runway of Keflavík airport was assessed by analyzing data on observed landing operations and the ROT impact of potential changes to the runway exit system was evaluated using the predictive models. This case-study demonstrated the effectiveness of the predictive models

in providing data-driven guidance to the airport operator regarding where to locate new high-speed exits to reduce ROT. The amount of available data on aircraft operations gives the opportunity today to replicate such a data-driven approach to alleviate other operational constraints at airports and propose appropriate airport-specific solutions.

THIS PAGE INTENTIONALLY LEFT BLANK

Bibliography

- [1] Eurocontrol. *Enhancing Airside Capacity, the Complete Guide, Ed. 2.0*. Tech. rep. 2003. URL: https://ext.eurocontrol.int/lexicon/index.php/Arrival_runway_occupancy_time.
- [2] Federal Aviation Administration. *JO 7110.65X: Air Traffic Organization Policy*. Tech. rep. US Department of Transportation - Federal Aviation Administration, 2017.
- [3] FAA. *Aeronautical Information Manual. Official Guide to Basic Flight Information and ATC Procedures*. Tech. rep. U.S. Department of Transportation, 2014, p. 726.
- [4] International Civil Aviation Organization. *Doc 4444, Procedures for Air Navigation Services - Air Traffic Management*. Tech. rep. 2016. URL: <https://ops.group/blog/wp-content/uploads/2017/03/ICAO-Doc4444-Pans-Atm-16thEdition-2016-OPSGROUP.pdf>.
- [5] Steven E Koenig. *Analysis of Runway Occupancy Times at Major Airports*. Tech. rep. McLean, Virginia: The MITRE Corporation, 1978. URL: <https://apps.dtic.mil/docs/citations/ADA056052>.
- [6] W E Weiss and J N Barrer. *Analysis of Runway Occupancy Time and Separation Data Collected at La Guardia, Boston, and Newark Airports*. Tech. rep. McLean, Virginia: MITRE Corporation, 1984. URL: <http://oai.dtic.mil/oai/oai?verb=getRecord&metadataPrefix=html&identifier=ADA154130>.
- [7] Derrick D. Lee et al. "NASA Low Visibility Landing and Surface Operations (LVLASO) Runway Occupancy Time (ROT) analysis". In: *AIAA/IEEE Digital Avionics Systems Conference - Proceedings*. Vol. 1. IEEE, 1999. DOI: [10.1109/dasc.1999.863754](https://doi.org/10.1109/dasc.1999.863754).
- [8] Vivek Kumar, Lance Sherry, and Rafal Kicingier. *Runway occupancy time extraction and analysis using surface track data*. Tech. rep. 2009.
- [9] Tamas Kolos-Lakatos. "The Influence of Runway Occupancy Time and Wake Vortex Separation Requirements on Runway Throughput". Doctoral dissertation. Massachusetts Institute of Technology (MIT), 2013. URL: <https://dspace.mit.edu/handle/1721.1/85804>.
- [10] Robert Horonjeff et al. "A Mathematical Model for Locating Exit Taxiways". In: (1959).
- [11] Hans G. Daellenbach. "Dynamic programming model for optimal location of runway exits". In: *Transportation Research* 8.3 (1974), pp. 225–232. ISSN: 00411647. DOI: [10.1016/0041-1647\(74\)90009-4](https://doi.org/10.1016/0041-1647(74)90009-4).

- [12] Terry A. Ruhl. “Empirical analysis of runway occupancy with applications to exit taxiway location and automated exit guidance”. In: *Transportation Research Record* 1257 (1988), pp. 44–57. ISSN: 03611981.
- [13] Antoine G. Hobeika et al. “Microcomputer model for design and location of runway exits”. In: *Journal of Transportation Engineering* 119.3 (1993), pp. 385–401. ISSN: 0733947X. DOI: [10.1061/\(ASCE\)0733-947X\(1993\)119:3\(385\)](https://doi.org/10.1061/(ASCE)0733-947X(1993)119:3(385)).
- [14] Antonio A Trani et al. *Flight Simulations of High Speed Runway Exits*. Tech. rep. 1995.
- [15] Xiaoling Gu, Antonio A. Trani, and Caoyuan Zhong. “Characterization of gate location on aircraft runway landing roll prediction and airport ground networks navigation”. In: *Transportation Research Record* 1506 (July 1995), pp. 52–60. ISSN: 03611981.
- [16] Carlos Barbas, Javier Vázquez, and Pablo López. “Development of an algorithm to model the landing operations, based on statistical analysis of actual data survey (proestop)”. In: *Proceedings of the 7th USA/Europe Air Traffic Management Research and Development Seminar, ATM 2007*. EUROCONTROL, 2007, pp. 73–83.
- [17] Federal Aviation Administration. *Airport Surface Detection Equipment, Model X (ASDE-X)*. URL: https://www.faa.gov/air_traffic/technology/asde-x/.
- [18] Federal Aviation Administration. *28 Day NASR Subscription*. URL: https://www.faa.gov/air_traffic/flight_info/aeronav/aero_data/NASR_Subscription/.
- [19] *Aircraft Characteristics Database – Airports*. URL: https://www.faa.gov/airports/engineering/aircraft_char_database/.
- [20] *SKYbrary Aviation Safety*. URL: <https://www.skybrary.aero/index.php/Category:Aircraft>.
- [21] National Weather Service US Department of Commerce NOAA. *Automated Surface Observing Systems*. URL: <https://www.weather.gov/asos/asostech>.
- [22] National Weather Service US Department of Commerce NOAA. *Automated Surface Observing System (ASOS)*. URL: <https://www.ncdc.noaa.gov/data-access/land-based-station-data/land-based-datasets/automated-surface-observing-system-asos>.
- [23] Christophe Leys et al. “Detecting outliers: Do not use standard deviation around the mean, use absolute deviation around the median”. In: *Journal of Experimental Social Psychology* 49.4 (July 2013), pp. 764–766. ISSN: 00221031. DOI: [10.1016/j.jesp.2013.03.013](https://doi.org/10.1016/j.jesp.2013.03.013).
- [24] Tin Kam Ho. “Random Decision Forests”. In: *Proceedings of the Third International Conference on Document Analysis and Recognition (Volume 1) - Volume 1*. ICDAR '95. Washington, DC, USA: IEEE Computer Society, 1995, pp. 278–. ISBN: 0-8186-7128-9. URL: <http://dl.acm.org/citation.cfm?id=844379.844681>.
- [25] Gilles Louppe. “Understanding Random Forests: From Theory to Practice”. In: (July 2014). URL: <http://arxiv.org/abs/1407.7502>.
- [26] H2O.ai. *Python Interface for H2O*. Mar. 2019. URL: <https://github.com/h2oai/h2o-3>.
- [27] Federal Aviation Administration. *AC 150/5300-13A, Airport Design*. Tech. rep. Federal Aviation Administration, 2014.

- [28] Federal Aviation Administration. *JO 7110.659C: Wake Turbulence Recategorization*. Tech. rep. US Department of Transportation - Federal Aviation Administration, 2016. URL: [https://employees.faa.gov/tools_resources/orders_notices/.](https://employees.faa.gov/tools_resources/orders_notices/)
- [29] Ian Goodfellow, Yoshua Bengio, and Aaron Courville. *Deep Learning*. MIT Press, 2016. URL: <http://www.deeplearningbook.org>.
- [30] Oriol Vinyals, Meire Fortunato, and Navdeep Jaitly. “Pointer networks”. In: *Advances in Neural Information Processing Systems*. Vol. 2015-January. Neural information processing systems foundation, 2015, pp. 2692–2700.
- [31] Rudolf Kadlec et al. “Text understanding with the attention sum reader network”. In: *54th Annual Meeting of the Association for Computational Linguistics, ACL 2016 - Long Papers*. Vol. 2. Association for Computational Linguistics (ACL), 2016, pp. 908–918. ISBN: 9781510827585. DOI: [10.18653/v1/p16-1086](https://doi.org/10.18653/v1/p16-1086).
- [32] François Chollet. *Keras*. 2015. URL: <https://keras.io>.
- [33] Abbas Khosravi et al. *Comprehensive review of neural network-based prediction intervals and new advances*. Sept. 2011. DOI: [10.1109/TNN.2011.2162110](https://doi.org/10.1109/TNN.2011.2162110).
- [34] ISAVIA. *Keflavík airport facts and figures 2018*. Tech. rep. 2019.

THIS PAGE INTENTIONALLY LEFT BLANK

Appendix A

List of Aircraft Used to Develop Predictive Models

This section presents the list of aircraft included in the predictive models, detailed in section [6](#).

Table A.1: List of aircraft used to develop predictive models

A124	B712	BE20	CRJ2	GALX
A20N	B732	BE40	CRJ7	GL5T
A21N	B733	BE99	CRJ9	GLEK
A306	B734	BE9L	DA40	GLF4
A310	B735	C172	DC10	GLF5
A319	B736	C182	DH8A	H25B
A320	B737	C208	DH8B	LJ31
A321	B738	C25A	DH8C	LJ35
A332	B739	C25B	DH8D	LJ45
A333	B744	C402	E120	LJ60
A339	B748	C510	E135	MD11
A343	B752	C525	E145	MD82
A345	B753	C550	E170	MD83
A346	B762	C560	E190	MD88
A388	B763	C56X	E45X	MD90
ASTR	B764	C650	E50P	PA31
AT72	B772	C680	E55P	PC12
B190	B77L	C750	F2TH	SF34
B350	B77W	CL30	F900	SH36
B38M	B788	CL35	FA50	SR22
B39M	B789	CL60	G150	SW4

THIS PAGE INTENTIONALLY LEFT BLANK

Appendix B

Performance of Predictive Model of Exit Use

This section presents the detailed performance of the predictive model of exit use for 218 runways in the US. This performance is described by four different metrics presented in Table B.1. These metrics include the categorical cross-entropy loss of the model, computed for each runway using the landing observations saved in the testing set. They also encompass a Top-1, Top-2 and Top-3 accuracy metrics. These Top-N metrics assess the number of times that the exit actually used by the aircraft in the observation is in the set of exits with the Top-N probabilities predicted by the model. Additional information is given on the number of exits of each runway and the number of observations in the testing set used to compute the metrics for each runway.

Table B.1: Detailed performance of the predictive model of exit use

Airport	Runway	Crossentropy loss	Top-1 accuracy	Top-2 accuracy	Top-3 accuracy	Number of observations
ATL	10	0.317	89.23%	99.51%	99.89%	3499
ATL	28	0.588	74.14%	98.76%	99.69%	5488
ATL	08L	0.478	82.68%	97.22%	99.44%	7086
ATL	09R	0.493	85.41%	96.45%	98.12%	5752
ATL	26L	1.124	67.57%	82.70%	94.05%	185
ATL	26R	0.437	84.18%	98.17%	99.28%	13662
ATL	27L	0.509	79.41%	98.27%	99.11%	11398
ATL	27R	1.237	52.54%	77.12%	89.83%	118
BDL	06	0.594	80.67%	93.32%	97.67%	1542
BDL	24	0.612	80.39%	94.53%	98.12%	1810
BDL	33	1.039	61.02%	80.32%	92.65%	803
BOS	27	0.473	81.51%	98.91%	99.65%	4510
BOS	32	0.180	96.49%	99.38%	99.79%	485

Continued on next page

Table B.1 – continued from previous page

Airport	Runway	Crossentropy loss	Top-1 accuracy	Top-2 accuracy	Top-3 accuracy	Number of observations
BOS	04L	0.858	67.48%	90.99%	97.00%	1399
BOS	04R	0.986	60.45%	85.72%	96.08%	5615
BOS	15R	1.165	61.07%	83.89%	90.60%	149
BOS	22L	0.967	60.50%	85.47%	95.58%	5312
BOS	22R	1.023	60.91%	88.18%	96.36%	110
BOS	33L	0.964	64.43%	86.56%	94.68%	3081
BOS	33R	0.406	90.12%	93.83%	96.30%	162
BWI	10	0.587	77.75%	96.01%	98.94%	2831
BWI	28	0.820	68.18%	95.45%	98.05%	154
BWI	15L	0.596	72.87%	98.40%	100.00%	188
BWI	15R	0.840	66.48%	93.71%	98.50%	731
BWI	33L	0.664	72.28%	96.45%	99.39%	8082
BWI	33R	0.592	74.59%	96.90%	99.59%	484
CLT	23	0.902	63.37%	85.44%	98.27%	4395
CLT	18C	1.112	55.84%	78.34%	93.01%	1574
CLT	18L	1.287	54.47%	77.50%	88.05%	929
CLT	18R	0.349	86.32%	99.61%	99.89%	6439
CLT	36C	1.060	55.42%	82.48%	95.67%	1918
CLT	36L	0.302	87.74%	99.66%	99.93%	7692
CLT	36R	1.087	61.14%	79.43%	88.04%	5679
DCA	01	0.941	63.48%	87.78%	97.08%	9207
DCA	15	1.124	65.17%	81.46%	94.38%	178
DCA	19	0.880	62.06%	91.85%	98.26%	4931
DCA	33	0.810	65.72%	94.14%	98.22%	563
DEN	07	0.181	96.50%	97.67%	100.00%	343
DEN	26	0.764	70.98%	93.40%	98.75%	803
DEN	16L	0.865	68.88%	89.73%	97.25%	7973
DEN	16R	0.715	73.48%	94.19%	98.22%	5008
DEN	17R	0.557	79.48%	96.38%	99.36%	2676
DEN	34R	0.627	82.34%	93.66%	96.95%	2129
DEN	35L	0.706	70.61%	95.87%	98.70%	7328
DEN	35R	0.596	75.17%	98.65%	99.15%	3186
DFW	13R	0.634	78.90%	95.78%	98.73%	474
DFW	17C	1.190	52.13%	81.13%	92.15%	9536
DFW	17L	0.377	87.54%	98.44%	99.60%	3982
DFW	17R	1.164	60.27%	80.13%	89.90%	594
DFW	18L	1.349	46.64%	72.26%	90.64%	566
DFW	18R	1.105	55.76%	84.89%	94.53%	10025
DFW	31R	0.748	73.82%	89.01%	99.48%	191
DFW	35C	0.784	78.63%	90.57%	95.01%	4146
DFW	35L	1.223	53.75%	83.00%	91.30%	253
DFW	35R	0.710	70.59%	95.84%	98.94%	2550
DFW	36L	0.772	75.22%	91.26%	96.54%	5376
DFW	36R	1.171	63.87%	83.46%	89.31%	393

Continued on next page

Table B.1 – continued from previous page

Airport	Runway	Crossentropy loss	Top-1 accuracy	Top-2 accuracy	Top-3 accuracy	Number of observations
DTW	03R	1.023	56.65%	88.08%	96.33%	1661
DTW	04L	0.373	87.95%	99.37%	99.64%	3310
DTW	04R	1.085	52.67%	84.89%	95.72%	1496
DTW	21L	0.927	64.95%	88.13%	96.75%	4365
DTW	21R	0.884	67.65%	84.71%	95.29%	170
DTW	22L	0.947	65.45%	84.45%	94.92%	2758
DTW	22R	0.490	81.85%	96.43%	99.26%	6893
EWR	11	1.665	48.44%	67.71%	80.73%	192
EWR	29	0.983	59.38%	81.32%	98.08%	1199
EWR	04L	1.644	36.32%	61.84%	77.11%	380
EWR	04R	1.123	54.24%	80.70%	93.56%	8755
EWR	22L	0.836	64.22%	92.60%	98.42%	11185
EWR	22R	1.269	58.55%	74.36%	83.55%	468
FLL	10L	0.950	59.48%	87.97%	96.88%	6052
FLL	10R	0.774	66.59%	95.18%	98.63%	2778
FLL	28L	0.855	63.63%	93.19%	98.05%	822
FLL	28R	0.956	59.01%	88.26%	98.06%	1959
HNL	04R	0.659	74.85%	95.42%	98.18%	3078
HNL	08L	0.891	71.71%	88.26%	94.83%	5529
HNL	26L	0.456	89.01%	97.86%	99.46%	373
HOU	04	0.778	66.80%	93.03%	96.91%	3271
HOU	17	0.919	65.91%	85.61%	94.70%	132
HOU	22	1.029	69.50%	81.08%	87.64%	259
HOU	13L	0.746	75.26%	90.00%	97.37%	190
HOU	13R	0.448	85.85%	97.41%	98.86%	4896
HOU	31L	0.926	62.39%	90.45%	96.72%	670
IAD	01C	0.879	68.89%	89.90%	96.52%	4742
IAD	01L	0.567	78.33%	98.28%	99.51%	406
IAD	01R	0.840	69.56%	90.63%	96.08%	3670
IAD	19C	0.808	71.46%	92.61%	96.06%	3557
IAD	19L	0.843	70.38%	90.39%	96.91%	2394
IAD	19R	0.734	77.08%	91.98%	97.42%	349
IAH	09	0.486	82.93%	97.07%	99.51%	205
IAH	27	0.874	60.75%	91.23%	98.65%	9395
IAH	08L	0.581	75.60%	98.38%	99.50%	2402
IAH	08R	0.643	76.82%	94.73%	97.80%	5051
IAH	15R	0.972	62.39%	85.47%	97.44%	117
IAH	26L	0.595	81.09%	95.81%	98.79%	7844
IAH	26R	0.658	68.52%	98.73%	99.51%	2440
JFK	04L	1.177	48.12%	79.08%	93.93%	478
JFK	04R	0.255	92.55%	98.91%	99.83%	2938
JFK	13L	1.120	55.12%	84.50%	92.45%	4465
JFK	13R	1.075	60.14%	85.14%	94.59%	148
JFK	22L	0.224	93.48%	98.87%	99.85%	3985

Continued on next page

Table B.1 – continued from previous page

Airport	Runway	Crossentropy loss	Top-1 accuracy	Top-2 accuracy	Top-3 accuracy	Number of observations
JFK	22R	1.229	46.35%	76.12%	89.33%	356
JFK	31L	1.048	54.64%	85.12%	96.44%	1768
JFK	31R	0.628	75.36%	96.73%	99.08%	5840
LAS	01L	0.747	67.08%	94.25%	99.32%	3982
LAS	01R	1.000	59.51%	87.79%	97.56%	1188
LAS	08R	0.788	65.41%	94.86%	99.14%	584
LAS	19L	1.013	58.63%	86.10%	95.98%	921
LAS	19R	0.798	67.03%	90.25%	98.60%	2287
LAS	26L	0.736	67.17%	95.15%	99.67%	13162
LAX	06L	0.575	74.26%	98.44%	99.38%	641
LAX	06R	1.115	58.48%	84.41%	93.76%	513
LAX	07L	1.033	69.40%	88.06%	91.79%	134
LAX	07R	0.974	63.08%	86.15%	95.90%	195
LAX	24L	0.886	63.11%	91.40%	98.51%	3231
LAX	24R	0.647	75.05%	90.96%	99.07%	12149
LAX	25L	0.933	62.69%	90.10%	96.92%	17915
LAX	25R	1.594	42.89%	68.03%	80.00%	760
LGA	04	1.360	43.62%	72.85%	88.87%	4221
LGA	13	0.841	64.52%	93.55%	98.28%	465
LGA	22	0.884	68.91%	91.37%	96.27%	10129
LGA	31	0.865	64.52%	92.12%	98.08%	5352
MCO	17L	0.331	89.48%	99.01%	99.76%	3822
MCO	17R	0.873	69.85%	91.63%	95.49%	932
MCO	18L	0.950	67.61%	87.78%	96.02%	352
MCO	18R	0.600	74.76%	97.98%	99.44%	5146
MCO	35L	1.087	55.92%	80.84%	94.60%	574
MCO	35R	0.566	77.34%	98.11%	99.77%	2586
MCO	36L	0.481	81.37%	97.11%	99.08%	3495
MCO	36R	0.822	67.41%	89.09%	98.32%	715
MDW	04L	0.760	78.48%	88.79%	94.62%	223
MDW	04R	0.734	75.44%	93.16%	96.85%	4577
MDW	13C	0.863	71.71%	89.24%	95.62%	251
MDW	22L	0.784	74.19%	90.71%	97.63%	2917
MDW	22R	0.556	76.88%	97.69%	98.27%	173
MDW	31C	0.346	88.68%	97.84%	99.01%	4159
MEM	09	0.994	66.40%	85.33%	92.00%	375
MEM	27	0.767	73.44%	91.01%	96.52%	1668
MEM	18C	1.310	57.84%	78.42%	87.63%	695
MEM	18L	0.702	77.17%	92.12%	97.28%	1472
MEM	18R	0.601	76.18%	97.89%	99.44%	1612
MEM	36C	1.435	60.57%	77.04%	83.99%	662
MEM	36L	0.568	82.77%	94.56%	97.12%	2537
MEM	36R	0.617	77.95%	95.62%	97.90%	2240
MIA	09	0.799	66.52%	92.51%	97.52%	8625

Continued on next page

Table B.1 – continued from previous page

Airport	Runway	Crossentropy loss	Top-1 accuracy	Top-2 accuracy	Top-3 accuracy	Number of observations
MIA	12	1.219	48.50%	80.53%	93.51%	4377
MIA	27	0.702	74.52%	95.22%	99.04%	314
MIA	30	0.706	71.21%	96.12%	99.58%	2164
MIA	08L	0.851	64.87%	91.55%	98.56%	2781
MIA	08R	1.015	58.65%	85.43%	96.21%	1531
MIA	26L	1.128	57.51%	84.53%	92.53%	1125
MIA	26R	0.819	65.49%	92.75%	98.69%	1985
MKE	01L	0.801	67.91%	91.99%	97.08%	1711
MKE	07R	1.003	68.79%	86.06%	91.97%	660
MKE	19R	0.748	72.35%	94.85%	98.03%	1573
MKE	25L	0.967	59.09%	86.11%	96.80%	1469
MSP	35	0.673	72.30%	96.22%	99.51%	2224
MSP	12L	0.854	62.14%	92.42%	98.99%	5066
MSP	12R	1.075	53.98%	84.75%	96.18%	5756
MSP	30L	1.181	54.20%	77.24%	89.91%	4362
MSP	30R	1.317	45.94%	73.73%	87.66%	4343
ORD	09L	0.098	98.40%	99.98%	99.98%	4758
ORD	09R	0.817	71.16%	91.63%	97.83%	1016
ORD	10C	1.161	56.29%	80.71%	92.21%	5774
ORD	10L	1.013	64.32%	86.49%	93.33%	555
ORD	10R	0.714	66.20%	98.09%	99.48%	577
ORD	14R	1.389	44.55%	73.27%	81.19%	101
ORD	22R	0.862	69.52%	79.05%	93.33%	105
ORD	27L	0.578	77.68%	95.27%	98.59%	11347
ORD	27R	0.079	98.51%	99.98%	99.98%	6507
ORD	28C	0.864	69.36%	90.54%	96.74%	7424
ORD	28R	0.865	71.73%	92.93%	96.15%	467
PHL	17	0.443	89.08%	96.68%	99.21%	632
PHL	26	0.268	92.53%	98.05%	99.92%	1285
PHL	35	0.665	69.49%	98.09%	99.60%	4245
PHL	09R	0.894	66.29%	91.82%	97.23%	4904
PHL	27L	0.718	78.22%	89.24%	95.14%	762
PHL	27R	0.930	63.08%	88.42%	96.62%	10149
PHX	08	1.116	53.13%	84.92%	94.68%	5882
PHX	26	1.048	56.12%	86.45%	96.85%	8231
PHX	07L	1.280	42.96%	75.82%	90.61%	703
PHX	07R	0.838	62.33%	93.90%	98.84%	3178
PHX	25L	0.655	73.93%	96.56%	99.53%	4212
PHX	25R	1.018	57.96%	87.98%	97.17%	1306
PVD	05	1.239	49.68%	78.56%	90.87%	942
PVD	23	0.499	83.50%	96.28%	98.45%	1291
SAN	09	1.392	51.39%	74.31%	86.81%	144
SAN	27	0.719	68.76%	95.80%	99.28%	9640
SDF	29	0.919	66.34%	92.08%	92.08%	101

Continued on next page

Table B.1 – continued from previous page

Airport	Runway	Crossentropy loss	Top-1 accuracy	Top-2 accuracy	Top-3 accuracy	Number of observations
SDF	17L	1.208	53.54%	79.65%	90.83%	2202
SDF	17R	0.911	67.55%	90.51%	94.47%	1285
SDF	35L	0.911	68.20%	90.18%	95.22%	2362
SDF	35R	0.842	67.05%	89.99%	97.03%	1648
SEA	16C	0.945	57.14%	88.57%	98.10%	105
SEA	16L	0.957	59.59%	89.41%	96.59%	2257
SEA	16R	0.713	71.08%	94.65%	99.50%	10831
SEA	34C	0.858	62.73%	94.41%	98.45%	322
SEA	34L	0.495	79.56%	98.90%	99.81%	5725
SEA	34R	0.852	68.82%	91.03%	96.98%	1193
SFO	19L	0.912	61.06%	92.71%	98.49%	398
SFO	28L	0.991	62.08%	84.84%	94.37%	8921
SFO	28R	0.948	63.59%	87.33%	95.93%	10894
SLC	17	0.981	63.87%	85.78%	93.90%	1132
SLC	32	0.075	99.12%	100.00%	100.00%	226
SLC	35	0.757	71.01%	90.31%	98.09%	1466
SLC	16L	1.255	50.02%	76.41%	87.65%	2081
SLC	16R	0.747	67.55%	95.25%	99.24%	2484
SLC	34L	0.836	65.27%	93.05%	98.58%	2891
SLC	34R	1.033	60.67%	86.19%	95.44%	2787
SNA	02L	1.022	58.33%	89.39%	95.45%	132
SNA	20L	0.926	64.47%	88.35%	93.80%	532
SNA	20R	0.390	86.85%	98.14%	99.03%	6679
STL	11	0.602	83.26%	92.34%	97.45%	705
STL	24	0.841	74.90%	84.94%	92.47%	239
STL	12L	0.633	75.89%	94.29%	98.82%	929
STL	12R	1.071	54.52%	85.91%	94.46%	2634
STL	30L	1.242	50.59%	78.69%	91.37%	765
STL	30R	0.723	72.46%	93.37%	98.13%	3740

Appendix C

Performance of Predictive Models of ROT

This section presents the detailed performance of the predictive models of Runway Occupancy Time for 218 runways in the US. This performance is described by the mean squared error and median squared error per runway of the model. These losses are computed using the landing observations kept in the testing set with a Runway Occupancy Time below 200s. Table C.1 present these results as well as the number of landing observations per runway present in the testing-set.

Table C.1: Detailed performance of the predictive models of average ROT

Airport	Runway	Median-squared error, s^2	Mean-Squared Error, s^2	Number of Observations
ATL	10	5.5	50.7	3498
ATL	28	5.0	52.7	5486
ATL	08L	5.4	36.0	7083
ATL	09R	9.0	40.8	5751
ATL	26L	18.7	75.6	185
ATL	26R	5.6	27.7	13656
ATL	27L	6.5	66.5	11393
ATL	27R	13.9	53.5	118
BDL	06	16.4	149.9	1541
BDL	24	13.4	81.9	1810
BDL	33	9.5	143.7	799
BOS	27	8.7	57.1	4510
BOS	32	10.3	72.1	485
BOS	04L	7.6	128.5	1398
BOS	04R	9.0	52.6	5609
BOS	15R	22.3	125.1	149
BOS	22L	9.0	48.2	5307
BOS	22R	21.5	74.7	110
BOS	33L	9.4	51.3	3081

Continued on next page

Table C.1 – continued from previous page

Airport	Runway	Median squared error, s^2	Mean squared error, s^2	Number of observations
BOS	33R	6.4	316.7	162
BWI	10	13.8	80.8	2827
BWI	28	21.2	79.2	154
BWI	15L	19.9	121.6	188
BWI	15R	10.5	65.9	730
BWI	33L	7.3	53.8	8081
BWI	33R	15.9	84.9	484
CLT	23	7.8	62.1	4386
CLT	18C	9.9	75.8	1574
CLT	18L	12.6	67.0	929
CLT	18R	5.5	65.0	6439
CLT	36C	9.8	41.2	1916
CLT	36L	5.3	30.4	7687
CLT	36R	9.7	51.6	5678
DCA	01	7.0	48.8	9206
DCA	15	8.7	199.8	177
DCA	19	7.4	47.3	4930
DCA	33	9.2	78.4	563
DEN	07	21.5	40.0	343
DEN	26	10.4	34.8	803
DEN	16L	9.9	43.8	7965
DEN	16R	17.3	65.6	5001
DEN	17R	9.2	64.3	2673
DEN	34R	8.9	38.0	2126
DEN	35L	9.4	43.3	7324
DEN	35R	12.0	36.9	3185
DFW	13R	17.0	66.0	471
DFW	17C	7.7	46.1	9525
DFW	17L	5.6	52.7	3980
DFW	17R	18.2	91.0	592
DFW	18L	12.8	88.4	566
DFW	18R	7.5	45.4	10011
DFW	31R	12.9	34.4	191
DFW	35C	10.9	44.7	4144
DFW	35L	18.8	58.2	252
DFW	35R	6.8	25.8	2549
DFW	36L	9.6	46.1	5376
DFW	36R	15.5	71.7	393
DTW	03R	8.5	50.7	1660
DTW	04L	8.3	59.8	3303
DTW	04R	9.4	96.5	1496
DTW	21L	10.9	58.7	4365
DTW	21R	18.8	250.7	169
DTW	22L	10.0	54.4	2754
DTW	22R	11.4	57.0	6889

Continued on next page

Table C.1 – continued from previous page

Airport	Runway	Median squared error, s^2	Mean squared error, s^2	Number of observations
EWR	11	18.2	275.6	192
EWR	29	7.7	48.9	1199
EWR	04L	15.2	61.6	379
EWR	04R	6.3	45.2	8751
EWR	22L	6.2	40.0	11177
EWR	22R	14.5	121.1	468
FLL	10L	7.8	41.0	6052
FLL	10R	10.7	55.3	2777
FLL	28L	10.1	48.7	822
FLL	28R	8.1	56.7	1958
HNL	04R	15.8	125.3	3077
HNL	08L	14.2	69.8	5523
HNL	26L	19.0	74.2	373
HOU	04	8.5	71.0	3269
HOU	17	8.5	36.3	132
HOU	22	7.2	27.1	259
HOU	13L	29.7	117.5	190
HOU	13R	6.7	67.6	4892
HOU	31L	8.9	99.7	670
IAD	01C	12.2	84.2	4740
IAD	01L	10.5	51.9	406
IAD	01R	12.3	53.3	3670
IAD	19C	11.2	44.3	3555
IAD	19L	11.0	73.7	2393
IAD	19R	16.8	179.4	349
IAH	09	7.8	109.2	205
IAH	27	11.8	71.3	9386
IAH	08L	7.6	39.8	2402
IAH	08R	8.7	62.9	5050
IAH	15R	27.8	155.2	117
IAH	26L	7.4	51.7	7836
IAH	26R	5.9	41.3	2436
JFK	04L	8.8	41.6	478
JFK	04R	9.0	58.8	2938
JFK	13L	9.8	84.9	4460
JFK	13R	12.2	121.1	148
JFK	22L	10.3	58.8	3981
JFK	22R	13.1	39.1	356
JFK	31L	10.5	57.0	1767
JFK	31R	11.0	61.9	5833
LAS	01L	12.4	49.6	3980
LAS	01R	14.1	54.5	1187
LAS	08R	8.6	99.3	584
LAS	19L	13.2	93.7	921
LAS	19R	10.4	94.4	2285

Continued on next page

Table C.1 – continued from previous page

Airport	Runway	Median squared error, s^2	Mean squared error, s^2	Number of observations
LAS	26L	7.2	61.9	13156
LAX	06L	15.6	84.5	641
LAX	06R	14.4	57.2	511
LAX	07L	33.7	161.1	134
LAX	07R	12.8	126.8	195
LAX	24L	7.0	38.9	3222
LAX	24R	8.9	57.7	12146
LAX	25L	8.2	53.2	17893
LAX	25R	11.5	85.4	760
LGA	04	7.8	72.8	4220
LGA	13	9.2	46.8	464
LGA	22	5.1	36.3	10123
LGA	31	6.3	46.6	5351
MCO	17L	6.8	54.9	3816
MCO	17R	28.2	82.4	930
MCO	18L	13.1	109.6	351
MCO	18R	10.5	79.4	5137
MCO	35L	21.1	46.0	573
MCO	35R	9.0	53.7	2585
MCO	36L	11.1	48.4	3493
MCO	36R	14.7	71.8	715
MDW	04L	23.8	200.0	222
MDW	04R	7.5	56.9	4576
MDW	13C	12.8	102.8	251
MDW	22L	7.6	50.9	2917
MDW	22R	33.7	88.2	173
MDW	31C	6.6	36.2	4159
MEM	09	20.1	64.7	375
MEM	27	13.8	52.8	1667
MEM	18C	12.4	91.7	694
MEM	18L	10.0	52.0	1471
MEM	18R	9.5	55.5	1610
MEM	36C	16.6	106.6	662
MEM	36L	14.4	52.9	2536
MEM	36R	14.2	69.4	2237
MIA	09	11.5	73.0	8618
MIA	12	11.3	67.7	4375
MIA	27	20.2	55.1	313
MIA	30	11.3	32.6	2163
MIA	08L	10.6	73.0	2781
MIA	08R	22.8	82.6	1531
MIA	26L	17.8	83.1	1125
MIA	26R	9.6	47.1	1982
MKE	01L	16.3	71.3	1711
MKE	07R	16.8	123.0	660

Continued on next page

Table C.1 – continued from previous page

Airport	Runway	Median squared error, s^2	Mean squared error, s^2	Number of observations
MKE	19R	14.5	90.7	1573
MKE	25L	9.3	48.2	1469
MSP	35	8.2	51.4	2223
MSP	12L	6.2	55.2	5065
MSP	12R	8.4	53.9	5756
MSP	30L	10.0	66.0	4362
MSP	30R	7.7	54.2	4341
ORD	09L	6.5	40.9	4757
ORD	09R	13.5	48.9	1016
ORD	10C	11.0	68.2	5770
ORD	10L	18.2	94.3	553
ORD	10R	6.1	43.5	577
ORD	14R	14.0	103.6	101
ORD	22R	7.3	122.7	105
ORD	27L	6.4	44.2	11340
ORD	27R	6.8	55.1	6501
ORD	28C	8.7	39.6	7421
ORD	28R	23.0	103.2	467
PHL	17	8.9	60.3	632
PHL	26	9.7	110.1	1285
PHL	35	5.7	33.7	4245
PHL	09R	7.5	51.2	4900
PHL	27L	13.6	55.1	761
PHL	27R	7.4	50.8	10147
PHX	08	11.1	63.3	5881
PHX	26	9.9	45.2	8225
PHX	07L	16.5	71.8	703
PHX	07R	9.6	50.3	3177
PHX	25L	8.3	37.3	4210
PHX	25R	21.6	56.7	1306
PVD	05	36.5	129.6	942
PVD	23	8.9	123.7	1291
SAN	09	12.5	117.6	144
SAN	27	9.2	56.4	9637
SDF	29	9.9	127.4	101
SDF	17L	9.4	83.0	2201
SDF	17R	12.1	79.4	1285
SDF	35L	14.0	60.1	2361
SDF	35R	12.8	53.6	1648
SEA	16C	9.4	60.4	105
SEA	16L	20.8	72.8	2256
SEA	16R	6.7	38.2	10822
SEA	34C	9.0	57.3	322
SEA	34L	6.7	63.0	5721
SEA	34R	14.7	94.9	1193

Continued on next page

Table C.1 – continued from previous page

Airport	Runway	Median squared error, s^2	Mean squared error, s^2	Number of observations
SFO	19L	11.1	36.0	398
SFO	28L	11.0	64.6	8914
SFO	28R	14.1	78.0	10881
SLC	17	18.7	113.9	1132
SLC	32	15.3	74.0	226
SLC	35	12.3	56.8	1464
SLC	16L	15.1	67.7	2080
SLC	16R	6.7	74.1	2476
SLC	34L	6.9	101.2	2890
SLC	34R	14.2	69.8	2785
SNA	02L	46.5	104.0	132
SNA	20L	69.5	421.8	527
SNA	20R	10.1	41.6	6678
STL	11	23.1	115.2	703
STL	24	12.3	196.1	239
STL	12L	6.5	45.4	929
STL	12R	15.6	58.5	2633
STL	30L	9.4	58.9	764
STL	30R	8.8	62.9	3739

Appendix D

ROT Distribution Prediction Performance

This section presents the detailed performance of the different predictive models in jointly predicting the Runway Occupancy Time distribution of a runway. This performance is assessed using the Kullback-Leibler divergence between observed and predicted distributions for 211 runways in the US. This metric is computed using solely the landing observations included in the testing set. Table D.1 presents these results as well as average and Median-Absolute-Deviation (MAD) of the distributions and the number of landing observations per runway in the testing set.

Table D.1: Performance of models in the prediction of Runway Occupancy Time distributions

Airport	Runway	$D_{KL}(P, Q)$, nats	Mean ROT, s		MAD, s		Number of observations
			Observed	Predicted	Observed	Predicted	
ATL	10	0.049	49.0	47.9	4.0	3.7	3499
ATL	28	0.064	43.0	45.1	4.0	4.1	5488
ATL	08L	0.023	45.0	45.2	4.0	3.9	7086
ATL	09R	0.044	45.0	46.0	4.0	4.1	5752
ATL	26L	0.177	58.0	59.1	7.0	7.9	185
ATL	26R	0.033	46.0	46.7	4.0	4.1	13662
ATL	27L	0.056	45.0	46.3	5.0	4.4	11398
ATL	27R	0.428	52.5	54.3	7.5	8.5	118
BDL	06	0.066	60.0	57.8	6.0	6.3	1542
BDL	24	0.086	56.0	57.1	4.0	5.8	1810
BDL	33	0.078	47.0	47.2	5.0	6.0	803
BOS	27	0.028	51.0	50.3	6.0	5.6	4510
BOS	32	0.102	46.0	44.9	5.0	5.4	485
BOS	04L	0.059	44.0	45.1	8.0	7.1	1399
BOS	04R	0.031	43.0	44.2	7.0	6.2	5615
BOS	15R	0.382	46.0	50.3	5.0	6.9	149
BOS	22L	0.047	45.0	47.3	5.0	5.7	5312

Continued on next page

Table D.1 – continued from previous page

Airport	Runway	$D_{KL}(P, Q)$, nats	Mean ROT, s		MAD, s		Number of observations
			Observed	Predicted	Observed	Predicted	
BOS	22R	0.417	56.0	54.1	10.0	6.5	110
BOS	33L	0.032	47.0	48.0	7.0	8.0	3081
BOS	33R	0.324	37.0	36.7	4.0	4.5	162
BWI	15L	0.227	41.0	44.3	8.0	8.3	188
BWI	15R	0.145	53.0	49.9	7.0	7.1	731
BWI	33L	0.028	49.0	49.3	4.0	5.1	8082
BWI	33R	0.176	46.0	45.8	9.0	6.9	484
CLT	23	0.026	49.0	48.3	7.0	7.3	4395
CLT	18C	0.051	49.0	49.9	7.0	6.5	1574
CLT	18L	0.099	45.0	46.3	6.0	6.5	929
CLT	18R	0.072	44.0	45.9	3.0	4.0	6439
CLT	36C	0.083	50.0	50.7	7.0	6.2	1918
CLT	36L	0.133	43.0	46.0	3.0	4.1	7692
CLT	36R	0.049	53.0	51.7	6.0	6.2	5679
DCA	01	0.025	41.0	41.7	3.0	3.5	9207
DCA	15	0.282	39.0	41.3	4.0	5.2	178
DCA	19	0.078	40.0	40.8	3.0	3.8	4931
DCA	33	0.079	43.0	42.4	4.0	3.8	563
DEN	07	0.401	52.0	57.4	4.0	5.4	343
DEN	26	0.126	53.0	55.0	5.0	5.9	803
DEN	16L	0.048	54.0	55.7	5.0	6.8	7973
DEN	16R	0.060	67.0	67.9	7.0	8.4	5008
DEN	17R	0.042	51.0	50.2	6.0	5.5	2676
DEN	34R	0.098	49.0	51.3	3.0	4.3	2129
DEN	35L	0.052	52.0	53.6	5.0	5.2	7328
DEN	35R	0.058	53.0	54.5	4.0	4.9	3186
DFW	13R	0.200	55.0	53.6	12.0	9.7	474
DFW	17C	0.103	47.0	51.2	6.0	7.5	9536
DFW	17L	0.024	46.0	46.9	3.0	3.6	3982
DFW	17R	0.116	66.0	63.7	8.0	8.1	594
DFW	18R	0.060	47.0	49.2	5.0	6.8	10025
DFW	31R	0.303	47.0	48.9	4.0	5.4	191
DFW	35C	0.060	52.0	53.2	5.0	5.5	4146
DFW	35L	0.253	60.0	59.0	6.0	7.0	253
DFW	35R	0.053	45.0	46.9	5.0	5.1	2550
DFW	36L	0.086	52.0	53.8	5.0	6.0	5376
DTW	03R	0.045	45.0	43.9	5.0	5.2	1661
DTW	04L	0.057	50.0	52.5	4.0	4.9	3310
DTW	04R	0.085	52.0	51.6	7.0	7.3	1496
DTW	21L	0.061	48.0	54.2	9.0	10.9	4365
DTW	21R	0.209	54.5	52.5	9.5	8.1	170
DTW	22L	0.056	50.0	49.6	5.0	4.9	2758
DTW	22R	0.042	51.0	52.3	5.0	4.9	6893
EWR	11	0.276	42.0	43.0	6.0	5.3	192

Continued on next page

Table D.1 – continued from previous page

Airport	Runway	$D_{KL}(P, Q)$, nats	Mean ROT, s		MAD, s		Number of observations
			Observed	Predicted	Observed	Predicted	
EWR	29	0.123	41.0	43.3	6.0	5.4	1199
EWR	04L	0.139	48.0	49.7	6.0	8.0	380
EWR	04R	0.035	41.0	42.5	5.0	6.0	8755
EWR	22L	0.023	42.0	42.7	4.0	4.6	11185
EWR	22R	0.131	51.0	51.1	8.0	7.1	468
FLL	10L	0.011	47.0	46.6	4.0	4.4	6052
FLL	10R	0.081	47.0	48.9	6.0	5.2	2778
FLL	28L	0.073	48.0	46.0	5.0	4.6	822
FLL	28R	0.031	48.0	48.3	4.0	4.5	1959
HNL	04R	0.033	54.0	56.5	13.0	14.0	3078
HNL	26L	0.191	61.0	63.6	6.0	6.9	373
HOU	04	0.031	48.0	46.7	5.0	4.6	3271
HOU	17	0.290	42.0	42.3	4.0	5.2	132
HOU	22	0.124	45.0	44.1	4.0	4.5	259
HOU	13L	0.284	54.5	50.9	11.5	8.7	190
HOU	13R	0.031	42.0	43.1	3.0	4.0	4896
HOU	31L	0.123	50.0	47.7	4.0	4.5	670
IAD	01C	0.044	45.0	46.9	6.0	6.6	4742
IAD	01L	0.158	45.0	47.8	5.0	5.1	406
IAD	01R	0.048	48.0	50.2	7.0	7.8	3670
IAD	19C	0.047	49.0	50.4	7.0	6.9	3557
IAD	19L	0.039	45.0	43.9	7.0	6.7	2394
IAD	19R	0.095	52.0	51.7	6.0	5.7	349
IAH	09	0.187	46.0	44.7	4.0	4.2	205
IAH	27	0.048	55.0	57.3	7.0	9.1	9395
IAH	08L	0.061	45.0	47.5	5.0	5.9	2402
IAH	08R	0.036	50.0	49.6	5.0	5.7	5051
IAH	15R	0.405	67.0	58.6	19.0	12.2	117
IAH	26L	0.036	49.0	49.5	4.0	5.0	7844
IAH	26R	0.031	47.0	47.0	5.0	5.7	2440
JFK	04L	0.128	49.0	50.0	5.0	6.4	478
JFK	04R	0.024	52.0	51.3	4.0	4.5	2938
JFK	13L	0.065	46.0	47.3	4.0	5.6	4465
JFK	13R	0.267	51.5	51.4	7.0	7.0	148
JFK	22L	0.024	51.0	51.0	4.0	4.6	3985
JFK	22R	0.141	53.0	52.9	8.0	8.3	356
JFK	31L	0.046	49.0	50.0	5.0	5.6	1768
JFK	31R	0.030	51.0	53.2	6.0	6.9	5840
LAS	01L	0.043	53.0	54.9	5.0	5.7	3982
LAS	01R	0.169	44.0	47.6	6.0	7.3	1188
LAS	08R	0.154	47.0	47.8	5.0	4.9	584
LAS	19L	0.189	52.0	51.7	9.0	7.2	921
LAS	19R	0.027	47.0	47.0	6.0	6.0	2287
LAS	26L	0.031	46.0	47.6	5.0	5.1	13162

Continued on next page

Table D.1 – continued from previous page

Airport	Runway	$D_{KL}(P, Q)$, nats	Mean ROT, s		MAD, s		Number of observations
			Observed	Predicted	Observed	Predicted	
LAX	06L	0.123	59.0	62.4	9.0	12.2	641
LAX	06R	0.136	60.0	61.1	12.0	12.5	513
LAX	07L	0.473	69.0	64.3	10.0	8.2	134
LAX	07R	0.312	59.0	57.4	10.0	10.7	195
LAX	24L	0.053	45.0	46.5	5.0	6.9	3231
LAX	24R	0.013	49.0	48.9	8.0	7.5	12149
LAX	25L	0.011	47.0	47.9	5.0	5.2	17915
LAX	25R	0.089	52.0	51.7	8.0	6.7	760
LGA	04	0.023	42.0	42.3	5.0	5.5	4221
LGA	13	0.104	41.0	41.0	5.0	4.3	465
LGA	22	0.058	41.0	41.4	4.0	4.9	10129
LGA	31	0.037	40.0	40.7	4.0	5.1	5352
MCO	17L	0.095	49.0	50.5	3.0	4.1	3822
MCO	17R	0.166	46.0	50.0	4.0	5.0	932
MCO	18L	0.099	51.0	53.1	6.0	7.6	352
MCO	18R	0.055	53.0	55.2	7.0	7.2	5146
MCO	35L	0.121	58.0	61.0	10.0	11.1	574
MCO	35R	0.035	53.0	52.4	4.0	5.1	2586
MCO	36L	0.040	58.0	57.9	6.0	6.6	3495
MCO	36R	0.106	65.0	62.8	13.0	14.7	715
MDW	04L	0.348	50.0	46.0	5.0	6.2	223
MDW	04R	0.035	45.0	45.5	3.0	3.8	4577
MDW	13C	0.179	45.0	44.3	4.0	4.4	251
MDW	22L	0.084	40.0	39.9	3.0	4.6	2917
MDW	22R	0.350	50.0	42.6	6.0	6.7	173
MDW	31C	0.094	38.0	40.6	3.0	4.5	4159
MEM	09	0.146	63.0	66.9	15.0	17.2	375
MEM	27	0.045	57.0	56.2	6.0	6.4	1668
MEM	18C	0.098	46.0	48.3	6.0	6.4	695
MEM	18L	0.056	49.0	50.9	6.0	6.5	1472
MEM	18R	0.029	52.0	52.3	5.0	5.6	1612
MEM	36C	0.132	57.0	57.1	9.0	9.3	662
MEM	36L	0.039	62.0	62.5	5.0	6.4	2537
MEM	36R	0.036	56.0	55.9	6.0	6.8	2240
MIA	09	0.062	54.0	56.9	7.0	7.0	8625
MIA	12	0.062	47.0	49.9	4.0	5.4	4377
MIA	27	0.208	60.0	61.2	7.0	6.6	314
MIA	30	0.052	48.0	49.2	5.0	4.3	2164
MIA	08L	0.021	48.0	48.3	5.0	5.1	2781
MIA	08R	0.061	61.0	62.2	8.0	9.6	1531
MIA	26L	0.063	56.0	56.6	7.0	7.5	1125
MIA	26R	0.041	47.0	47.4	4.0	5.1	1985
MKE	01L	0.058	54.0	54.9	6.0	6.1	1711
MKE	07R	0.087	49.0	50.4	5.0	5.2	660

Continued on next page

Table D.1 – continued from previous page

Airport	Runway	$D_{KL}(P, Q)$, nats	Mean ROT, s		MAD, s		Number of observations
			Observed	Predicted	Observed	Predicted	
MKE	19R	0.067	49.0	49.3	7.0	5.8	1573
MKE	25L	0.057	48.0	48.9	6.0	5.8	1469
MSP	35	0.054	46.0	47.3	5.0	4.9	2224
MSP	12L	0.020	47.0	47.2	4.0	3.9	5066
MSP	12R	0.014	52.0	52.5	4.0	4.9	5756
MSP	30L	0.026	52.0	53.0	4.0	5.4	4362
MSP	30R	0.023	47.0	47.3	4.0	4.7	4343
ORD	09L	0.025	49.0	49.3	3.0	3.4	4758
ORD	09R	0.069	47.0	48.5	4.0	4.4	1016
ORD	10C	0.084	47.0	50.3	5.0	6.5	5774
ORD	10L	0.105	61.0	62.3	6.0	7.9	555
ORD	10R	0.060	46.0	45.9	4.0	4.3	577
ORD	14R	0.378	59.0	56.2	8.0	8.6	101
ORD	22R	0.486	44.0	47.0	4.0	6.6	105
ORD	27L	0.030	41.0	42.3	4.0	5.3	11347
ORD	27R	0.005	49.0	48.9	4.0	3.9	6507
ORD	28C	0.041	46.0	48.0	5.0	5.9	7424
ORD	28R	0.154	60.0	59.5	13.0	12.3	467
PHL	17	0.074	48.0	46.8	4.0	5.2	632
PHL	26	0.039	49.0	47.7	5.0	5.1	1285
PHL	35	0.024	42.0	42.8	6.0	6.2	4245
PHL	09R	0.031	49.0	49.7	6.0	7.2	4904
PHL	27L	0.116	53.0	50.1	6.0	5.0	762
PHL	27R	0.023	47.0	46.7	7.0	6.6	10149
PHX	08	0.153	53.0	56.9	5.0	7.4	5882
PHX	26	0.069	49.0	50.5	4.0	5.1	8231
PHX	07L	0.152	56.0	60.0	7.0	9.6	703
PHX	07R	0.083	46.0	48.0	4.0	4.6	3178
PHX	25L	0.023	47.0	48.1	5.0	5.3	4212
PHX	25R	0.141	47.0	50.9	4.0	6.3	1306
PVD	05	0.118	58.0	60.4	7.0	7.5	942
PVD	23	0.060	48.0	49.5	5.0	5.2	1291
SAN	09	0.316	48.0	47.7	4.0	4.5	144
SAN	27	0.013	48.0	46.8	6.0	5.3	9640
SDF	29	0.406	45.0	47.3	7.0	7.4	101
SDF	17R	0.056	52.0	53.4	6.0	6.3	1285
SDF	35L	0.051	51.0	53.3	6.0	6.8	2362
SEA	16C	0.409	47.0	47.6	6.0	5.2	105
SEA	16L	0.050	68.0	69.4	10.0	12.1	2257
SEA	16R	0.064	44.0	45.9	4.0	4.5	10831
SEA	34C	0.149	46.0	44.7	7.0	6.2	322
SEA	34L	0.050	44.0	45.1	5.0	4.8	5725
SEA	34R	0.075	59.0	58.2	7.0	7.9	1193
SFO	19L	0.093	50.0	51.2	4.0	4.9	398

Continued on next page

Table D.1 – continued from previous page

Airport	Runway	$D_{KL}(P, Q)$, nats	Mean ROT, s		MAD, s		Number of observations
			Observed	Predicted	Observed	Predicted	
SFO	28L	0.026	58.0	58.6	11.0	9.8	8921
SFO	28R	0.050	52.0	55.0	7.0	8.0	10894
SLC	17	0.084	51.0	53.1	9.0	9.4	1132
SLC	32	0.204	50.0	51.4	4.0	5.7	226
SLC	35	0.059	47.0	48.7	6.0	6.5	1466
SLC	16L	0.038	55.0	55.6	9.0	9.0	2081
SLC	16R	0.019	49.0	49.2	4.0	4.3	2484
SLC	34L	0.033	46.0	46.9	4.0	4.3	2891
SLC	34R	0.067	47.0	48.5	4.0	5.7	2787
SNA	02L	0.575	53.0	47.0	6.0	4.1	132
SNA	20L	0.136	39.0	41.3	8.0	7.7	532
SNA	20R	0.036	45.0	46.5	4.0	4.2	6679
STL	11	0.390	80.0	64.6	7.0	16.0	705
STL	24	0.276	54.0	53.0	5.0	6.3	239
STL	12L	0.059	43.0	43.9	6.0	6.0	929
STL	12R	0.020	63.0	62.9	9.0	9.1	2634
STL	30L	0.071	47.0	47.5	6.0	6.5	765
STL	30R	0.030	48.0	47.7	5.0	5.1	3740